LBL-35489
UC-408

Lawrence Berkeley Laboratory
UNIVERSITY OF CALIFORNIA

STRUCTURAL BIOLOGY DIVISION

Fluorescence Spectroscopic Studies of DNA Dynamics

B.A. Scalettar
(Ph.D. Thesis)

April 1987

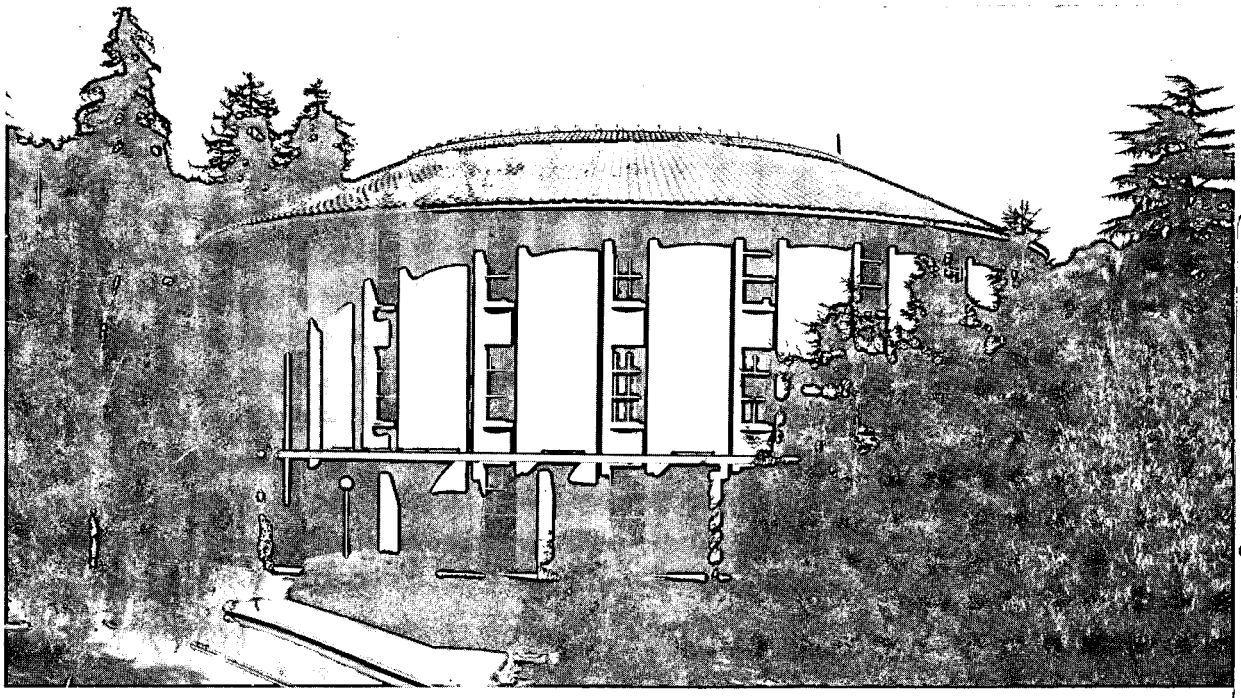

Prepared for the U.S. Department of Energy under Contract Number DE-AC03-76SF00098

DISCLAIMER

LBL-35489
UC-408

Fluorescence Spectroscopic Studies of DNA Dynamics

Bethe Anne Scalettar
Ph.D. Thesis

Department of Biophysics
University of California

and

Division of Structural Biology
Lawrence Berkeley Laboratory
University of California
Berkeley, California

April 1987

This work was supported by the Director, Office of Energy Research, Office of Health Effects Research, of the U.S, Department of Energy under Contract No. DE-AC03-76SF00098, NIH grant number GM30781and by a University of California Graduate Opportunity Fellowship.

Fluorescence Spectroscopic Studies of DNA Dynamics

by

Bethe A. Scalettar

Fluorescence Spectroscopic Studies of DNA Dynamics

Bethe A. Scalettar

Abstract

Random solvent induced motions of DNA are manifest as nanosecond torsional oscillations of the helix backbone, nanosecond through millisecond bending deformations and overall rotational and translational diffusion of the polymer. Cellular processes may superimpose coordinated energy-dissipative motion on this Brownian background. Fluorescence spectroscopy is used to study this spectrum of DNA motions. The fluorescent probe, ethidium monoazide, is covalently bound to the nucleic acid. The steady state fluorescence depolarization data indicate that the covalent monoazide/DNA complex exhibits internal motions characterized by an average angular amplitude of 26 degrees. This result confirms reports of fast torsional oscillations in 'noncovalent' ethidium bromide/DNA systems. A new polarized photobleaching recovery technique (FPR) is used to monitor slow DNA reorientation. The FPR data reflect both the rotational dynamics of the polymer and the reversible photochemistry of the dye. To isolate the reorientational motion of the DNA, the FPR experiments are run in two modes that differ only in the polarization of the bleaching light. A quotient function constructed from the data obtained in these two modes monitors only the rotational component of the FPR recovery. In specific applications those bending deformations

of long DNA molecules that have characteristic relaxation times on the order of 100 microseconds have been resolved. The extent of unresolved, rapid motion is quantified with a 'wobble' model. A fluorescence correlation technique that relates fluctuations in particle number to center-of-mass motion is used to measure translational diffusion coefficients of the plasmid PBR322 ($D = 1.7 \times 10^{-8} \frac{cm^2}{sec}$) and a short oligomeric DNA ($D \approx 10^{-7} \frac{cm^2}{sec}$). A theory that describes angular correlation in systems exhibiting cyclic, biologically directed reorientation and random Brownian rotation is developed. The angular correlation function exhibits an exponential decay that is modulated by a periodic term arising from the nonrandom force. DNA/RNA polymerase, muscle and flagellar systems to which the analysis is applicable are discussed.

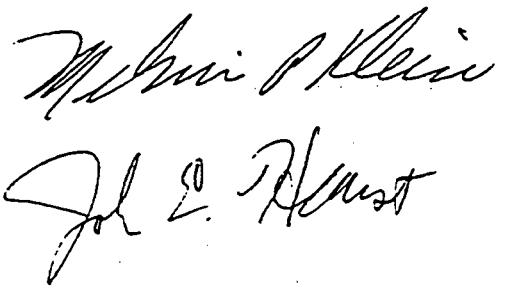

Acknowledgements

I wish to thank my two thesis advisors, John E. Hearst and Melvin P. Klein, for providing me with an intellectually stimulating graduate career. My first foray into the world of scientific research was both a profitable and enjoyable experience. I thank Robert A. Harris, Michael J. Saxton, John C. Owicki, Aaron B. Kantor and Harold Lecar for the many enlightening discussions we had. My experimental work also profitted considerably from the electronic and optical expertise of M.J. Saxton and the biochemical skills of Howard Gamper. Finally, I thank Daniel Axelrod and Paul R. Selvin for providing me with an opportunity to do the photobleaching experiments.

This work has been supported by NIH grant number GM30781, by the Office of Energy Research, Office of Health and Environmental Research of the U.S. Department of Energy under contract number DE AC03-76SF00098 and by a University of California Graduate Opportunity Fellowship.

I have had the love and support of my family throughout my graduate career. I thank my father, Richard Scalettar, my brother, Richard T. Scalettar and my husband, James R. Abney, for helping to make this all possible. Above all I thank my mother, Florence C. Scalettar, for all the wonderful things that she did for me. This thesis is dedicated to her.

Table of Contents

Chapter 1

Introduction and Overview

The dynamic characteristics of macromolecules influence many important biological phenomena. For example, the physical interactions between nucleic acids and proteins are modulated by conformational fluctuations in the two interacting species. The packaging of viral nucleic acid into phage heads and the folding of chromatin require that the DNA be a flexible (bendable) molecule. This dissertation research has probed the nature of macromolecular dynamics and its influence on the mechanisms that underlie important biological processes, particularly those involving DNA. It is hoped that the experimental tools and theoretical ideas presented here will find continued application in studies of biological systems and will thereby help further deepen our understanding of the role of molecular dynamics in cellular events.

The experimental component of this research has centered primarily on the development of fluorescence methods for monitoring slowly relaxing (microsecond and longer) DNA motion. A special significance may be attached to the longer-lived components of biomolecular motion because a number of fundamental cellular processes have been hypothesized to involve slow macromolecular reorientation. As an example, let us consider the phenomenon of transcription. During transcription the enzyme RNA polymerase binds to the DNA template and produces an mRNA molecule that is

complementary to the template (see figure 1). As depicted in the figure, the insertion of the correct complementary bases into the growing mRNA chain hinges on the establishment of hydrogen bonds between the incoming RNA bases and the DNA. Therefore, as the polymerase proceeds down the helical template there must be a relative rotation of the two molecules.[1] The turning frequency or period of this motion can easily be estimated from the known rate of transcription in *in vivo* or *in vitro* systems. The period is found to be on the order of 100 milliseconds. It would be of considerable scientific significance if one could label DNA or the enzyme with a fluorescent tag and then study the slow reorientational motion of transcribing RNA polymerase/DNA complexes.

Slow molecular rotation may also underlie the mechanism by which RNA polymerase searches for the transcriptional start signal, the promoter. Specifically, it has been suggested that the enzyme does a one-dimensional search for the promoter by spiraling down one of the grooves of the DNA.[2] This phenomenon could also be studied with the spectroscopic techniques that are discussed in the coming chapters.

Finally we note that biologically associated rotational motion is not confined to processes that involve nucleic acids. It has been elegantly demonstrated that long-axis flagellar rotation underlies bacterial locomotion,[3] and some experimental evidence suggests that repetitive reorientation of myosin S1 moieties occurs during muscle contraction.[4]

The spectroscopic approach adopted here has many advantages over alternative techniques; the fluorescence method is very sensitive and selective and it is relatively easy to attach a fluorophore rigidly to nucleic acids (via intercalation). However, the most

widely exploited fluorescence method of monitoring molecular reorientation, fluorescence depolarization, will only resolve motions that relax characteristically in $\lesssim$100 nanoseconds (see chapter 3). Therefore, this work has centered largely on the development and initial application of two fluorescence methods that are sensitive to more slowly relaxing rotational motion—polarized Photobleaching Recovery and Correlation Spectroscopy. We have demonstrated that these techniques can be used to monitor DNA reorientations that are 1000 times longer-lived than those probed in a depolarization experiment. Therefore the data presented here, when combined with the results obtained in depolarization work, help establish a complete, integrated fluorescence description of DNA dynamics.

Our experimental studies have led rather naturally to complementary theoretical work. For example, we have shown theoretically that angular correlation measurements will reveal the presence of cyclical biological rotation even if the driven motion is superimposed on a background of random Brownian reorientation. Our studies of DNA dynamics in spatially constrained systems have also led us to hypothesize that when DNA is suspended in a gel-like matrix the larger amplitude bending deformations of the molecule are suppressed. Therefore, local conformational fluctuations and long-axis rotational diffusion are believed to constitute the major reorientational motions of a sterically hindered polymer. If this hypothesis turns out to be correct, it may be possible (using constrained systems) to monitor slow biologically directed rotational motion in the absence of competing large amplitude intramolecular DNA deformations.

The basic construct of this thesis is as follows. The work has been both experimental and theoretical in nature. The purely theoretical work is discussed in chapter 4 after

reviewing what is known about DNA dynamics in chapter 2 and introducing the fluorescence techniques that were used in the experimental studies in chapter 3. Chapters 5, 6 and 7 will then contain the bulk of the experimental work with the photobleaching and correlation techniques. Chapter 8 contains concluding remarks.

Figure 1

Proposed mechanism underlying the phenomenon of transcription. The enzyme RNA polymerase (depicted by the two ovals) will contact the double-stranded helix (the DNA molecule) and copy the DNA into the single-stranded mRNA. An 18 base region surrounding the point of interaction between the enzyme and the DNA is in a locally unwound state. RNA polymerase inserts a base into the growing mRNA if the hydrogen bonding between the DNA and the mRNA is correct. Therefore, as transcription proceeds the proper orientation of these two molecules must be maintained. Because DNA has a helical structure there must then be a relative rotation of the enzyme/mRNA/DNA complex. It has been suggested that rotation occurs because RNA polymerase exerts a torque on the DNA that causes it to turn. For more detail see reference 1.

Figure 1

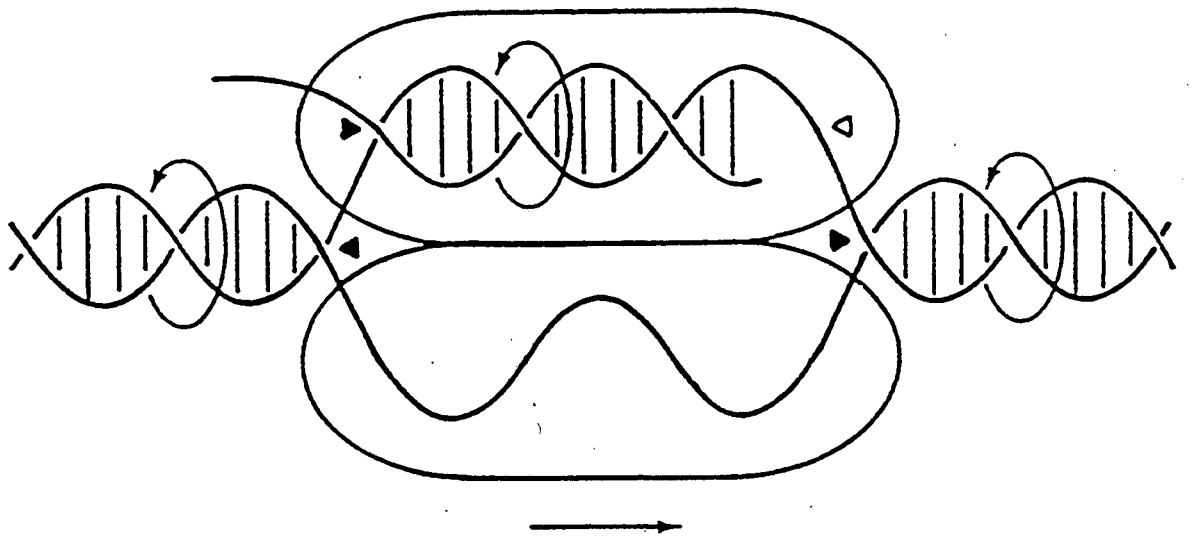

References for Chapter 1

1. H. Gamper and J.E. Hearst (1982) A topological model for transcription based on unwinding analysis of *E. Coli* RNA polymerase. Binary, initiation and ternary complexes. Cell **29**: 81.

2. J.M. Schurr (1979) The one-dimensional diffusion coefficient of proteins absorbed on DNA. Hydrodynamic considerations. Biophys. Chem. **9**: 413.

3. B. Alberts, D. Bray, J. Lewis, M. Raff, K. Roberts and J.D. Watson (1983) *Molecular Biology of the Cell.* Garland Publishing Inc., New York, 757-758.

4. J. Borejdo, S. Putnam and M.F. Morales (1979) Fluctuations in polarized fluorescence: Evidence that muscle cross bridges rotate repetitively during contraction. Proc. Natl. Acad. Sci. USA **76**: 6346.

Chapter 2

Historical Background of DNA Dynamics

Once it had been demonstrated that DNA played a fundamental role in biological processes, a major effort was directed at characterizing the motion of nucleic acids in solution. Here we first describe the development of an experimental 'picture' of DNA dynamics. Theoretical models of DNA motion will be considered separately. In reality there has, of course, been considerable interplay and ideological exchange between the experimental and theoretical branches of the field.

2.1 Experimental History

2.1.1 The Average Conformation of DNA in Solution

Electron micrographs of *dry* DNA typically reveal long cylindrical molecules that bend gently over distances of many hundreds of angstroms. Such pictures provided some of the first unequivocal evidence that DNA was a semi-flexible rod-like polymer. A number of years passed, however, before scientists began to monitor the structural characteristics of DNA in a solution environment like that found *in vivo*.

In the early 1960's hydrodynamic measurements of the sedimentation coefficient, s^0_{20}, and intrinsic viscosity, $[\eta]$, of DNA provided compelling evidence that 'long' DNA molecules are also bent or coiled in solution. (Note that because s^0_{20} monitors the rate at which a molecule sediments it is sensitive to shape and that $[\eta]$ will also depend on

conformation).[1] As an example, consider the sedimentation and viscosity data of Eigner and Doty in figure 2.[2] The curves were fit to a relationship of the form $s^0_{20} \propto (M.W.)^{\alpha}$ and $[\eta] \propto (M.W.)^{\beta}$ (see figure 2). The experimental dependence of sedimentation and viscosity on molecular weight differs from that predicted theoretically for a rigid rod or a random coil.[3-4] It is suggested, then, that (in the size regime examined by Eigner and Doty) neither a rigid-rod nor a completely flexible coil description of DNA conformation is correct.

It was found instead that the molecular weight dependence of DNA sedimentation can be described by modeling the polymer as 'semi-flexible.'[4] Very short pieces of DNA do behave more or less like rods but as the molecular weight of the polymer increases the flexibility of the DNA has a substantial effect on its sedimentation properties. The characteristic length at which the DNA begins to assume a coiled conformation is termed the persistence length, a, of the polymer. Hearst has used sedimentation data to demonstrate that the persistence length of DNA in solution is 500-600 angstroms.[4] (The 100 angstrom variation is attributable to salt effects; low salt concentration leads to a more extended, rigid DNA).

Total intensity light scattering measurements confirmed the conclusions drawn from the hydrodynamic data. Light scattering can be used to extract another important shape parameter—the radius of gyration. The radii of gyration extracted from a number of scattering studies are consistent with a coiled picture of DNA conformation.[5] Nevertheless, it is worth noting that scattering studies of DNA dimension have suffered somewhat from problems associated with low angle data extrapolation.

In conclusion static measurements of DNA shape indicated that the polymer is bent in solution (if it is more than about 200 base pairs in length). The root mean square bend per base pair of DNA is about 6 degrees.[6]

2.1.2 The Dynamic Conformation of DNA

The hydrodynamic and spectroscopic experiments discussed above provided valuable information about the time averaged conformation of the DNA molecule. Soon investigators began to direct their efforts toward characterizing solvent induced DNA motions and the *temporal variation* in DNA conformation. Quasi-Elastic Light Scattering (QELS) has figured prominently in time resolved studies of DNA dynamics. In the QELS experiment the autocorrelation function $C(\tau)$ (see chapter 3) of the scattered light is measured as a function of scattering vector, q. The correlation function is expected to decay as predicted by the relationship $C(\tau) = exp(-2q^2 D_{app}\tau)$.[7] For small scattering angles it was found the the decay of correlation is governed by the center of mass motion of the DNA (*i.e.* $D_{app} = D_0$ where D_0 is the translational diffusion coefficient of the DNA).[7] However, at larger scattering angles the loss of correlation is dictated primarily by segmental or bending motions of the polymer. For relatively long pieces of DNA the light scattering approach has resolved bending deformations in the microsecond and millisecond time regimes.[8] The data have been adequately interpreted in terms of theoretical models of polymer dynamics to be discussed in section 2.2.

The birefringence (or dichroism) decay technique also proved a fruitful method of monitoring relatively slow microsecond and millisecond bending deformations of DNA. In the birefringence experiment the polymer is oriented either with a flow or an applied

electric field. The oriented sample then possesses a different index of refraction, n, (or extinction coefficient, ϵ) along directions parallel and perpendicular to the alignment axis of the DNA. This difference in refractive index can be monitored as a function of time after an orienting 'pulse.' The rate of decay of anisotropy in n or ϵ will reveal the temporal characteristics of Brownian rotational and bending motions. Callis and Davidson have conducted thorough studies of DNA dynamics with the flow dichroism technique.[9] Their results are generally in agreement with the QELS studies. The Callis and Davidson work led to an empirical relationship between Brownian relaxation time, τ, and DNA molecular weight (M.W.):

$$\tau = 5.0 \times 10^{-14}(M.W.)^{1.6\pm0.1}. \qquad (2-1)$$

More recently evidence pointing toward the existence of very rapid (10-100 nanosecond) torsional oscillations in DNA has begun to mount. Torsional oscillations were first detected in fluorescence depolarization studies of ethidium-bromide/DNA complexes.[10] This technique is discussed in detail in chapter 3; here we merely note that the depolarization experiment involves creating an anisotropic angular pattern of excited dye molecules and then monitoring the reorientation induced decay of the anisotropy. Depolarization experiments of Wahl *et al.*,[10] and others, in the early 1970's revealed a sub-microsecond decay in anisotropy that could not have its origin in more slowly relaxing Brownian rotations or bending motions. It was postulated, therefore, that DNA undergoes torsional motions about its long axis. Barkley and Zimm have developed a continuum theory of DNA torsional flexibility.[11]

Magnetic resonance studies of rapid DNA reorientation have served to confirm the

conclusions of the depolarization experiments although, in general, the amplitude of fast motions detected in either nuclear magnetic resonance (NMR) or electron spin resonance (ESR) studies is substantially larger than the corresponding fluorescence result. In a standard magnetic resonance experiment, line widths can be used to monitor molecular rotation. If reorientation is fast (on the time-scale of the technique) the absorption lines appear sharp. If the system is static they are broad. For long DNA molecules it was found that the lines were narrow and that their width did not vary appreciably with DNA length.[12] This result implicates a local motion such as twisting as the principle determinant of line width.

The current estimate of the root mean square amplitude of DNA torsional motion is 8 degrees per base pair.[6]

2.2 Theoretical Models of DNA Conformation and Motion

Theoretical treatments of DNA flexibility and dynamics generally model the polymer either as a discrete set of beads connected together by Hookian springs or as a continuously bending chain (see figures 3 and 4). The models serve both to correlate flexibility with the average dimensions of the macromolecule in solution and to make predictions about the temporal and spatial characteristics of polymer dynamics. Here we discuss four well known models of DNA flexibility and present their important conclusions.

2.2.1 The Freely Rotating Chain and Wormlike Coil Models

The Kratky-Porod wormlike coil is the continuum extension of a very simple stick model of flexible polymers—the freely rotating (FR) chain (see figure 3a).[13-14] A

freely rotating polymer is composed of N stick subunits of length, l. The i^{th} subunit is oriented along $\vec{l}_i$. In the model the angle, θ, between $\vec{l}_i$ and $\vec{l}_{i-1}$ is fixed and independent of i. Subunit i can, however, undergo unhindered azimuthal rotation about subunit $i-1$; hence this chain is called freely rotating.

The FR model can be used to calculate important measures of polymer dimension—the mean square end to end length, $\langle R^2 \rangle$ and the persistence length, a (where $\langle\rangle$ denotes ensemble average). For the freely rotating chain, $\langle R^2 \rangle$ is defined, quite naturally, by the expression

$$\langle R^2 \rangle = \langle [\sum_{i=1}^{N} \vec{l}_i]^2 \rangle. \qquad (2-2)$$

It is easy to show that, for the FR chain,

$$\langle R^2 \rangle = Nl^2 [\frac{1+\alpha}{1-\alpha} - \frac{2\alpha}{N} \frac{1-\alpha^N}{(1-\alpha)^2}]. \qquad (2-3)$$

Here $\alpha = cos\,\theta$. The persistence length (see figure 3b) is the average sum of each bond's projection onto the direction $\vec{l}_1$ (in the limit that N becomes infinite). Hence

$$a = \lim_{N \to \infty} \langle \sum_{i=1}^{N} \vec{l}_i \cdot \hat{l}_1 \rangle. \qquad (2-4)$$

The persistence length of the FR chain is simply

$$a = \frac{l}{1-\alpha}. \qquad (2-5)$$

We now allow the bond length l of the FR chain to approach zero while maintaining the persistence length and contour length $L = Nl$ at their predetermined values. This limiting process yields the Porod-Kratky worm-like coil. For this model one has the important relationship[13-14]

$$\langle R^2 \rangle = 2aL[1 - \frac{a}{L}(1 - exp(-\frac{L}{a}))]. \qquad (2-6)$$

Note that as the persistence length of the polymer becomes very large, *i.e.* the molecule become very stiff, expression 2-6 reduces to the appropriate rigid rod relationship

$$\langle R^2 \rangle = L^2. \qquad (2-7)$$

2.2.2 The Rouse-Zimm Model

We now move to a dynamic model of polymeric molecules first introduced by Rouse and Zimm.[15-17] In the Rouse-Zimm (RZ) description the polymer is composed of a set of beads that are connected by springs (see figure 3c). Each bead moves under the influence of Brownian, viscous drag and harmonic restoring (transverse and longitudinal) forces. The dynamics of the contour of the polymer is represented by the combined motion of the beads. If we let $\vec{x}$ contain the x components of the position vectors of each of the N beads, the Rouse-Zimm equation of motion will read

$$m\frac{d^2\vec{x}}{dt^2} = -f\frac{d\vec{x}}{dt} - \sigma A\vec{x} + \vec{F}_{Brown}. \qquad (2-8)$$

In equation 2-8, f is the friction factor, m is the mass of a bead, σA is a matrix that describes the restoring forces, and $\vec{F}_{Brown}$ is the Brownian force. The solution for the temporal and spatial characteristics of the polymer conformation is written as a superposition of the normal modes, n, of the equation of motion. The normal modes are simple sinusoidal functions. An equation that describes temporal variation in the normal coordinates follows directly from 2-8.

The normal mode equation of motion is most easily solved in the long wavelength limit, i.e when $\frac{\pi n}{N} << 1$. In this limit it can be shown that the relaxation time, τ_n, of mode n is given by the expression[17]

$$\tau_n = \frac{2R_G^2}{\pi^2 n^2 D_0} \qquad (2-9a)$$

and that the equilibrium mean square displacement, $\langle \delta_n^2 \rangle$, of mode n is

$$\langle \delta_n^2 \rangle = \frac{N R_G^2}{6\pi^2 n^2}. \qquad (2-9b)$$

Here R_G is the radius of gyration of the polymer. The Rouse-Zimm model has been extensively used to interpret both dynamic light scattering and birefringence data.

2.2.3 The Hearst-Harris Model

Hearst and Harris extended the RZ model of polymer dynamics by introducing chain stiffness into the equation of motion.[18] The Hearst-Harris model was formulated in both a discrete and a continuum form. In the continuum picture, the position, $\vec{x}$, of a point on the polymer is described parametrically *i.e.* $\vec{x} = \vec{x}(s,t)$ where s is a contour distance along the length of the chain. The equation of motion for $\vec{x}(s,t)$ contains the Brownian, viscous and restoring terms of the RZ model and a stiffness term proportional to $\frac{\partial^4 \vec{x}}{\partial s^4}$. The full equation of motion is

$$\rho \frac{\partial^2 \vec{x}}{\partial t^2} + f \frac{\partial \vec{x}}{\partial t} + \epsilon \frac{\partial^4 \vec{x}}{\partial s^4} - \kappa \frac{\partial^2 \vec{x}}{\partial s^2} = \vec{F}_{Brown}(s,t). \qquad (2-10)$$

Here ρ is the chain density, and ϵ and κ are, respectively, the force constants for bending and stretching of the chain. The solution of 2-10 can also be formulated as a normal mode expansion.

Both equilibrium and dynamic properties of the polymer can be extracted from the Hearst-Harris model. It can be shown that for long chains the relaxation times and mean square amplitudes of the modes have the same form as in the RZ model.

2.2.4 The Tuna-Fish Can Model

In the Tuna-Fish Can model the polymer is viewed as a linear array of connected rods[19] (see Figure 4). In general the macromolecule will rotate and deform under the

influence of global and internal Brownian motions. The evolution of macromolecular orientation can be followed by defining a local set of body fixed axes for each subunit. It is assumed that the mean square angular displacements $\langle \Delta_x^2 \rangle$ and $\langle \Delta_y^2 \rangle$ about the transverse (x and y) body axes are the same. We note in passing that if the polymer were rigid $\langle \Delta_x^2 \rangle$ and $\langle \Delta_y^2 \rangle$ would be proportional to an appropriate diffusion coefficient and the time. However, for a deformable macromolecule this standard result does not hold.

A diffusion equation that governs the temporal evolution of the fraction, $f(\Phi)$, of a given subunit at orientation Φ (in the laboratory frame) is then written down. This equation contains effective time dependent diffusion coefficients. Angular correlation functions for the Tuna-Fish molecule (related to those discussed in chapters 3 and 4) can then be calculated.

Figure 2

Viscosity and sedimentation data of Eigner and Doty. The sedimentation data in figure 2 fit the expressions $s^0_{20} \propto (M.W.)^{0.325}$ for $3 \times 10^5 < M.W. < 4 \times 10^6$ and $s^0_{20} \propto (M.W.)^{0.405}$ for $M.W. > 4 \times 10^6$. The predicted relationship between s^0_{20} and molecular weight is $s^0_{20} \propto (M.W.)^{0.5}$ for a long random coil. Therefore the DNA is not behaving strictly like a random coil (nor a rigid rod). However, the data do manifest a quasi random coil sedimentation relationship at the higher end of the molecular weight spectrum. For the smaller DNA molecules the plot is more accurately described by a rod model. Similar considerations hold for the intrinsic viscosity. Adapted from Reference 2.

Figure 2

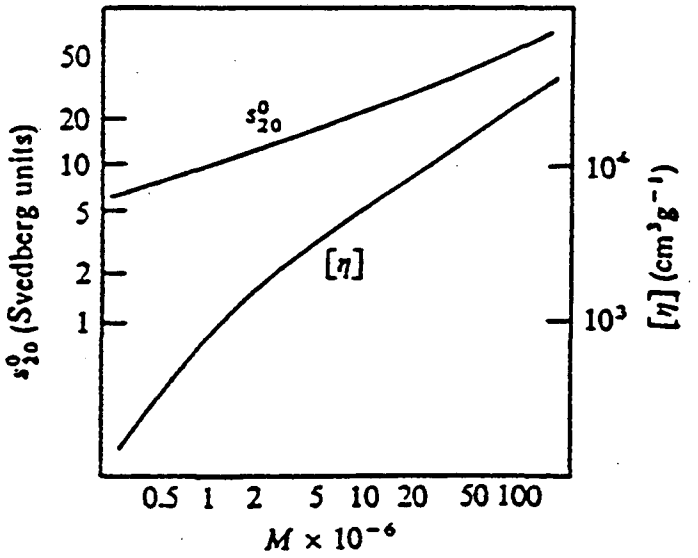
50
20
10
5
2
1
s^0_{20}
$[\eta]$
10^4
10^3
s^0_{20} (Svedberg units)
$[\eta]$ (cm^3g^{-1})
0.5 1 2 5 10 20 50 100
$M \times 10^{-6}$

Figure 3

Schematic representation of the persistence length (3b), a section of a freely rotating (FR) polymer (3a) and a bead spring (RZ) macromolecule (3c). In (3b) the persistence length, a, of a stick (FR) polymer is shown. The persistence length is the average sum of the projection of each bond on the direction of the first bond (for an infinitely long molecule). Therefore, a measures the extent to which the contour of the polymer persists in the original direction. For the FR chain (in 3a) the azimuthal angle ϕ assumes all values with equal probability while θ is fixed. Adapted from References 1 (3a,b) and 17 (3c).

Figure 3

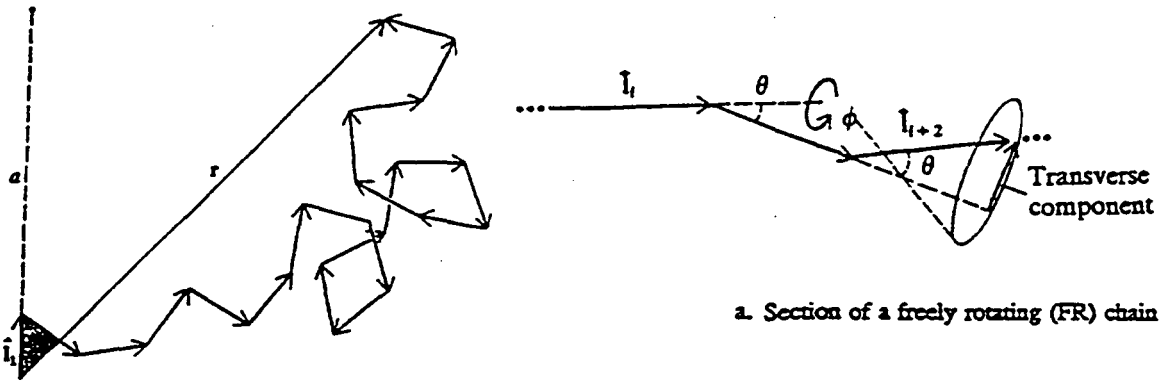

a. Section of a freely rotating (FR) chain

b. Definition of the persistence length, a, of a freely rotating polymer

$$a = \lim_{N \to \infty} \langle \sum_{i=1}^{N} \vec{l}_i \hat{l}_1 \rangle$$

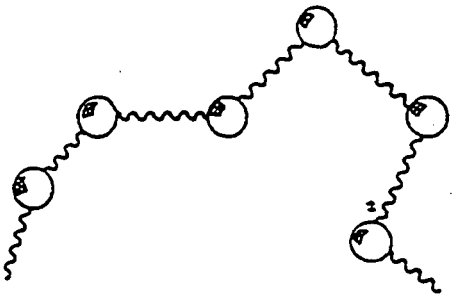

c. Section of a bead spring (RZ) macromolecule

Figure 4

The Tuna-Fish Can representation of polymer reorientation.. In this model the macromolecule can exhibit a wide spectrum of rotational motions. However, it is assumed that the mean square angular displacement about the x and y body axes is the same *i.e.* the polymer maintains a mean local cylindrical symmetry. Expressions for the angular correlation of a twisting, bending and diffusing 'Tuna-Fish' molecule have been derived. Adapted from Reference 20.

Figure 4

THE ROD (or TUNA FISH CAN) MODEL

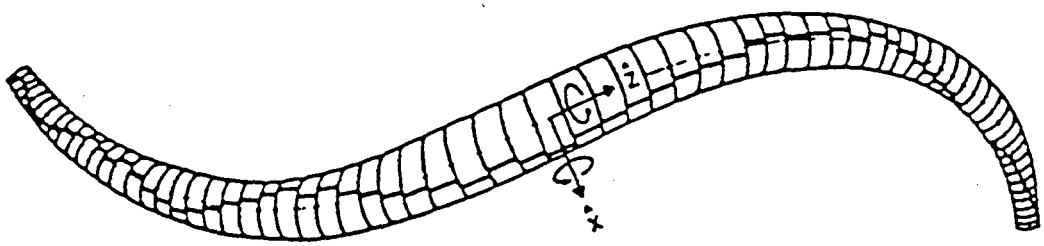

TWISTING

$\langle \Delta_Z(t)^2 \rangle$ = MEAN SQUARED ANGULAR DISPLACEMENT ABOUT BODY-FIXED $\hat{Z}$-AXIS

TUMBLING (BENDING)

$\langle \Delta_X(t)^2 \rangle$ = MEAN SQUARED ANGULAR DISPLACEMENT ABOUT BODY-FIXED $\hat{X}$-AXIS

$= \langle \Delta_Y(t)^2 \rangle$ (ASSUMED)

References for Chapter 2

1. C.R. Cantor and P.R. Schimmel (1980) *Biophysical Chemistry, Vol. II.* W.H. Freeman and Company, San Francisco, 461.

2. J. Eigner and P. Doty (1965) The native, denatured and renatured states of deoxyribonucleic acid. J. Mol. Biol. **12**: 549.

3. C.R. Cantor and P.R. Schimmel (1980) *Biophysical Chemistry, Vol. II.* W.H. Freeman and Company, San Francisco, 1026-1027.

4. J.E. Hearst and D.A Reese (1980) Sedimentation of wormlike coils. II. J. Chem. Phys. **73**: 3007.

5. C.W. Schmid, F.P. Rinehart and J.E. Hearst (1971) Statistical length of DNA from light scattering. Bipolymers **10**: 883.

6. M.D. Frank-Kamenetskii (1981) Fluctuations in DNA. Comm. Mol. Cell. Biophys. **1**: 105.

7. V.A. Bloomfield (1981) Quasi-elastic light scattering applications in biochemistry and biology. Ann. Rev. Biophys. Bioeng. **10**: 421.

8. K.S. Schmitz and J.M. Schurr (1973) Rotational relaxation of macromolecules determined by dynamic light scattering. II. Temperature dependence for DNA. Biopolymers **12**: 1543.

9. P.R. Callis and N. Davidson (1969) Hydrodynamic relaxation times of DNA from decay of flow dichroism measurements. Biopolymers **8**: 379.

10. Ph. Wahl, J. Paoletti and J.-B. LePecq (1970) Decay of fluorescence emission anisotropy of the ethidium bromide-DNA complex. Evidence for an internal motion

in DNA. Proc. Nat. Acad. Sci. USA **65**: 417.

11. M.D. Barkeley and B.H. Zimm (1979) Theory of twisting and bending of chain macromolecules; analysis of the fluorescence depolarization of DNA. J. Chem. Phys. **70**: 2991.

12. M.E. Hogan and Oleg Jardetzky (1979) Internal motions in DNA. Proc. Nat. Acad. Sci. USA **76**: 6341.

13. P.J. Flory (1969) *Statistical Mechanics of Chain Molecules*. John Wiley and Sons, Inc., New York, 401-403.

14. O. Kratky and G. Porod (1949) Röntgenuntersuchung gelöster fadenmolekule. Rec. Trav. Chim. **68**: 1106.

15. P.E. Rouse (1953) A theory of the viscoelastic properties of dilute coiling polymers. J. Chem. Phys. **21**: 1272.

16. B.H. Zimm (1956) Dynamics of polymer molecules in dilute solution: Viscoelasticity, flow birefringence and dielectric loss. J. Chem. Phys. **24**: 269.

17. B.J. Berne and R. Pecora (1976) *Dynamic Light Scattering*. John Wiley and Sons, Inc., New York, 182-188.

18. R.A. Harris and J.E. Hearst (1966) On polymer dynamics. J. Chem. Phys. **44**: 2595.

19. J.M. Schurr (1984) Rotational diffusion of deformable macromolecules with mean local cylindrical symmetry. Chem. Phys. **84**: 71.

20. J.H. Shibata B.S. Fujimoto and J.M. Schurr (1985) Rotational dynamics of DNA from 10^{-10} to 10^{-5} seconds: Comparison of theory with optical experiments.

Biopolymers **24**: 1909.

Chapter 3

Fluorescence Spectroscopy as a Probe of Rotational Motion

Here we present an overview of the basic principles that underlie three of the most widely utilized fluorescence methods of monitoring molecular motion: depolarization, photobleaching and correlation spectroscopy. The physics that describes all three techniques is very similar. Fundamentally all fluorescence experiments utilize light to induce electronic excitation of dye molecules. The excited state typically decays away after several nanoseconds and, concurrently, a fluorescence photon is produced. It is this photon that is experimentally detected. The probability that an excitation beam photon is absorbed by a dye molecule is determined by the angle between the transition moment, $\hat{\mu}$, of the fluorophore and the polarization of the exciting quantum of light. Specifically if light with polarization direction $\hat{p}$ impinges on a sample, the absorption probability will be proportional to[1]

$$(\hat{\mu} \cdot \hat{p})^2 = cos^2\,\theta \qquad (3-1)$$

where θ is the angle between the unit vectors $\hat{\mu}$ and $\hat{p}$. It is apparent from equation 3-1 that fluorescence spectroscopy can be used to monitor rotational motion because reorientation of the dye molecules will lead to changes in the angle θ and associated variation in the emitted fluorescence. Let us look at the specific way that the depolarization technique monitors rotation induced changes in θ.

3.1 Fluorescence Depolarization

In a time resolved fluorescence depolarization experiment the sample is typically hit with a short pulse of plane polarized light. If the dye molecules do not completely reorient during the pulse the number of excited molecules at orientation θ will be greatest for small angles and will approach zero for θ=90 degrees. The components of the fluorescence emission parallel, $I_{||}$, and perpendicular, $I_{\perp}$, to the direction of polarization of the exciting light are then followed as a function of the time, t, after the pulse. The component of the fluorescence along an axis is simply proportional to the square of the projection of the emission dipole on the given direction.

It is qualitatively clear that (if the absorption and emission moments of the dye are parallel) the intensity of the parallel component will be bigger than that of the perpendicular component for small t and that $I_{||}$ and $I_{\perp}$ will approach one another as molecular rotation leads to the reestablishment of an isotropic angular pattern of fluorescing molecules. It is also important to realize that the number of excited molecules will decay as a function of time because the excited state has a finite ($\approx$ 10 nanosecond) lifetime. When the effects of lifetime and rotational diffusion are combined it can be shown that for spherically rotating particles[1]

$$I_{||} = [\frac{1}{3} + \frac{4}{15} exp(-6D_{rot}t)(\frac{3\,cos^2\,\xi - 1}{2})]exp(-\frac{t}{\tau_f}) \qquad (3-2a)$$

$$I_{\perp} = [\frac{1}{3} - \frac{2}{15} exp(-6D_{rot}t)(\frac{3\,cos^2\,\xi - 1}{2})]exp(-\frac{t}{\tau_f}) \qquad (3-2b)$$

and that the anisotropy

$$r(t) = \frac{I_{||} - I_{\perp}}{I_{||} + 2I_{\perp}} \qquad (3-2c)$$

is given by the expression

$$r(t) = \frac{2}{5} exp(-6D_{rot}t)[\frac{3\,cos^2\,\xi - 1}{2}]. \qquad (3-2d)$$

In the above expressions ξ is the angle between the absorption and emission moments, D_{rot} is the rotational diffusion constant of the molecule, and τ_f is the fluorescence lifetime of the dye. It is typical in a time resolved fluorescence depolarization experiment to monitor r(t) and to fit the data to find the rotation rate.

Fluorescence depolarization has provided a wealth of data on molecular motion. The chief disadvantage of the technique is that the signals $I_{||}$ and $I_{\perp}$ will disappear with a characteristic time τ_f and, hence, depolarization will not resolve microsecond and millisecond macromolecular motions.

The temporal constraints that exist in depolarization experiments stimulated an interest in developing fluorescence techniques that can probe more slowly relaxing molecular motions. Fluorescence Photobleaching Recovery (FPR) and Correlation Spectroscopy (FCS) are two such techniques. Both the FPR and FCS methods have been primarily applied to the study of translational diffusion. We now review the way in which rotational and translational motion manifest themselves in FCS and FPR experiments. The FPR approach will be considered first because of analogies that can be drawn with fluorescence depolarization experiments.

3.2 Fluorescence Photobleaching Recovery

In the fluorescence depolarization experiment a short pulse of light was used to create an anisotropic angular pattern of excited molecules. In a photobleaching experiment the sample is also hit with a short pulse of light, however, the FPR flash is so intense that

excited molecules are actually bleached (*i.e.* they become non-fluorescent) with some probability. Because the establishment of the non-fluorescent state depends fundamentally on the absorption of light, a polarized bleach beam will create an anisotropic angular concentration of fluorophore by preferentially destroying dye molecules whose absorption moments are parallel to the polarization of the light (see section 3.2.1).

After the dye molecules have been hit with the bleach pulse, an attenuated probe beam is directed onto the sample and the temporal dependence of the fluorescence excited under weak illumination is monitored. During the probe phase of the experiment rotational motion leads to the return of a uniform angular distribution of dye; the changes in dye distribution are manifest as systematic changes in the fluorescence signal. Because this work includes one of the first polarized FPR studies of microsecond rotational motion, a reasonably detailed description of the theory that describes the polarized FPR experiment will be presented.

There are essentially two versions of polarized FPR theory. The first, developed by Smith *et al.*,[2] provided a framework within which to interpret FPR measurements of 'slow' rotational relaxation rates. In the Smith treatment the characteristics of the FPR data were described by a theoretical model which attributes post-bleach anisotropy decay purely to molecular rotation. Here we first review the theoretical ideas developed in reference 2. We then discuss a theory of polarized FPR that has been extended to deal with a more complex system in which there exist both rotational and, competing, nonreorientational processes in the sample.[3,4] This generalized theory is the one that is applicable to the microsecond FPR study of DNA dynamics studies conducted here.

3.2.1 Theory of Pure Rotational FPR

Polarized photobleaching experiments typically are conducted in two modes (see figure 5). The fluorescent molecules are exposed to a very intense pulse of light that is polarized along the y axis (parallel experiment) or the x axis (perpendicular experiment). Immediately after bleaching (t=0), the intensity of the light is reduced by a factor of $\approx$10,000 and the temporal dependence of the fluorescence is then monitored. The polarization of the weaker (probing) beam is always parallel to the y axis.

Simple qualitative arguments make it clear that the fluorescence intensity, $F_{\|}(t)$, should rise as a function of time when an experiment is run in the parallel mode. In a parallel experiment the intense polarized light preferentially destroys dye molecules that are aligned along the y axis at the time of the bleach. Moreover, during observation the probe beam will preferentially excite fluorophores that are oriented parallel to the y axis. Immediately after the bleach the number of fluorescent molecules aligned along the observation axis is reduced and therefore, initially, the fluorescence emitted by the sample under probe illumination is diminished relative to the pre-bleach level, F_0. Moreover, as the bleached dye molecules begin to distribute themselves more uniformly over angular space, the parallel fluorescence rises (see figure 5).

In a perpendicular ($\perp$) experiment, one expects to observe a photobleaching decay curve since there is minimal destruction of fluorophores whose absorption dipoles are aligned about the observation axis (see figure 5); post-bleach molecular rotation serves, therefore, to reduce the number of fluorescent molecules that are parallel to the x direction.

These statements can be made mathematically precise for simple systems.[2-4] The

analysis shows that the photobleaching curves will exhibit a bi-exponential recovery/decay in the parallel/perpendicular mode respectively. These predictions have been qualitatively verified for a liposome-diI system in which the relaxation times were several hundred milliseconds or longer.[2]

3.2.2 Theory of Coupled Rotational and Nonrotational FPR

The above description of photobleaching curves has assumed that reorientational motion is the only physical process producing recovery. However, there may exist other mechanisms by which the fluorescence can recover.[3,4] Axelrod has noted that a bleached molecule (*e.g.* a dye-oxygen complex) might regain its fluorescent properties because the establishment of the nonfluorescent state is reversible.[3] Wegener and Rigler have suggested that if a complex multi-component system is under study the translational recovery of one species may overlap the rotational relaxation of a different component.[4] The presence of competing recovery modes will clearly modify the predicted form of FPR curves. However, if we assume that only rotational processes are sensitive to the polarization of the incident light, there is a relatively straightforward way to isolate the component of the recovery that is derived from purely reorientational motion.[3–5]

Wegener and Rigler have presented a method for separating the contributions of orientation dependent and independent phenomena. For the case where fluorescence is gathered by 4π steradian collection optics, only nonrotational processes contribute to the recovery if the observation beam polarization is rotated 54.7 degrees with respect to the polarization of the bleach beam. The rotational motions are characterized from parallel and perpendicular FPR experiments and an anisotropy function is derived that is valid in

the limit of shallow bleaches.[4]

For the very common case of epi-illumination microscope optics and arbitrary bleach depth (bleach depth in mode m is defined as $\frac{F_0 - F_m(0)}{F_0}$) Axelrod has derived expressions for the ratio of parallel and perpendicular FPR data that likewise eliminates the orientation independent processes.[3] Since the experimental configuration used here is the same as that analyzed in Axelrod's treatment a more detailed review of his results is presented.

Consider the quantity R(t) defined as follows:

$$R(t) = \frac{F_0 - F_\perp(t)}{F_0 - F_\parallel(t)}. \qquad (3-3)$$

Recall that F_0 denotes the pre-bleach fluorescence of the sample; $F_\perp(t)$ and $F_\parallel(t)$ refer to the post bleach fluorescence at time t in the perpendicular and parallel modes respectively. The ratio R(t) is predicted to start at a value less than unity at t=0 (immediately after bleaching). This mathematical statement can be reformulated in a way that displays a clear analogy with the theory of pure rotational FPR. If R(0)<1 we have $F_0 - F_\perp(0) < F_0 - F_\parallel(0)$, *i.e.* the depth of bleach is larger in the parallel mode than in the perpendicular. Hence, even if there exist nonrotational recovery modes for the sample we *still* expect the deepest bleach when the observation beam polarization (*i.e.* the direction of preferential excitation) is parallel to the direction of greatest bleaching. (Note in figure 5 that the bleach is also deeper for a parallel experiment when *only* rotational recovery is considered). Then as time progresses and the bleached molecules distribute themselves uniformly over angular space $F_\parallel(t)$ and $F_\perp(t)$ will approach one another and the ratio will tend toward one. The time scale associated with the rise of the ratio mirrors the purely reorientational processes in the sample.

Axelrod has made quantitative predictions for the behavior of the ratio R(t) when the system is immobile during the bleach and when the molecules undergo isotropic spherical rotational diffusion in 3 dimensions (with diffusion constant D_{rot}) during the observation period. His results for the optical geometry used in these experiments are (see Appendix 1)

$$R(0) = 0.20 \qquad (3-4)$$

and

$$R(t) = \frac{A - Bexp(-6D_{rot}t) - Cexp(-20D_{rot}t)}{A + 2B\,exp(-6D_{rot}t) - \frac{8}{3}C\,exp(-20D_{rot}t)}. \qquad (3-5)$$

Here A, B and C can be expressed in terms of incomplete Gamma functions and a parameter that characterizes the depth of bleach. The ratio itself is relatively insensitive to the depth of bleach. Expressions 3-4 and 3-5 are valid if the absorption and emission dipoles of the dye are parallel and the numerical aperture of the microscope objective is small.

To account adequately for the microsecond photobleaching data obtained from a complex polymer like DNA, the assumption that the fluorophore is static during the bleach must be modified. If the pulse is 10 microseconds long, the small amplitude torsional oscillations and bending deformations exhibited by nucleic acids will cause substantial deviations from an instantaneous bleach pattern. In fact even for relatively simple systems dye wobble will cause depolarization during a microsecond pulse of light. It is possible mathematically to model the effect of fast, restricted motion during the bleach using a 'uniform wobble in a cone' model (see figure 6 and Appendix 1). A discussion of this model can also be found in reference 4. Qualitatively, the existence of motion during

the bleach will cause an increase in R(0) because the distinction between the destruction profile in the parallel and perpendicular modes is reduced when a fluorophore wobbles and has increased probability of being destroyed by light of either polarization. If it is assumed that a dye molecule explores a cone of half angle α uniformly during the bleach then it can be shown that for the geometry used in these experiments:

$$R(0) = \frac{1 - \frac{\chi^2}{35}}{\frac{2}{35}\chi^3 + \frac{3}{5}\chi^2 + 1}. \qquad (3-6)$$

Here $\chi = cos\alpha(cos\alpha + 1)$. Note that R(0) is indeed an increasing function of α and that if α=0 we recapture the result R(0)=0.20. Moreover, if the fluorophore moves very extensively during the bleach (*i.e.* $\alpha \approx 90$ degrees), R(0)=1 and the FPR technique is unable to resolve the rotational recovery of the molecule to which the fluorophore is attached.

3.3 Fluorescence Correlation Spectroscopy

Finally we discuss the FCS technique. The conceptual foundation of FCS differs somewhat from that of FPR and fluorescence depolarization. In an FPR or depolarization study the average fluorescence emitted by the sample, $\langle i \rangle$, is measured; in an FCS experiment the *temporal variation* in the signal about the mean, $\delta i(t) = i(t) - \langle i \rangle$, is followed. It is intuitively clear that the fluctuations, $\delta i(t)$, will be manifest only if the number of molecules under observation is 'small.' Therefore, in a correlation experiment the fluorescence emitted by $\lesssim 10^6$ molecules is monitored.

In an FCS experiment the autocorrelation function $C(\tau) = \langle \delta i(t) \delta i(t+\tau) \rangle$ of the fluorescence signal is computed. The autocorrelation function measures the similarity between the fluorescence at a time t and this signal at a later time t+τ. The temporal

behavior of the correlation function mirrors the characteristic relaxation of the physical processes producing the fluorescence fluctuations. A physical picture of the correlation function is drawn as follows. For times τ that are short relative to relaxation rates $i(t) \approx i(t+\tau)$ and the degree of correlation is high (*i.e.* $C(\tau)$ is large). As τ increases and the configuration of the system changes the similarity between $i(t)$ and $i(t+\tau)$ will diminish; $C(\tau)$ therefore decays with time. The rate at which correlation is lost is determined by the characteristic relaxation of the underlying physical processes. Here a brief review of the relationship between translational diffusion and the concentration correlation function will be presented; rotational diffusion and angular correlation will then be discussed in somewhat greater detail.

3.3.1 Translational FCS

Translational diffusion leads to fluctuations in the fluorescence emitted by a sample that is illuminated in a small region because molecules outside the area of excitation can move into the beam and begin to contribute to the signal and fluorescing dye can diffuse out of the spot (see figure 7). This physical statement can be made mathematically precise. If it is assumed that the sample is illuminated with light having a nondiverging Gaussian intensity profile $I(r) = \frac{2P}{\pi\omega_0^2} exp(\frac{-2r^2}{\omega_0^2})$ (r is the radial cylindrical polar coordinate of a point $\vec{r}$ from the position of maximal light intensity, ω_0 is the e^{-2} radius of the illuminated spot and P is the power in the beam), it can be shown that the translational correlation function has the form:[6]

$$C(\tau) = \frac{C(0)}{1+\frac{\tau}{\tau_d}} \qquad (3-7a)$$

where

$$\tau_D = \frac{\omega_0^2}{4D_0}. \qquad (3-7b)$$

In 3-7b D_0 is the translational diffusion coefficient of the molecule. An explicit expression for the zero time value of the autocorrelation function, C(0), is

$$C(0) = \frac{\langle i \rangle^2}{\pi \omega_0^2 LC}. \qquad (3-8)$$

Here C is the concentration of dye and L is the length of the sample. Note that the commonly used TEM_{00} mode of a laser has a transverse Gaussian irradiance profile and, therefore, the assumption that the beam is Gaussian is not very restrictive.

There are several important features to the above equations. First, the characteristic time for relaxation of translational fluctuations, τ_D, is dependent on the size of the illuminated region of the sample, ω_0. The relationship 3-7b between τ_D and ω_0 can easily be rationalized if one recalls the two dimensional expression for a random walker's mean square displacement $\langle r^2 \rangle = 4D_0 t$. If we take r=$\omega_0$ and t=τ_D equation 3-7b follows. Second, if the decay of correlation has its origin in translational motion (or in fact *any* number fluctuation) the amplitude, C(0), of the correlation function and the mean of the signal, $\langle i \rangle$, will be related to the average number of fluorescing molecules, N, as dictated by the equation:

$$\frac{C(0)}{\langle i \rangle^2} = \frac{1}{N}. \qquad (3-9)$$

Equations 3-8 and 3-9 are identical: substitution of the relationship $N = \pi \omega_0^2 LC$ in 3-8 will yield 3-9. It is also worth noting that since C(0)=σ^2 where σ is the standard deviation of the signal, relationship 3-9 is characteristic of a process that obeys Poisson

statistics. The most important feature of equation 3-9 is that it provides a way to isolate spurious, systematic sources of correlation.

3.3.2 Rotational FCS

The fluorescence signal can also fluctuate with time because the orientation of the absorption and emission dipoles of the probes vary with respect to the direction of polarization of the excitation beam and the direction of observation. (It is assumed in this discussion that translational motion is separable from molecular rotation because molecules typically translate very slowly relative to their rate of reorientation).

We present a review of the quantitative relationship between angular variables and the fluorescence autocorrelation function. A more complete discussion may be found in the article by Aragon and Pecora.[7] The measured quantity is the fluorescence photocurrent produced when photons impinge on the photocathode of a photomultiplier tube and an electron cascade is released. The current from a population of N singly-labeled molecules is given by

$$i(t) = geQ(\lambda)\sum_{j=1}^{N} n_j(t) \qquad (3-10)$$

where g is the gain of the photomultiplier, e the electronic charge, Q(λ) the efficiency of the photocathode at wavelength λ, and $n_j(t)$ the number of photons emitted per second by the j^{th} fluorophore. The basic quantity of interest is the ensemble averaged autocorrelation function

$$C(\tau) = \langle \delta i(t)\delta i(t+\tau)\rangle. \qquad (3-11)$$

$C(\tau)$ may be rewritten using the above expression for the photocurrent as

$$C(\tau) = \langle \delta i(t)\delta i(t+\tau)\rangle = g^2e^2Q^2(\lambda)\langle\sum_{j=1}^{N}\delta n_j(t)\sum_{i=1}^{N}\delta n_i(t+\tau)\rangle. \qquad (3-12)$$

This expression simplifies for a dilute solution in which the cross correlation terms, $i \neq j$, may be neglected. If we note that the ensemble average is the same for each molecule

$$C(\tau) = g^2 e^2 Q^2(\lambda) \langle \sum_{i=1}^{N} \delta n_i(t) \delta n_i(t+\tau) \rangle = N g^2 e^2 Q^2(\lambda) \langle \delta n(t) \delta n(t+\tau) \rangle. \quad (3-13)$$

Finally, since the process under consideration is stationary, *i.e.*, invariant under time translation,

$$C(\tau) = N g^2 e^2 Q^2(\lambda) \langle \delta n(0) \delta n(\tau) \rangle. \quad (3-14)$$

The number of photons emitted per second by a fluorophore, $n(t)$, monitors the orientation of the rotating molecule with respect to an external lab frame because it depends on the cosine of the angle between the polarization of the excitation beam and the absorption dipole of the probe. If a particular direction of polarization of the emitted fluorescence is monitored, then the expression for the photocurrent will also contain a term depending on the component of the fluorescence in the direction of detection. In this later case sensitivity to orientation is greater, but this extra complexity has no bearing on the basic physical result; hence, we will assume isotropic detection of the fluorescence.

The mathematical expression for $n(t)$ is discussed by Aragon and Pecora. They find that the number of photons emitted per second by a fluorophore is given by

$$n(t) = \frac{q_f \epsilon(\lambda) I_0}{\tau_f} \int_{-\infty}^{t} (\hat{\mu}(t') \cdot \hat{p})^2 \, exp[-(\frac{t-t'}{\tau_f})] dt'. \quad (3-15)$$

Here q_f is the fluorescence quantum yield of the dye, $\epsilon(\lambda)$ is the extinction coefficient at wavelength λ, I_0 is the incident light intensity, and τ_f is the fluorophore lifetime. The quantity $\hat{\mu}(t) \cdot \hat{p}$ denotes the dot product of the transition dipole, $\hat{\mu}(t)$, and the constant polarization vector, $\hat{p}$. The physical content of equation 3-15 is easy to understand. At

time t the number of photons/sec emitted by a dye molecule is given by the integral over all earlier times t' of the probability of absorption of the polarized incident light, $(\hat{\mu}(t') \cdot \hat{p})^2 I_0 \epsilon(\lambda)$, multiplied by the probability that a photon absorbed at t' will be reemitted as fluorescence at time t, $\frac{1}{\tau_f} exp[-(\frac{t-t'}{\tau_f})]$. In the case of interest here the fluorescence emission is extremely rapid relative to the physical processes under study; hence, it is an excellent approximation to assume that the emission probability is given by its value in the limit that the fluorescent lifetime approaches zero. In this approximation we have

$$\lim_{\tau_f \to 0} \frac{1}{\tau_f} exp[-(\frac{t-t'}{\tau_f})] = \delta(t-t') \qquad (3-16)$$

and

$$C(\tau) = Ng^2 e^2 Q^2(\lambda) \epsilon^2(\lambda) q_f^2 I_0^2 [\langle (\hat{\mu}(0) \cdot \hat{p})^2 (\hat{\mu}(\tau) \cdot \hat{p})^2 \rangle - \langle (\hat{\mu}(0) \cdot \hat{p})^2 \rangle^2]. \qquad (3-17)$$

The correlation function must now be related to rotational diffusion. In chapter 4 one method of determining the dependence of C(τ) on the rotational diffusion coefficient is presented. For the moment we merely note that the angular correlation of rigid cylindrical molecules undergoing long-axis rotational diffusion will decay exponentially with time *i.e.*

$$C(\tau) \propto \frac{sin^4 \beta}{15} exp(-4\gamma(b\tau - 1 + exp(-b\tau)))$$

$$+ \frac{4 sin^2 \beta cos^2 \beta}{15} exp(-\gamma(b\tau - 1 + exp(-b\tau))) + \frac{4}{45}(\frac{3 cos^2 \beta}{2} - \frac{1}{2})^2. \qquad (3-18)$$

In the above equation γ is related to the moment of inertia of the DNA and the frictional drag on the polymer and β is the angle that the transition moment makes with respect to the long-axis of the helix. This formula is discussed in more detail in chapter 4.

Figure 5

Schematic representation of the different bleaching and excitation events involved in the parallel and perpendicular modes of an FPR experiment. In the parallel mode an intense 10 microsecond pulse of light ($\Longleftrightarrow$) creates a cylindrically symmetric pattern of bleached dye molecules about the y axis (we assume here that the system is static during the bleach). The shading of the 'darkness' profile indicates that fluorophores (absorption dipoles) that are parallel to the y axis at the time of the bleach are most likely to be destroyed. In the parallel mode the observation beam ($\longleftrightarrow$) preferentially excites dye molecules that are oriented along the direction of most intense bleaching. If post-bleach molecular rotation alone eliminates any anisotropy in the angular distribution of fluorophore the parallel mode FPR curve will exhibit a post-bleach recovery.

In the perpendicular experiment the 10 microsecond pulse is polarized about the x axis and therefore the bleach profile is also oriented about the x direction. The observation beam preferentially excites dye molecules whose absorption dipoles are parallel to the y axis. In the perpendicular mode the post-bleach signal decays if molecular rotation alone produces an isotropic distribution of dye. The rotational correlation times can be extracted either from the recovery of the parallel curve or the decay of the perpendicular curve.

Figure 5

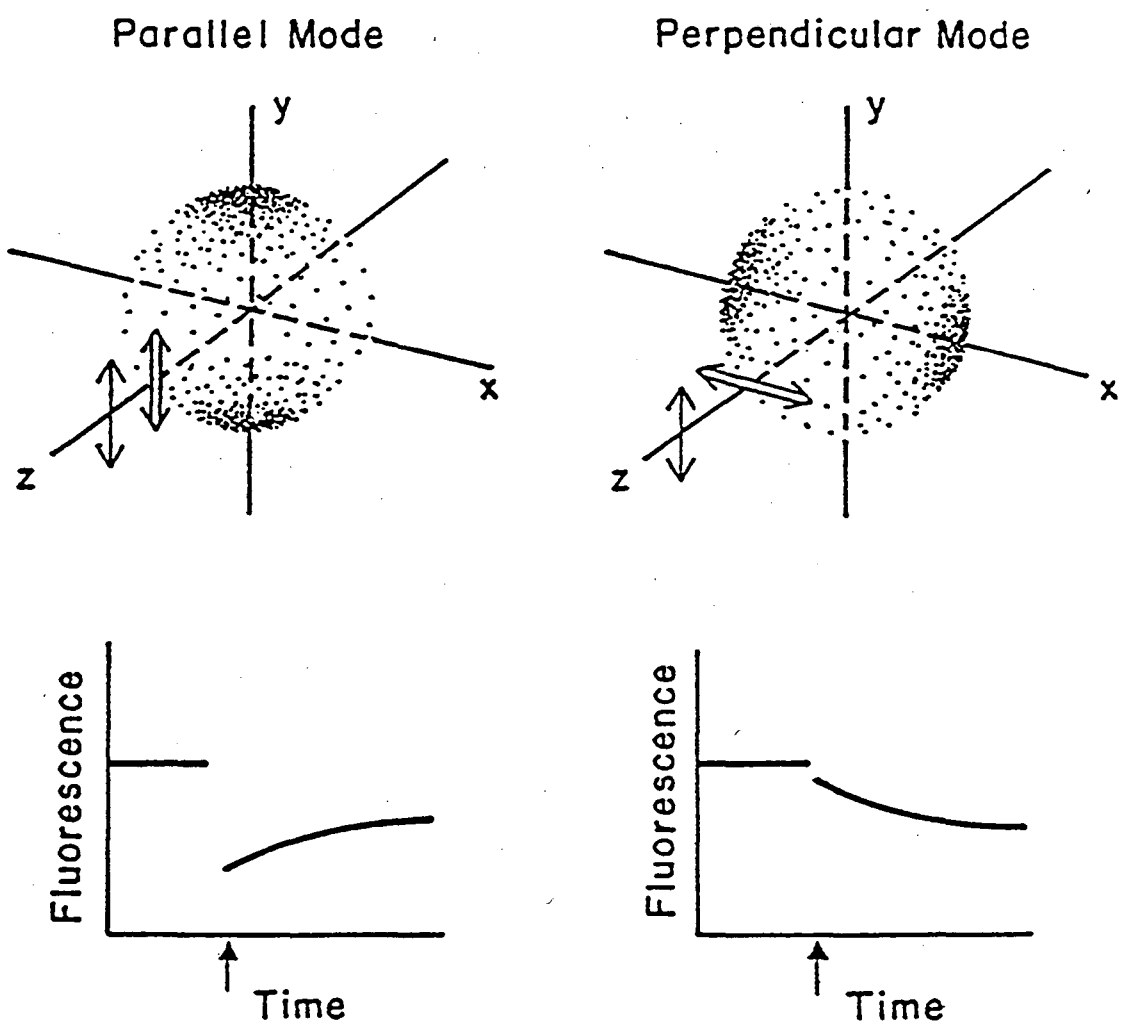
Parallel Mode
Perpendicular Mode
y
x
z
y
x
z
Fluorescence
Time
Fluorescence
Time

Figure 6

Mathematical basis for the wobble model of fast internal motion in a macromolecule. The absorption dipole is assumed to maintain an average angle θ_0 with respect to the direction of polarization of the bleach beam (taken here as the z axis for mathematical convenience). During the bleach period the absorption dipole uniformly explores a cone of half angle α centered about θ_0. Therefore, the probability of absorbing the z polarized light is not strictly proportional to $cos^2\,\theta$ but must be computed as the average of $cos^2\,\theta$ over the cone.

Figure 6

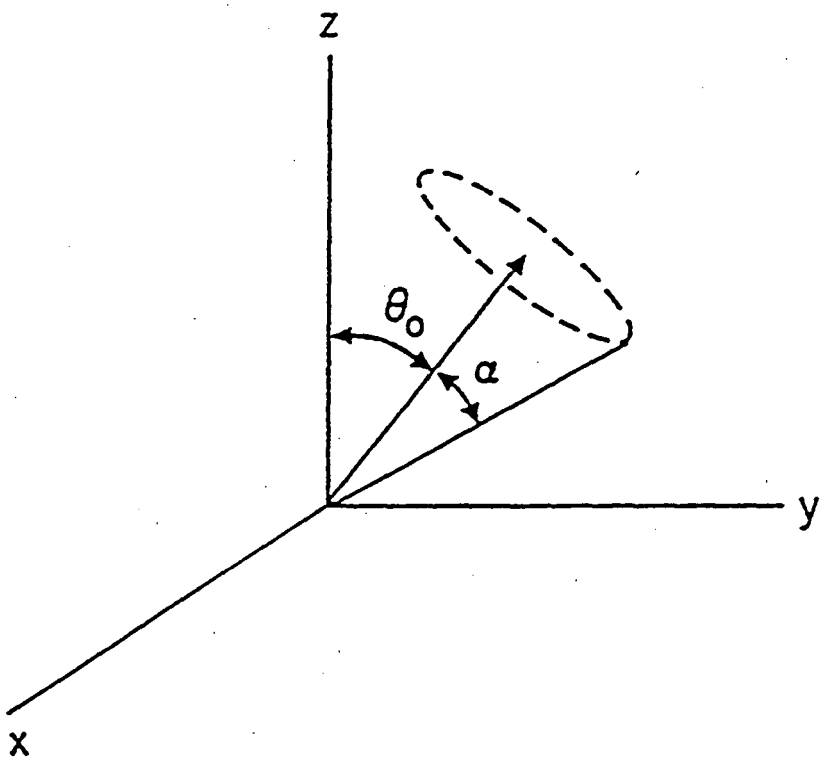

Figure 7

The origin of the translational FCS signal. The laser beam is assumed to define an open illuminated (circular) region. A certain number of molecules are in the beam; they are depicted as ovals. The surrounding area contains circular molecules that are not fluorescing. Diffusive forces will cause ovals to move out of the illuminated region and circles to move in. This motion leads to fluctuations in the number of molecules in the beam and corresponding temporal variation in the fluorescence emitted by the sample.

Figure 7

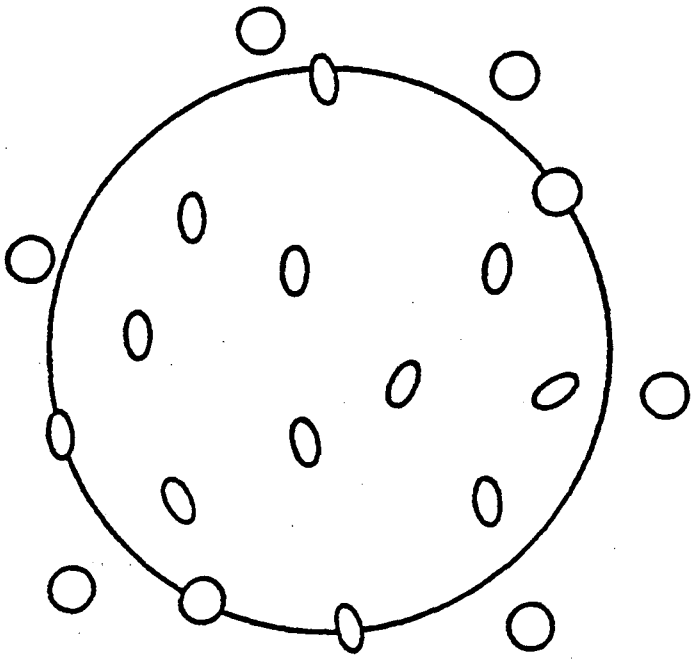

References for Chapter 3

1. C.R. Cantor and P.R. Schimmel (1980) *Biophysical Chemistry, Vol. II.* W.H. Freeman and Company, San Francisco, 455-463.

2. L.M. Smith, R.M. Weis and H.M. McConnell (1981) Measurement of rotational motion in membranes using fluorescence recovery after photobleaching. Biophys. J. **36**: 73.

3. M. Velez and D. Axelrod (1987) Polarized fluorescence photobleaching recovery for measuring fast rotational diffusion. Biophys. J. **51**: 240a.

4. W.A. Wegener and R. Rigler (1984) Separation of translational and rotational contributions in solution studies using fluorescence recovery after photobleaching. Biophys. J. **46**: 787.

5. R.E. Dale (1987) Depolarized fluorescence photobleaching recovery. Eur. Biophys. J. **14**: 179.

6. E.L. Elson and D. Magde (1974) Fluorescence correlation spectroscopy. 1. Conceptual basis and theory. Biopolymers **13**: 1.

7. S.R. Aragon and R. Pecora (1975) Fluorescence correlation spectroscopy and Brownian rotational diffusion. Biopolymers **14**: 119.

Chapter 4

Rotational Correlation in Biological Systems

The ubiquity of systems that display a coupling of random diffusion to driven rotation (see chapter 1) has inevitably led to an interest in spectroscopic probes for these motions. In order to elucidate the operative biological mechanisms it is desirable to distinguish those components of a complex reorientation that have their origin in random fluctuations from those that are in some sense biologically directed. Correlation measurements are ideally suited to the task of discriminating random macromolecular motions from repetitive reorientation. Here we have adopted a Langevin-Operator approach to address the analysis of rotational correlation in a biological system subject to purely diffusive and driven rotational motion. It is demonstrated that, despite the existence of competing modes of reorientation such as those arising from diffusion, correlation measurements should reveal the presence of driven motion. Specifically, the power spectrum of noise containing a repetitive rotational component should exhibit a resonance at characteristic 'forcing' frequencies. For the sake of concreteness a fluorescence correlation experiment is considered although the concept of modulation is more generally applicable.

4.1 Theory

In this work we have been motivated primarily by an interest in the motion of DNA in solution. Hence, our model system is a cylindrical DNA subject to an enzymatic torque and solvent induced Brownian rotation. The DNA is assumed to be labeled with one covalently bound intercalated fluorophore whose transition dipole makes a fixed angle β with respect to the long axis of the polymer; the orientation of the DNA is defined by its spherical polar coordinates θ_0 and ϕ_0 with respect to a set of lab fixed axes (see figure 8). It is reasonable to assume that a long macromolecule will have two equivalent diffusion constants that are much smaller than the long-axis rotational diffusion coefficient. Hence, for a system such as an actively transcribing RNA polymerase, rotational diffusion about two axes will be negligible, while there will be a coupling of the long-axis rotational diffusion of the enzyme-DNA complex and the driven motion.

In chapter 3 we discussed the relationship between angular variables and the fluorescence autocorrelation function. It is apparent from equation 3-17 that orientational information is contained in the autocorrelation function $\langle(\hat{\mu}(0)\cdot\hat{p})^2(\hat{\mu}(\tau)\cdot\hat{p})^2\rangle$. Hence, the basic mathematical problem is to follow the evolution of the quantity $\hat{\mu}(t)\cdot\hat{p}$ in time. The solution is most easily formulated in a coordinate system whose z axis is along the long axis of the macromolecule. Let $\theta(t)$ denote the angle of rotation of the absorption dipole projection about this z axis in time t (see figure 8); then the stochastic behavior of $\hat{\mu}(t)\cdot\hat{p}$ will be governed by the Langevin equation for $\theta(t)$. The Langevin equation will contain a term representing the Brownian random torque and a driving torque. The external torque is assumed to be constant; this is probably not an unreasonable model for

long-lived rotational phenomena such as flagellar motion or the transcription of DNA by a processive enzyme such as RNA polymerase. We have

$$I\frac{dw(t)}{dt} = -fw(t) + L(t) + L_{ext}. \qquad (4-1)$$

Here f is the frictional factor, I is the long axis moment of inertia of a DNA molecule, L(t) is the random torque, L_{ext} is the constant external torque and $w(t) = \frac{d\theta}{dt}$.

To compute expectation values from equation 4-1 we follow an operator technique for solving the Langevin equation.[1] The idea is to generate the time dependent orientation of the transition dipole with a rotation operator. Specifically, we write

$$\hat{\mu}(t) = R(t)\hat{\mu}(0). \qquad (4-2)$$

Here, the rotation operator R(t) is given by the standard matrix expression

$$R(t) = \begin{pmatrix} cos\,\theta(t) & -sin\,\theta(t) & 0 \\ sin\,\theta(t) & cos\,\theta(t) & 0 \\ 0 & 0 & 1 \end{pmatrix}. \qquad (4-3)$$

R(t) is stochastic because its matrix elements are random functions of the time. In fact, by expressing $\hat{\mu}(t)$ in terms of $\hat{\mu}(0)$ and the rotation operator, the stochasticity in the problem is entirely confined to R(t). Hence, if we wish to compute ensemble averages of functions of θ, the problem reduces to the determination of the ensemble average of R(t). We now proceed with the computation of $\langle R(t) \rangle$ for a fixed initial orientation of the transition moment. Of course the evaluation of the correlation function will require a second average over the initial distribution; this double average will be considered explicitly later.

We move from the Langevin equation of motion for the basic physical variable of interest, in this case the angle θ, to an associated equation for R(t). The equations

governing the temporal behavior of these two quantities are related because the matrix R(t) is explicitly defined in terms of θ. If R(t) is given by 4-3 then

$$\frac{dR(t)}{dt} = \begin{pmatrix} -\sin\theta(t) & -\cos\theta(t) & 0 \\ \cos\theta(t) & -\sin\theta(t) & 0 \\ 0 & 0 & 0 \end{pmatrix} \frac{d\theta(t)}{dt}. \qquad (4-4)$$

Setting

$$J = \begin{pmatrix} 0 & -i & 0 \\ i & 0 & 0 \\ 0 & 0 & 0 \end{pmatrix} \qquad (4-5)$$

we have the evolution equation

$$\frac{dR(t)}{dt} = -iJw(t)R(t). \qquad (4-6)$$

The equation 4-6 for R(t) may be related to the Brownian torque through the equation of motion, that is the Langevin equation, for $w(t)$. First note that equation 4-1 differs from the undriven Langevin equation by just the constant external torque. It is helpful therefore to reexpress $w(t)$ in terms of quantities characteristic of the simpler problem. If we take the undriven equation, in which L_{ext} is zero, to have a solution $w_0(t)$ then it can be easily verified by substitution into 4-1 that

$$w(t) = w_0(t) + \frac{L_{ext}}{Ib}. \qquad (4-7)$$

Here b=f/I.

Upon substituting expression 4-7 for $w(t)$ into equation 4-6 we have

$$\frac{dR(t)}{dt} = -iJ[w_0(t) + \frac{L_{ext}}{Ib}]R(t). \qquad (4-8)$$

It is advantageous to make the change of variable

$$R(t) = S(t)\,exp(-i\alpha Jt) \qquad (4-9)$$

where $\alpha = L_{ext}/Ib$. It is apparent that S(t) will satisfy the equation

$$\frac{dS(t)}{dt} = -iJw_0(t)S(t). \qquad (4-10)$$

Comparison of equation 4-10 with the original evolution equation 4-6 for R(t) shows that S(t) is nothing more than the rotation operator associated with the Langevin equation in the absence of any driving torque. The average of S(t) is known.[1] The general method used in obtaining the expectation value of S(t) centers around a power series expansion in some small parameter characteristic of the stochastic differential equation 4-10. This approach is outlined in appendix 2.

For the stochastic equation 4-10 the power series method of determining the expectation value of an operator yields an exact solution:

$$\langle S(t)\rangle = \begin{pmatrix} exp(-\gamma(bt-1+exp(-bt))) & 0 & 0 \\ 0 & exp(-\gamma(bt-1+exp(-bt))) & 0 \\ 0 & 0 & 1 \end{pmatrix}. \qquad (4-11)$$

Here $\gamma = k_BT/Ib^2$ where k_B is Boltzmann's constant. Since R(t) and S(t) differ only by the multiplicative factor

$$exp(-i\alpha Jt) = \begin{pmatrix} cos\,\alpha t & -sin\,\alpha t & 0 \\ sin\,\alpha t & cos\,\alpha t & 0 \\ 0 & 0 & 1 \end{pmatrix} \qquad (4-12)$$

we obtain the following expression for the expectation value of R(t):

$$\langle R(t)\rangle = exp(-\gamma(bt-1+exp(-bt))) \begin{pmatrix} cos\,\alpha t & -sin\,\alpha t & 0 \\ sin\,\alpha t & cos\,\alpha t & 0 \\ 0 & 0 & 0 \end{pmatrix} + \begin{pmatrix} 0 & 0 & 0 \\ 0 & 0 & 0 \\ 0 & 0 & 1 \end{pmatrix}. \qquad (4-13)$$

It is now possible to determine the temporal behavior of $\langle sin\,\theta(t)\rangle$ and $\langle cos\,\theta(t)\rangle$. From equation 4-3

$$\langle R(t)\rangle = \begin{pmatrix} \langle cos\,\theta(t)\rangle & -\langle sin\,\theta(t)\rangle & 0 \\ \langle sin\,\theta(t)\rangle & \langle cos\,\theta(t)\rangle & 0 \\ 0 & 0 & 1 \end{pmatrix}. \qquad (4-14)$$

Upon equating associated matrix elements in equations 4-13 and 4-14 we obtain

$$\langle cos\,\theta(t)\rangle = exp(-\gamma(bt - 1 + exp(-bt)))\,cos(\alpha t) \qquad (4-15a)$$

$$\langle sin\,\theta(t)\rangle = exp(-\gamma(bt - 1 + exp(-bt)))\,sin(\alpha t). \qquad (4-15b)$$

The quantity of real experimental interest is the autocorrelation function of the absorption probability. A determination of this average requires a knowledge of the expectation values of the second powers of cosine and sine of θ. This follows from the matrix expressions for $\hat{\mu}(t)$ and R(t). We have

$$\langle(\hat{\mu}(0)\cdot\hat{p})^2(\hat{\mu}(t)\cdot\hat{p})^2\rangle = \langle(\mu^+(0)H^+p)^2(\mu^+(0)R^+(t)H^+p)^2\rangle. \qquad (4-16)$$

In equation 4-16 $\mu^+(0)$ and $R^+(t)$ denote the transpose of the matrices (written in the molecular frame) representing $\hat{\mu}(0)$ and R(t) respectively, p is a laboratory referenced column matrix and H^+ is the transpose of the matrix that converts the coordinates of a vector in the molecule fixed axes into the corresponding components in the laboratory frame. We take $\hat{p}$ parallel to the laboratory z axis. An explicit expression for H is

$$H = \begin{pmatrix} sin\,\phi_0 & cos\,\phi_0\,cos\,\theta_0 & cos\,\phi_0\,sin\,\theta_0 \\ -cos\,\phi_0 & sin\,\phi_0\,cos\,\theta_0 & sin\,\phi_0\,sin\,\theta_0 \\ 0 & -sin\,\theta_0 & cos\,\theta_0 \end{pmatrix}. \qquad (4-17)$$

Once again note that the brackets in equation 4-16 really denote a two time average.

Upon performing the indicated matrix manipulations the desired autocorrelation function may be expressed as:

$$\langle(\hat{\mu}(0)\cdot\hat{p})^2(\hat{\mu}(\tau)\cdot\hat{p})^2\rangle =$$

$$\langle(-\mu_2(0)\,sin\,\theta_0 + \mu_3(0)\,cos\,\theta_0)^2[-sin\,\theta_0(sin\,\theta\mu_1(0) + cos\,\theta\mu_2(0)) + cos\,\theta_0\mu_3(0)]^2\rangle. \qquad (4-18)$$

The subscripts 1, 2 and 3 in equation 4-18 denote the 1, 2 and 3 components of the vectors relative to the molecular axes. The initial distribution of the projection of $\hat{\mu}$ onto the plane perpendicular to the long axis of the DNA is assumed to be uniform. Therefore, when expression 4-18 is expanded all terms that involve odd powers of the components of the transition moment average to zero and the correlation function becomes

$$\langle(\hat{\mu}(0)\cdot\hat{p})^2(\hat{\mu}(\tau)\cdot\hat{p})^2\rangle = \langle sin^2\,\theta\rangle\langle\mu_1(0)^2\mu_2(0)^2\,sin^4\,\theta_0+\mu_1(0)^2\mu_3(0)^2\,sin^2\,\theta_0\,cos^2\,\theta_0\rangle_0$$

$$+\langle cos^2\,\theta\rangle\langle\mu_2(0)^2\mu_3(0)^2\,cos^2\,\theta_0\,sin^2\,\theta_0+\mu_2(0)^4\,sin^4\,\theta_0\rangle_0$$

$$+\langle cos\,\theta\rangle\langle 4\mu_3(0)^2\mu_2(0)^2\,sin^2\,\theta_0\,cos^2\,\theta_0\rangle_0$$

$$+\langle\mu_3(0)^2\mu_2(0)^2\,sin^2\,\theta_0\,cos^2\,\theta_0+\mu_3(0)^4\,cos^4\,\theta_0\rangle_0. \qquad (4-19)$$

In equation 4-19 the notation $\langle\rangle_0$ explicitly indicates an average over the initial distribution.

It is clear from equation 4-19 that we need to know the expectation values of $cos^2\,\theta$ and $sin^2\,\theta$. The higher powers of the trigonometric functions may be reexpressed as

$$cos^2\,\theta = \frac{1}{2}(1+cos\,2\theta) \qquad (4-20a)$$

$$sin^2\,\theta = \frac{1}{2}(1-cos\,2\theta). \qquad (4-20b)$$

It is now a relatively simple extension of the previous derivation of the averages of $cos\,\theta$ and $sin\,\theta$ to show that for any k

$$\langle cos\,k\theta\rangle = exp(-k^2\gamma(bt-1+exp(-bt)))\,cos(k\alpha t) \qquad (4-21a)$$

$$\langle sin\,k\theta\rangle = exp(-k^2\gamma(bt-1+exp(-bt)))\,sin(k\alpha t). \qquad (4-21b)$$

These results can be verified simply by repeating the mathematical steps outlined for the case k=1; in this more general situation the relevant matrix generates a rotation by an angle $k\theta$.

To determine the averages indicated in equation 4-19, we require the case k=2:

$$\langle cos\, 2\theta \rangle = exp(-4\gamma(bt - 1 + exp(-bt)))\, cos(2\alpha t) \qquad (4-22a)$$

$$\langle sin\, 2\theta \rangle = exp(-4\gamma(bt - 1 + exp(-bt)))\, sin(2\alpha t). \qquad (4-22b)$$

Inserting 4-22a into equation 4-19 and explicitly computing the initial averages the correlation function 4-18 is found to have the form

$$\langle(\hat{\mu}(0)\cdot\hat{p})^2(\hat{\mu}(\tau)\cdot\hat{p})^2\rangle \propto \frac{sin^4\beta}{15} exp(-4\gamma(b\tau - 1 + exp(-b\tau)))\, cos(2\alpha\tau)$$

$$+\frac{4\, sin^2\beta\, cos^2\beta}{15} exp(-\gamma(b\tau - 1 + exp(-b\tau)))\, cos(\alpha\tau) + \frac{4}{45}(\frac{3\, cos^2\beta}{2} - \frac{1}{2})^2 + \frac{1}{9}. \qquad (4-23a)$$

It can be shown that $\langle(\hat{\mu}(0)\cdot\hat{p})^2\rangle^2 = \frac{1}{9}$, therefore

$$C(\tau) \propto \frac{sin^4\beta}{15} exp(-4\gamma(b\tau - 1 + exp(-b\tau)))\, cos(2\alpha\tau)$$

$$+\frac{4\, sin^2\beta\, cos^2\beta}{15} exp(-\gamma(b\tau - 1 + exp(-b\tau)))\, cos(\alpha\tau) + \frac{4}{45}(\frac{3\, cos^2\beta}{2} - \frac{1}{2})^2. \qquad (4-23b)$$

Finally, it is illustrative to examine the Fourier transform of the autocorrelation function 4-23b. We focus attention on the time dependent term and compute the power spectrum J(ω) as

$$J(\omega) = \int_0^\infty cos(\omega t)[\frac{sin^4\beta}{15} exp(-4\gamma(bt - 1 + exp(-bt)))\, cos(2\alpha t)$$

$$+\frac{4\, sin^2\beta\, cos^2\beta}{15} exp(-\gamma(bt - 1 + exp(-bt)))\, cos(\alpha t)]dt. \qquad (4-24)$$

If the exponential in equation 4-24 is expanded in powers of $exp(-bt)$ and then the integration is performed term by term it can be demonstrated that

$$J(\omega) \propto \frac{sin^4\beta\tau_D}{30[1+\tau_D^2(\omega+2\alpha)^2]} + \frac{2\,sin^4\beta\tau_D\gamma[1+4\gamma-\tau_D\tau_F(\omega+2\alpha)^2]}{15[1+\tau_D^2(\omega+2\alpha)^2][(1+4\gamma)^2+\tau_F^2(\omega+2\alpha)^2]} + ...$$

$$+\frac{2\,sin^2\beta\,cos^2\beta\tau_D}{15[1+\tau_D^2(\omega+\alpha)^2]} + \frac{2\,sin^2\beta\,cos^2\beta\tau_D\gamma[1+\gamma-\tau_D\tau_F(\omega+\alpha)^2]}{15[1+\tau_D^2(\omega+\alpha)^2][(1+\gamma)^2+\tau_F^2(\omega+\alpha)^2]} + ... \quad (4-25)$$

In equation 4-25 $\tau_D = \frac{f}{k_BT}$ and $\tau_F = \frac{I}{f}$. J(ω) also contains four other terms that can be obtained by replacing the quantity α by $-\alpha$ in expression 4-25.

4.2 Interpretation

The fluorescence photocurrent autocorrelation function arising from a dilute sample of cylindrical molecules subject to random Brownian and constant external torques is given by equation 4-23b. This correlation function exhibits an exponential decay that is modulated by a cosine term. The modulation frequency is $\alpha = L_{ext}/Ib$. The exponential contribution arises from the random Brownian torque; in fact by setting L_{ext}=0 we obtain the purely exponential decay corresponding to the undriven case

$$C(\tau) \propto \frac{sin^4\beta}{15}\,exp(-4\gamma(b\tau-1+exp(-b\tau)))$$

$$+\frac{4\,sin^2\beta\,cos^2\beta}{15}\,exp(-\gamma(b\tau-1+exp(-b\tau))) + \frac{4}{45}(\frac{3\,cos^2\beta}{2}-\frac{1}{2})^2. \quad (4-26)$$

The oscillatory terms, on the other hand, are manifestations of the correlation that would be observed from molecules moving under the influence of constant and frictional torques. Consider the equation of motion of a cylinder in the absence of random torques

$$I\frac{dw}{dt} = -fw(t) + L_{ext}. \quad (4-27)$$

Under steady state conditions the angular acceleration is equal to zero, and the steady state angular velocity has the form

$$f w_{ss} = L_{ext} \qquad (4-28a)$$

$$w_{ss} = \frac{L_{ext}}{f}. \qquad (4-28b)$$

The modulation frequency appearing in equation 4-23b, $\alpha = L_{ext}/Ib = L_{ext}/f$, is the steady state angular velocity. Hence, the sinusoidal term in equation 4-23b gives the correlation that would be observed from a molecule subject to frictional and constant torques, under steady state conditions. The second harmonic arises because the expression for the probability of absorbing polarized light depends on the quantity $(\hat{\mu}(\tau) \cdot \hat{p})^2$; there is, therefore, a $2w_{ss}$ periodicity associated with antiparallel orientations of the transition dipole.

If the Fourier transform of the correlation function, the power spectrum 4-25 is examined, it is apparent that there are peaks or resonances in the spectrum at $\pm w_{ss}$ and $\pm 2w_{ss}$. Thus, characteristic driving frequencies are also manifest in the power spectrum of the signal.

Finally we note that long cylindrical molecules such as DNA exhibit internal bending and torsional motions that will affect the fluorescence photocurrent autocorrelation function. As long as these motions are of restricted amplitude they should not destroy the long time reorientational correlations discussed here.

Figure 8

Coordinate system used to describe the orientation of a rotating cylindrical particle. The absorption dipole $\hat{\mu}(t)$ makes an angle β with respect to the long axis of the polymer. A given DNA molecule has an angular orientation specified by its spherical polar coordinates θ_0 and ϕ_0 with respect to the laboratory axes. The polarization of the light, defined by $\hat{p}$, is along the z axis of the laboratory frame. The DNA can undergo coupled rotational diffusion and driven reorientation about its long axis.

Figure 8

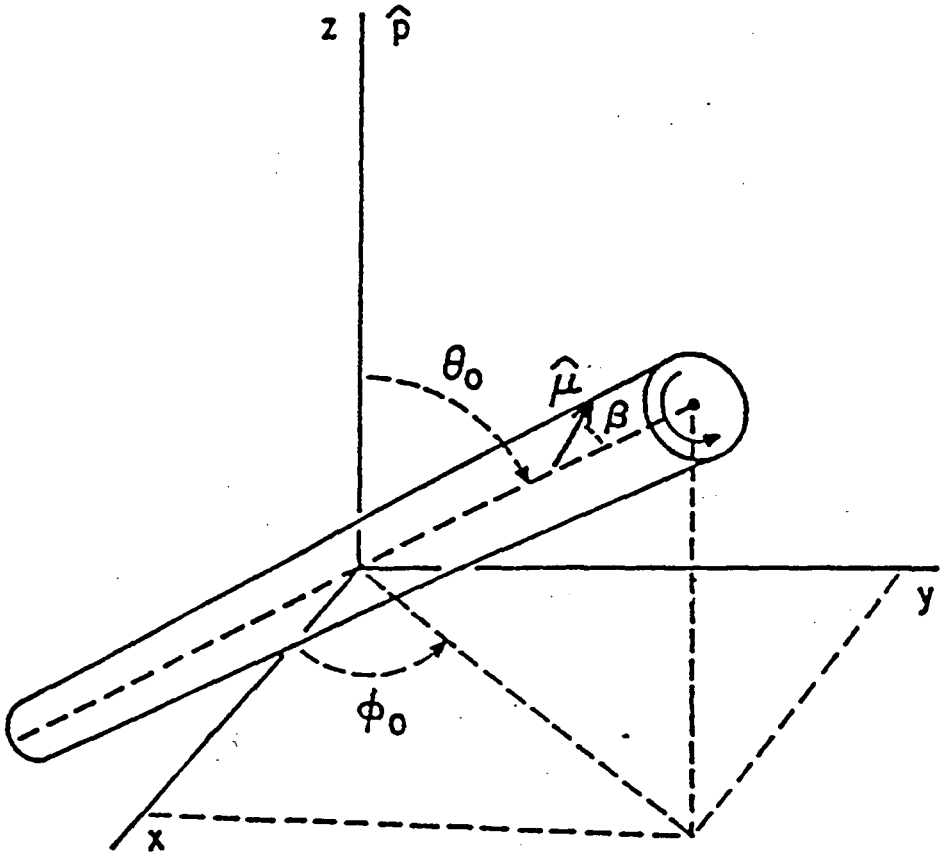

References for Chapter 4

1. J. McConnell (1980) *Rotational Brownian Motion and Dielectric Theory.* Academic Press, New York, 136.

Chapter 5

Synthesis and Characterization of Fluorophore

The nucleic acid fluorophore used in the FCS and FPR experiments was an analog of ethidium bromide called ethidium monoazide. The structures of ethidium and two of its azide derivatives are shown in figure 9. It is apparent that ethidium bromide and ethidium monoazide differ only in having, respectively, an amino, NH_2, or an azide, N_3, group at the 8 position of the molecule. Ethidium monoazide was the chosen dye because it is quite a good fluorophore and its covalent interaction with nucleic acids has been shown to mimic intercalated ethidium bromide-DNA complexes.[1-4] The work that has been done to characterize the nature of the azide-DNA interaction will be reviewed in section 5.2 in conjunction with the relevant information obtained from our fluorescence experiments.

5.1 Synthesis of Ethidium Monoazide

Graves *et al.* have published a protocol for synthesizing the azide that produces the desired product in high yield.[1] The procedure is straightforward, with the caveat that both the synthesis and isolation must be done in a darkroom under red safety light. We present our adaptation of the protocol, noting problems we encountered and their solutions.

The following materials were required: 0.5 grams of ethidium bromide dissolved in

40 milliliters of double distilled water (pH 1.6), sodium azide in water ($\frac{30mg}{4ml}, pH = 3$), $NaNO_2$ in water ($\frac{30mg}{4ml}, pH \approx 3$) and a stock of 10 normal NaOH. A pH meter and a vacuum filter were placed in the dark room before the synthesis was started. The filtration set-up utilized a large Buchner funnel and Whatman 50 grade, 7 centimeter diameter filter paper.

The reaction was conducted as follows. The $NaNO_2$ was added dropwise from a 10 ml glass pipet to a stirred, iced ethidium solution. Stirring was continued for approximately 5 minutes after addition of all of the $NaNO_2$. The pH of the ethidium/$NaNO_2$ mixture was checked and adjusted to about 2.5 if necessary. The NaN_3 was then added dropwise to the stirred ethidium/$NaNO_2$ solution, and stirring was again continued for several minutes after the addition was completed. The pH of the final solution was then raised to 11.5 with a few drops of sodium hydroxide; the high pH served to precipitate the product. The precipitated solution was then poured onto a pre-wetted filter and the liquid removed under vacuum. The solid product was scraped from the dry paper and stored, covered, in the refrigerator to await separation.

The azide was separated from diazide product and unreacted ethidium bromide on a carboxymethyl cellulose (CMC or Cellex) cation exchange column. We discuss our column preparation protocol in detail, particularly with regard to the elimination of small particles that can cause clogging.

Approximately 100 grams of the original dry CMC stock were used to yield the required quantity of appropriately sized Cellex particles. The resin was first hydrated by placing 10 gram aliquots of CMC in 500 mls of 0.25 normal HCl and allowing the Cellex

to swell for 30 minutes. The resin was not stirred during the hydration procedure to avoid particle breakage. The resin was then filtered and rinsed and the CMC suspended in 0.25 molar NaOH for 10 minutes. The Cellex was then filtered and rinsed, and the initial HCl hydration and rinse were repeated.

The column was run with a standard phosphate buffer prepared at pH=7. (If the pH of the buffer is greater than 4, the resin will be in the anionic form and can, therefore, bind the positively charged ethidium molecules). Cellex was equilibrated with the buffer and all the fine particles subsequently removed. The elimination of small resin material was accomplished by very gently stirring the buffer-resin mixture and then allowing the solution to settle a few minutes. The fine material did not have time to sediment to the bottom of the beaker and could therefore be decanted off the top. This procedure was repeated many times until all the residual resin sedimented within a few minutes of the end of stirring.

Even when the fine particles were meticulously removed, clogging was still a problem. An adequate solution was to remove the fret from the column and replace it with a little piece of lightly packed glass wool. With this done, a dilute solution of buffer and resin was poured into a funnel at the top of the column and the first 2-3 centimeters of Cellex were allowed to settle under gravity. The rest of the packing was done under flow.

After the column was rinsed with buffer, the sample was loaded and fractions were collected. The diazide was the first compound to come off the column and was identified by its yellow color. The monoazide eluted next and was red-orange. There was very

little diazide product. The success of the monoazide synthesis was verified by mass-spectrometry and visible absorption.

The yield of monoazide was sufficient for all the work discussed in this thesis. Product was stored in the dark and under refrigeration. Periodic checks assured the integrity of the monoazide.

5.2 Characterization of Covalent Ethidium-DNA Complex

The azide reacts covalently with DNA upon exposure to light. During the course of these studies a synthetic 18mer, calf thymus DNA, PBR 322 and phage Lambda were labeled. To attain a desired dye-DNA ratio, a solution of nucleic acid (several hundred $\frac{\mu g}{ml}$ in Tris-EDTA buffer pH=7.5) was typically combined with a 2 to 3 fold molar excess of azide. Intercalated complexes were formed in the dark and then covalent addition was achieved upon exposure of the dye-DNA solution to room light for about 10 minutes. The unreacted azide is effectively removed by ethanol precipitation of the DNA.

At an early stage in this work we were concerned that the dye might be nicking the nucleic acid. Therefore a sample of PBR 322 (primarily in the closed circular form) was labeled with fairly large amounts of the dye and a gel of the unmodified and labeled DNA was examined. There was no detectable change in the banding pattern after photolabeling; we conclude therefore that, under our conditions, DNA nicking is probably not a common occurrence.

The nature of the covalent interaction can be elucidated by monitoring the fluorescence properties of the photolysed dye-DNA complex. Garland *et al.* have monitored the steady state and time resolved fluorescence spectra of the azide and a

variety of dye-DNA complexes.[4] (See also reference 5 for updated measurements). In the presence of DNA the fluorescence excitation maximum of the unphotolysed dye exhibits a marked red shift and the relative fluorescence yield of the dye increases by a factor of 20. Garland *et al.* have also shown that the fluorescence lifetime of the covalent adduct is 10 times longer than that of unbound dye. All of these changes are analogous to spectral shifts that are observed when ethidium bromide intercalates into DNA.[2–4] Therefore, it is highly likely that the azide is intercalated into the nucleic acid.

In figure 10 below are shown the fluorescence excitation spectra we obtained for solutions of the azide alone and photolysed oligomer samples. For the azide alone the peak is at 462 nanometers (as reported in reference 5). The maximum shifts to about 510 nm if the dye is photolysed in the presence of DNA. The fluorescence emission spectrum of the covalent adduct was also monitored for a number of different excitation wavelengths. The emission maximum of the dye was found to be 610 nm independent of the wavelength of the exciting light. Therefore, it is likely that just one major fluorescent moiety is formed upon photoreaction with DNA.

An accurate interpretation of the photobleaching data required a precise knowledge of the angle between the absorption and emission dipoles of the the covalent adduct. It is generally believed that these moments are parallel for intercalated ethidium bromide molecules; nevertheless the steady state polarization of the covalent adduct was monitored to see if the dipoles are also parallel for the analog. The steady state polarization, P, of a sample that is rotationally immobile on the time scale of the fluorescent lifetime of the dye is related to the angle between the absorption and emission moments, ξ, according

to the relationship[6]

$$P = \frac{3\cos^2\xi - 1}{\cos^2\xi + 3}. \qquad (5-1)$$

If the sample is not rotationally static the polarization will be influenced both by the angle ξ and the motion of the fluorophore (see section 8.1). If the system is immobile and ξ=0, P will attain the theoretical fluorescence maximum of 0.50.[6]

The steady state polarization of solutions of sonicated calf thymus DNA ($\approx 500\frac{\mu g}{ml}$) was monitored in a Spex Industries Fluorolog 212T. The polarization over a wide range of wavelengths was determined by exciting the sample with vertically polarized light and simultaneously collecting the vertically (VV) and horizontally (VH) polarized component of the emission. The sample is then excited with horizontally polarized light and the emission is again monitored in the vertical (HV) and horizontal (HH) directions. This rather extensive amount of data is required to correct for differences in the degree to which diffraction gratings pass light of differing polarization.[7] Specifically, it can be shown that the intrinsic polarization of a molecule is correctly determined by the expression[7]

$$P = \frac{\frac{VV}{VH}\frac{HH}{HV} - 1}{\frac{VV}{VH}\frac{HH}{HV} + 1}. \qquad (5-2)$$

P is typically monitored for a range of wavelengths spanning the transition of interest; a polarization spectrum will establish a more accurate value for P and can also provide evidence for energy transfer.

The experimental results for calf thymus in Tris-EDTA buffer and in saturated sucrose solutions are shown in figure 11. For the DNA in buffer the polarization was found to be about 0.32. This experimental result indicates either that there is some motion in the DNA buffer system on the time-scale of 100 nanoseconds or that the absorption and

emission moments are not parallel. However, the data from the DNA/sucrose solution demonstrates that it is possible to attain a polarization that is very nearly the limiting value of 0.5. Therefore the absorption and emission moments of the photoreacted dye are in fact parallel and the reduced value of P in the buffer system is probably indicative of some sort of nanosecond torsional motion or dye wobble in the nonviscous solution.

Figure 9

The structures of ethidium bromide, and its monoazide and diazide analogs. The synthesis of the monoazide and diazide proceeds, respectively, through diazonium and bis-diazonium salt intermediates. Nucleophilic substitution then yields the azide product. Adapted from Reference 1.

Figure 9

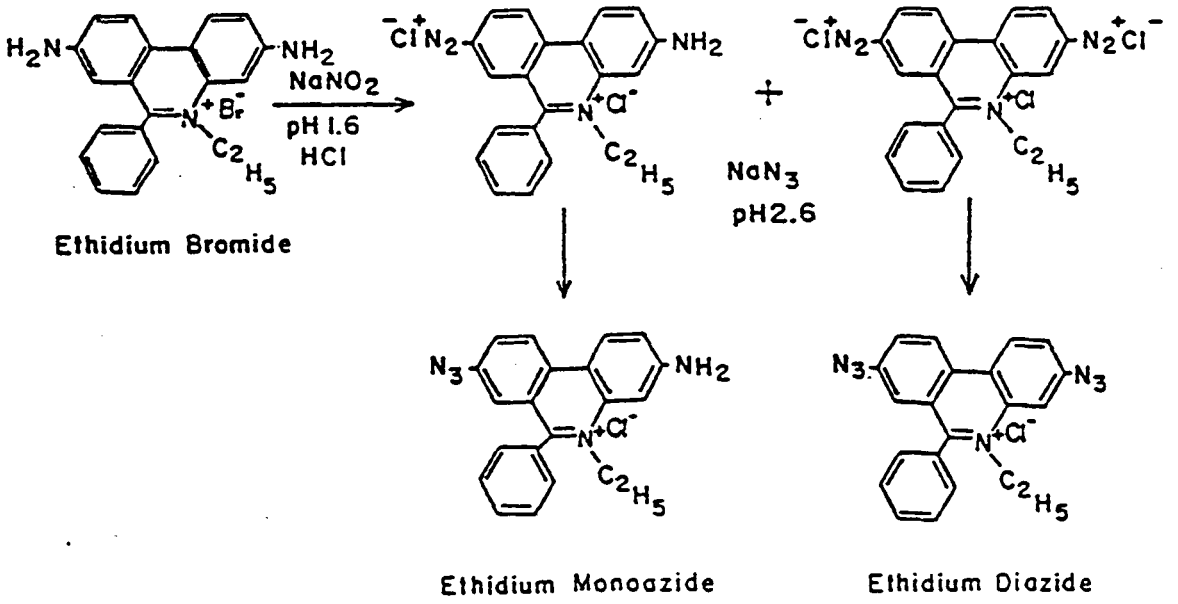
NaNO2
pH 1.6
HCl
NaN3
pH2.6
Ethidium Bromide
Ethidium Monoazide
Ethidium Diazide

Figure 10

Fluorescence excitation spectra of a solution of azide alone and an 18 base pair oligomer that has been photoreacted with the dye. Emission was monitored at 610 nanometers. The raw data have been smoothed. Note that the azide spectrum has the characteristic peak at 462 nanometers and that the maximum for the covalent dye/DNA solution is at about 510 nanometers. The relative height of the peaks in this figure means nothing.

Figure 10

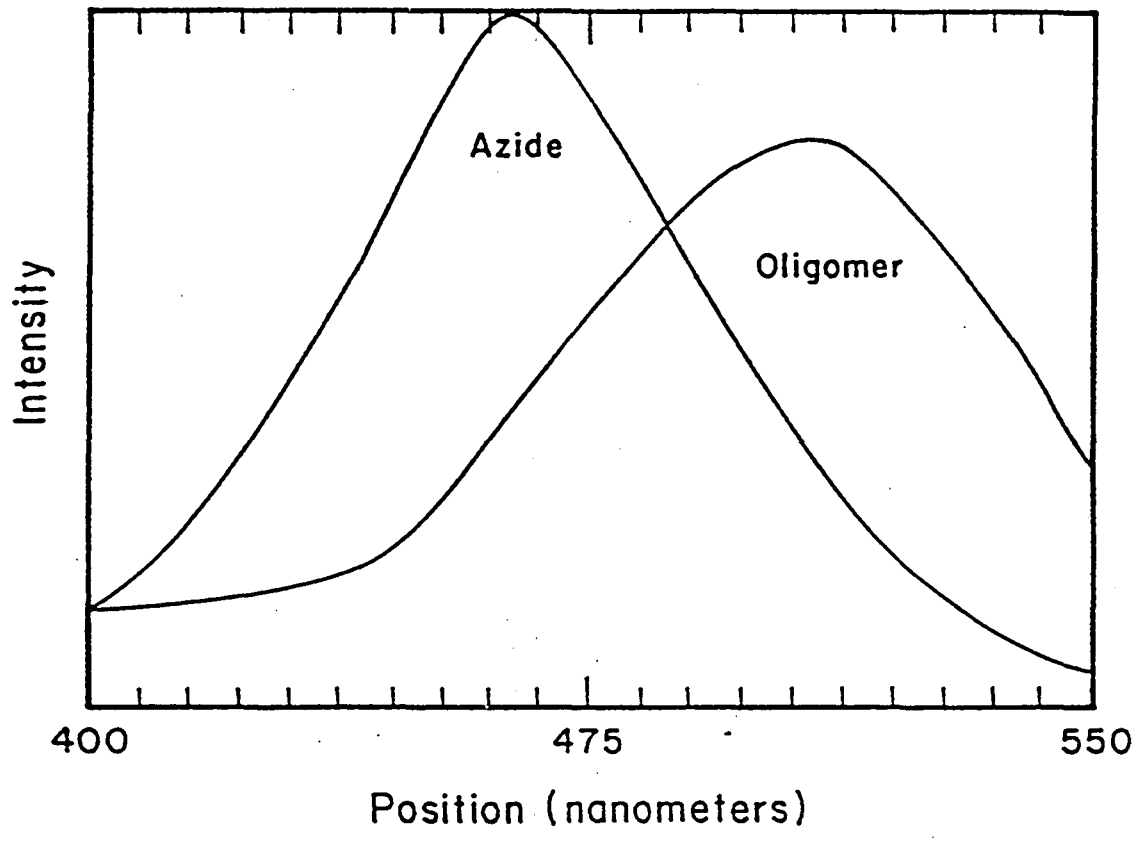

Figure 11

Polarization spectra for a solution of labeled calf-thymus DNA in TE buffer (11a) and in a saturated sucrose solution (11b). Emission was monitored at 610 nanometers. Corrected/baseline subtracted horizontal and vertical data sets were used in the calculation of the polarization. However, the effect of sample scatter on the measured value of P was not considered. Both sets of data were obtained at room temperature. Note that the polarization near the maximum in the excitation spectrum of figure 10 (510 nanometers) is 0.32 for the buffer solution and increases to 0.44 in sucrose. This latter value of P is close to the theoretical maximum attained by a rotationally immobile fluorophore that possesses parallel absorption and emission moments. The increase in noise at each end of the two polarization spectra reflects a decrease in signal as one moves away from the absorption peak at 510 nanometers.

Figure 11a

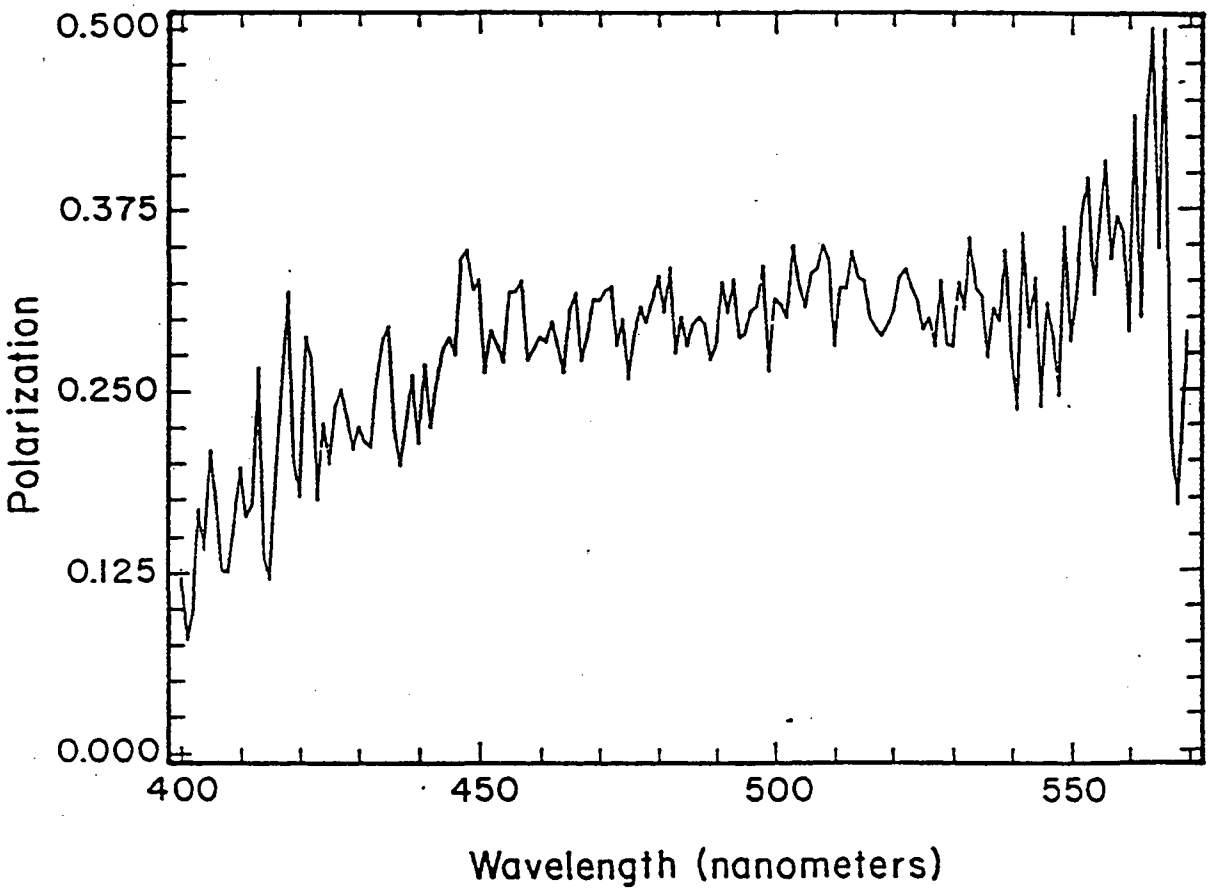
0.500
0.375
0.250
0.125
0.000
Polarization
400
450
500
550
Wavelength (nanometers)

Figure 11b

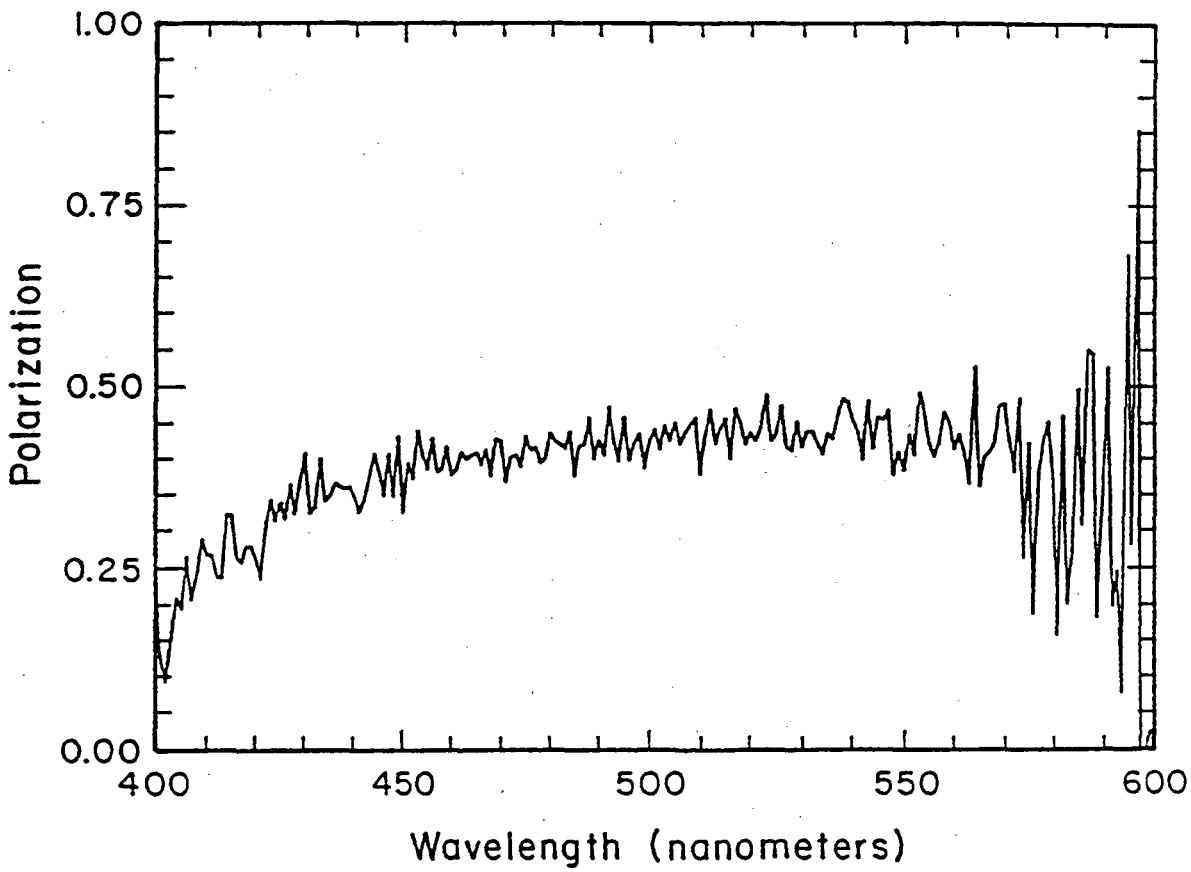
1.00
0.75
0.50
0.25
0.00
Polarization
400
450
500
550
600
Wavelength (nanometers)

References for Chapter 5

1. D.E. Graves, L.W. Yielding, C.L. Watkins and K.L Yielding (1977) Synthesis, separation and characterization of the monoazide and diazide analogs of ethidium bromide. Biochim. Biophys. Acta **479**: 98.

2. J.-B. LePecq and C. Paoletti (1967) A fluorescent complex between ethidium bromide and nucleic acids. Physical-chemical characterization. J. Mol. Biol. **27**: 87.

3. J. Olmsted and D.R. Kearns (1977) Mechanism of the ethidium bromide fluorescent enhancement on binding to nucleic acids. Biochem. **16**: 3647.

4. F. Garland, D.E. Graves, L.W. Yielding and H.C. Cheung (1980) Comparative studies of the binding of ethidium bromide and its photoreactive analogues to nucleic acids by fluorescence and rapid kinetics. Biochem. **19**: 3221.

5. W.J. Firth, III., C.L. Watkins, D.E. Graves and L.W. Yielding (1983) Synthesis and characterization of ethidium analogs: Emphasis on amino and azido substituents. J. Heterocyclic Chem. **20**: 759.

6. C.R. Cantor and P.R. Schimmel (1980) *Biophysical Chemistry, Vol. II.* W.H. Freeman and Company, San Francisco, 461.

7. J.R. Lackowicz (1983) *Principles of Fluorescence Spectroscopy.* Plenum Press, New York, 128-130.

Chapter 6

Photobleaching Experiments on Phage Lambda DNA

6.1 Experimental Apparatus

Fast polarized FPR studies were conducted in the laboratory of Prof. Daniel Axelrod at the University of Michigan because the experiments require a powerful laser and specialized optical equipment that were not a part of the fluorescence set-up at Berkeley. A brief discussion of the essential features of the photobleaching apparatus follows (see figure 12). The excitation beam is the 514.5 nanometer line of a 15 watt Coherent argon-ion laser. The light that emerges from the laser is deflected into a set of diffraction spots by an acousto-optic modulator. Only the first order spot is directed through an aperture; therefore, the intensity of the laser light incident on the sample is controlled by varying the amount of light sent into the first order deflection. During the bleach phase of an experiment the modulator directs approximately 50 percent of the 514.5 nanometer light (2 watts) into the first order; the probe beam is about 10,000 times less intense than the bleach.

The photobleaching experiments were run in two alternate modes that differ in bleach beam polarization (see the discussion in chapter 3 for motivation). The direction of light polarization is controlled by a Pockels Cell. The light that is sent into the Pockels cell has been circularly polarized by a quarter wave plate. The beam emerges plane polarized

in one of two orthogonal directions. The probe beam always has the same polarization; the bleach is parallel to the observation (probe) beam in one mode and perpendicular to it in the alternate mode.

A series of secondary apertures are placed along the optical path. These extra diaphragms serve to block any residual zeroth order light that has passed through the first aperture. If zeroth order light is allowed to illuminate the sample the contrast (the ratio of the intensities of the bleach and probe beams) is reduced. The contrast as well as the ratio of bleach intensity for the two possible bleach polarizations can be measured with an analyzing photodiode and polarizer.

The exciting laser light is directed onto the sample through an inverted epi-illumination microscope. The objective employed in these experiments had a 10x magnification and a numerical aperture of 0.25. Typically the illuminated region was 3 microns in radius. The sample was mounted on fused silica to avoid background luminescence from glass which will persist for about 100 microseconds after bleaching.

In all the experiments described here the sample was subjected to a 10 microsecond bleach pulse. The fluorescence intensity emitted by the sample under weak illumination was photon counted in intervals of 10 microsecond duration. The total experimental time following the bleach pulse was 1500-1700 microseconds (150-170 points at 10 μsec/point); the pre-bleach fluorescence level was monitored for 200 microseconds (20 points at 10 μsec/point). Only one polarization component of the fluorescence is passed to the photomultiplier tube. There is a 10 microsecond delay between the end of the bleach and the onset of photon counting during the probe phase of the experiment. The

bleach-probe cycle was repeated a minimum of 3000 times on the same sample to assure the statistical significance of the curves; signal to noise was also improved with a 5 point cubic smooth of the data. As mentioned in chapter 3, the difference between the pre and post-bleach fluorescence (normalized by the pre-bleach fluorescence) immediately after the 10 microsecond pulse is referred to as the 'depth of bleach.' In these experiments the depth of bleach was typically between 0.35 and 0.60. The number of photon counts per second was about 150,000. The stage was minutely translated between each round of pulse-probe to avoid cumulative bleaching problems.

Curve fits were performed by IMSL routine ZXSSQ. Data were fit to a single exponential of the form $A - Bexp(-t/\tau)$.

6.2 Experimental Results

To test for the presence of nonrotational recovery processes (see section 3.2.2) in the DNA samples all FPR experiments were run, under identical conditions, in both the parallel and perpendicular modes. It was found that the perpendicular curves did not exhibit a post-bleach decay (see figure 13). Therefore, the FPR data must be monitoring more than pure molecular reorientation and we focus attention on R(t) to see what information about DNA rotation can be extracted from the temporal dependence of the ratio.

Two classes of experiments were conducted in this study. First, we explored the polarized FPR data obtained from an immobilized DNA system. This simple experiment provides a test of the ability of the ratio method to monitor the bleach-induced anisotropy in the angular distribution of fluorophore. A value of R(t) that is less than unity

implies that the region of the sample under observation possesses (after the bleach) a nonuniform angular concentration of dye. Therefore, if at time t the ratio is less than unity, we conclude that the DNA molecule has not yet undergone complete post-bleach reorientation.

6.2.1 Immobilized DNA Results

Lambda DNA was dried onto fused silica coverslips and then subjected to a 10 microsecond bleach followed by a probe of 1500 microsecond duration (150 points at 10 μsec/point). An example of the individual parallel and perpendicular mode photobleaching curves obtained from such a sample is displayed in figure 13. It will be noticed that both the parallel and perpendicular curves exhibit a partial post-bleach recovery. The bleach is, however, twice as deep in the parallel mode. The ratio determined from such an experiment is shown in figure 14. Note that R(0) is about 0.5 and that the 'temporal evolution' of the ratio for the dry DNA sample is indicative of a highly immobilized system. The ratio is effectively constant over the entire 1.5 millisecond time interval under examination, hence we conclude that, in this sample, there are no large amplitude molecular reorientations that would allow the ratio to rise back up to unity.

6.2.2 FPR on DNA Solutions

We have also conducted a set of microsecond FPR experiments on DNA solutions. An example of the data obtained when phage Lambda (2 $\frac{mg}{ml}$ in TE buffer) is subjected to a 10 microsecond bleach is displayed in figure 15. The observation time was about 1500 microseconds. Note that both the parallel and perpendicular curves exhibit a partial recovery and that, once again, the bleach is deeper in the parallel mode.

The behavior of ratio changes markedly when the DNA is suspended in solution. The initial value of the ratio increases to 0.87. Moreover, the ratio is not 'static': after about 300 microseconds R(t) has risen back up to unity. To make this statement more precise a best-fit exponential has been drawn over the ratio. The exponential time constant, τ, associated with the rise of the ratio was found to be 120μsec; these three digits were estimated to be significant by the IMSL routine ZXSSQ. Both R(0) and τ will be related to the dynamic behavior of the dye-DNA complex in section 6.3.5.

The success of these FPR experiments hinged on the use of a low power objective with a small numerical aperture. In our work with DNA solutions it was found that a high power objective (n.a.$\gtrsim$0.85) forces R(0) toward unity; no dynamic information can then be extracted from the data (see section 6.3.4).

6.3 Discussion of FPR Data

6.3.1 Factors Affecting the Initial Ratio

The measured value of R(0) for a dry DNA system, 0.5, deviates substantially from the value of 0.2 predicted by a simple model in which it is assumed that the dye is static during the bleach, has parallel absorption and emission dipoles and the numerical aperture of the microscope objective is small. The rather high measured value for the initial ratio could have its origin in a number of phenomena. We discuss several possibilities. Residual dye wobble in these 'immobilized' samples could force R(0) up to 0.5. If the motion is adequately described by a wobble model, equation 3-6 predicts that the fluorophore would have to explore a region of half angle 45 degrees to account for the observed values of R(0). If the wobble is actually harmonic in character the uniform

model will overestimate the extent of the motion contributing to the change in R(0). In an oscillatory mode positions deviating farther from the mean should be weighted more heavily because more time is spent near the extrema of the motion.

The numerical aperture of the microscope objective also influences the initial value of the ratio. In these experiments with the 10x objective this lens effect should raise the ratio less than 10 percent over the zero aperture value.[1,2]

For all immobilized samples the initial value of the ratio is found to be substantially less than one. This fact argues strongly that an anisotropic angular distribution of dye is created by the bleaching light and is detected during the probe phase of the experiment. Moreover, if the system under study is expected to reorient rapidly (on the nanosecond time scale) R(0)=1 (*i.e.* no anisotropy remains at the end of the bleach[3]). Most probably some sort of residual dye wobble is elevating the ratio above the theoretical lower bound.

6.3.2 Statistical Significance of Results

It is important to demonstrate that the photon statistics in these experiments are good enough to make the conclusions reliable. Here a detailed analysis of the data obtained from the DNA solutions will be presented. Once it has been demonstrated that the ratio is statistically different from unity for the solution samples it will be apparent that the ratio results are also significant in the case of the experiments on immobilized systems. Let us analyze the statistics of the first data point for the Lambda solution. The total number of counts per second (pre-bleach) was about 150,000. Hence in 10 microseconds the first bin accumulates about 1 photon. After an experiment is repeated 3,000 times there are 3,000±55 counts at the first time point. Therefore the standard

deviation in the counts divided by the pre-bleach is 0.012. The data were given a 5 point cubic smooth that improves the signal to noise by about a factor of $\sqrt{5}$.[4] If the depth of bleach is 0.35 the relative uncertainty in the numerator, $\frac{F_0 - F_\perp(0)}{F_0}$, of the ratio will then be $\frac{\sigma_{num}}{num} = \frac{0.0054}{0.35} = 0.016$. The depth of bleach is somewhat greater in the parallel mode (see section 3.2.2) but for the purposes here it is sufficient to say that the denominator is known to the same accuracy. The relative uncertainty in the ratio is then $\frac{\sigma_{rat}}{rat} = \sqrt{2}(0.016) = 0.022$. Finally, we conclude that $R(0) = 0.87 \pm 0.02$.

The statistical uncertainty in the number of counts per time point also leads to an uncertainty in the time constant associated with the rise of the ratio. As mentioned previously, the best fit τ is estimated to be reliable to 3 digits.

6.3.3 Thermal Effects in 3 Dimensional FPR Studies

In any FPR experiment it is necessary to analyze the magnitude of the light induced thermal effects. Here we present a brief discussion of sample heating in three dimensional FPR studies. In appendix 3 it is demonstrated that if the sample is infinite in extent the bleach induced temperature rise, ΔT, at the position of maximal light intensity is bounded above by the expression

$$\Delta T = \frac{9.2\epsilon C P}{w_0^2 \pi c_p \rho} \Delta t. \qquad (6-1)$$

In equation 6-1 Δt is the length of the bleach, c_p is the specific heat of the sample, ρ is the solution density, ϵ represents the extinction coefficient of the dye, C is the concentration of the fluorophore and w_0 is the beam waist of the Gaussian intensity profile of the laser light.

We now use expression 6-1 to examine the importance of thermal effects in these

experiments. The total laser power in the 514.5 nanometer line of the laser is 4 watts. About 2 watts is typically diffracted into the first order spot during a bleach. The beam waist was about 3 microns. The extinction coefficient of ethidium is approximately $5 \times 10^3 cm^{-1} molar^{-1}$.[5] The dye concentration was about 1 micromolar and the sample thickness was about 150 microns. The thermal parameters of the solution are taken to be those of water. It then follows that $\Delta T = 0.8°$ Celsius. This calculation indicates that the DNA samples were not heated excessively by the FPR bleach pulse.

6.3.4 Effects of Numerical Aperture on the Ratio

During the early stages of the FPR work we tried to maximize the light intensity at the sample by focusing the laser with a high power objective. However this approach was eventually abandoned because lenses with a large numerical aperture tend to elevate the measured value of the ratio.[1,2] The origin of this effect may be understood as follows. The theoretical analysis of polarized FPR assumes that all detected photons propagate parallel to the z axis. Therefore, if the objective collects light traveling in directions that deviate substantially from the z axis the ratio will differ significantly from the theoretical zero numerical aperture limit. It can be shown that the ratio will increase as the numerical aperture of the lens goes up.[1,2] Therefore, for mobile systems that have intrinsically high ratios, and ample fluorescence, it is advantageous to focus the laser light with a low power objective.

6.3.5 Dynamic Interpretation of FPR Results

As discussed in Chapter 3, the temporal rise of the ratio is attributed purely to rotational recovery mechanisms. Translational diffusion produces a polarization

independent recovery that will not contribute to R(t). We first consider the possibility that the dye or DNA exhibits substantial reorientation during the period of time (20 microseconds) encompassing the bleach and the reopening of the photomultiplier tube. Any such fast motion will affect the initial value of the ratio. The measured value of R(0) for a Lambda solution, 0.87, is substantially larger than the static R(0)=0.20; therefore the DNA molecule and the reporter ethidium reorient considerably during the bleach. Within the confines of the wobble model an R(0) of 0.87 is indicative of motion in a cone of half angle $\alpha = 70$ degrees. Again we note that the internal dynamics of DNA are fundamentally harmonic in character; hence a uniform 'wobble in a cone' analysis probably does overestimate the extent of the motion during this initial 20 microseconds.

The reorientations that are assumed to be contributing to the temporal rise of the ratio are the larger amplitude bending deformations and the Brownian rotational diffusion of DNA. We characterize the motions that contribute to the several hundred microsecond FPR recovery with the Hearst-Harris (HH) model of the dynamics of a semi-flexible rod-like DNA molecule. Remember that in such models the motion of the contour of the polymer is decomposed into a set of normal modes whose time dependence is given by $exp(-t/\tau_n)$.[6-8] The spatial character of an HH mode is governed by an eigenfunction of the differential equation that specifies the flexibility of the molecule. The normal mode motions of the polymer can be thought of much as one envisions the modes of a string. The longest wavelength normal mode contains no nodes and corresponds to a large amplitude motion of the entire molecule. Higher order modes contain progressively more and more nodes and correspond to local motions of the macromolecule.

Equations 2-9a and 2-9b express the characteristic relaxation time and amplitude of a given Rouse-Zimm mode, n, in terms of measurable properties of the polymer. In the continuum Hearst-Harris model these relationships become (in the random coil limit)[9]

$$\langle \delta_n{}^2 \rangle^{\frac{1}{2}} = \left(\frac{2}{3}\frac{\langle R^2 \rangle}{\pi^2 n^2}\right)^{\frac{1}{2}} \qquad (6-2)$$

and

$$\tau_n = \frac{\langle R^2 \rangle}{3D_0\pi^2 n^2}. \qquad (6-3)$$

Here, $\langle R^2 \rangle$ denotes the mean square end to end length of a molecule and D_0 is the translational diffusion constant of the DNA. Phage Lambda consists of 50,000 base pairs; the mean square end to end length of the molecule is, therefore, approximately 2 μm^2. We take $D_0 = 2 \times 10^{-8} \frac{cm^2}{sec}$.[10] For the Lambda molecule equations 6-2 and 6-3 then become

$$\langle \delta_n{}^2 \rangle^{\frac{1}{2}} = \frac{350\ nanometers}{n} \qquad (6-4)$$

and

$$\tau_n = \frac{30\ milliseconds}{n^2}. \qquad (6-5)$$

Thus the relaxations monitored in these experiments are governed largely by modes 20 and higher. (Note that excluded volume effects have been ignored in this analysis. However, because higher order motions are less influenced by steric factors it is felt that this description is reasonably valid).

The correlation time associated with overall rotational motion of phage Lambda DNA is expected to be many milliseconds. Therefore, Brownian relaxation of the entire Lambda molecule probably is not the major mechanism underlying the anisotropy decay monitored in this study.

Figure 12

Apparatus used in fast rotational photobleaching experiments. The light source is a Coherent 15 watt argon-ion laser. The beam emerges from the acousto-optic modulator as a series of diffraction spots. Note that the first order deflection is directed through an aperture and onto the sample. During the bleach pulse about 2 watts of laser power is directed into the first order; the probe beam is about 10,000 times less intense than the bleach.

To counteract depolarizing effects of the modulator the beam is sent through a plane polarizer; the light is then given a circular polarization by a quarter wave plate. At this point the beam in incident on a Pockels Cell. The light emerges from the Pockels Cell in one of two perpendicular plane polarized states. An analyzing polarizer and photodiode (shown to the right of the optic train) are used to monitor the polarization of the light that is output by the Pockels Cell. The photodiode can also be used to measure the ratio of the bleach to probe beam intensity.

Finally, the light is directed onto the sample through a standard epi-illumination microscope set-up. In our experiments the ethidium azide labeled DNA was mounted on fused silica coverslips. In solution studies the sample was about 150 microns thick. The objective was always focused onto the center of the sample to ensure that an image-plane diaphragm (see figure) blocked most photons emitted by any silica-bound DNA.

A polarizer passes one polarization component of the fluorescence on to the phototube. The fluorescence photons are counted for intervals of 10 microsecond duration; the data is then stored in a NOVA 3/12 minicomputer.

Figure 12

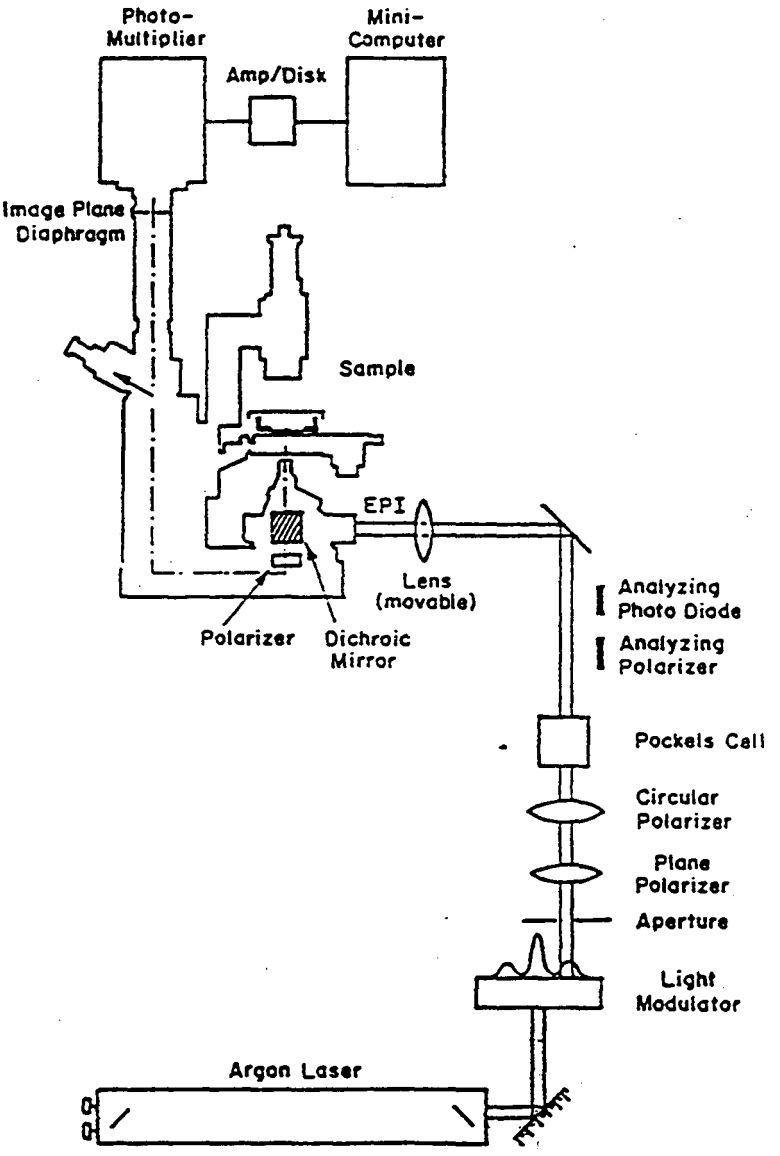
Photo-
Multiplier
Amp/Disk
Mini-
Computer
Image Plane
Diaphragm
Sample
EPI
Lens
(movable)
Polarizer
Dichroic
Mirror
Analyzing
Photo Diode
Analyzing
Polarizer
Pockels Cell
Circular
Polarizer
Plane
Polarizer
Aperture
Light
Modulator
Argon Laser

Figure 13

The parallel and perpendicular mode FPR curves for an immobilized DNA sample. The pre-bleach fluorescence level is approximately 1 on the graph. Data were collected in 10 microsecond intervals; therefore the entire x axis corresponds to an elapsed time of about 1.6 millisecond. Note that both parallel (triangles) and perpendicular (circles) fluorescence signals recover but that the bleach depth is twice as large in the parallel experiment. Even in the presence of nonrotational recovery mechanisms if the sample retains some of the bleach pattern at an observation time t, the fluorescence signal at time t must be lowest when excitation (*i.e.* the probe polarization) is along the direction of greatest bleaching. This physical argument is equivalent to our mathematical statement that $R(0)=\frac{F_0-F_\perp(0)}{F_0-F_\parallel(0)}$ is less than unity if the sample has not completely depolarized at the end of the bleach period. If R(0)<1 then $F_0 - F_\perp(0) < F_0 - F_\parallel(0)$, *i.e.* the depth of bleach is larger in the parallel experiment than in the perpendicular.

Figure 13

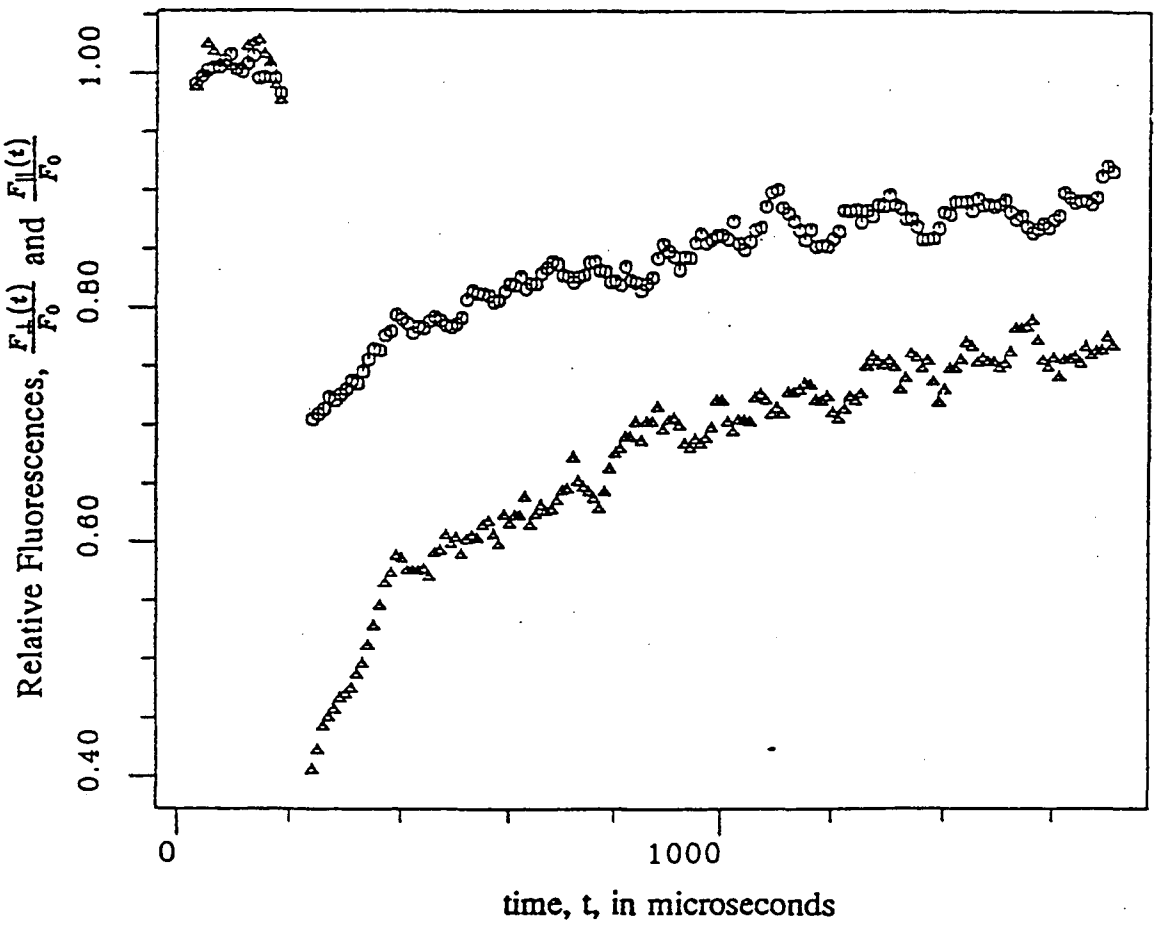
Relative Fluorescences, $\frac{F_\perp(t)}{F_0}$ and $\frac{F_\parallel(t)}{F_0}$
0.40
0.60
0.80
1.00
0
1000
time, t, in microseconds

Figure 14

The ratio $R(t)=\frac{F_0-F_\perp(t)}{F_0-F_\parallel(t)}$ computed from the individual FPR curves shown in figure 13. As mentioned in the text R(0) is about 0.5, and in fact the ratio does not differ significantly from 0.5 for the entire 1.5 millisecond observation period. Therefore, despite the fact that the individual parallel and perpendicular FPR curves manifest some degree of recovery, the ratio exhibits the static behavior one would expect from a rotationally restricted sample.

Figure 14

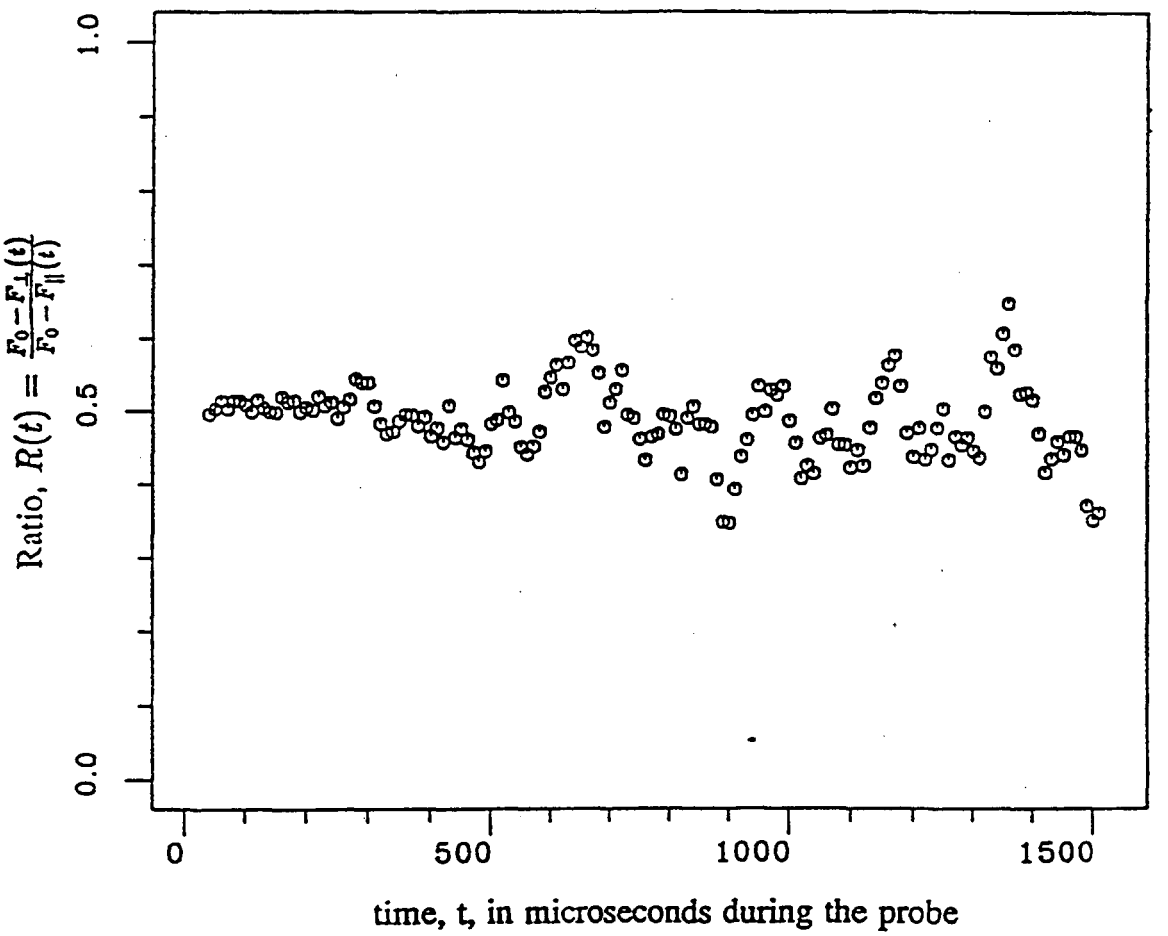
Ratio, $R(t) = \frac{F_0 - F_\perp(t)}{F_0 - F_\parallel(t)}$
1.0
0.5
0.0
0
500
1000
1500
time, t, in microseconds during the probe

Figure 15

The parallel (15a) and perpendicular (15b) photobleaching curves and ratio R(t) (15c) for a solution of phage Lambda at 2 mg/ml in TE buffer. Superimposed on the ratio is a best fit exponential of the form $A - B\,exp(\frac{-t}{\tau})$. Note the different characteristics of the ratio when the DNA is in solution and when it is stuck on the silica slide (see figure 14). When the molecules are in solution R(0) increases substantially to 0.87 and the ratio rises back up to unity as the DNA experiences rotational recovery. The time constant associated with the rise of the ratio, approximately one hundred microseconds, must reflect rotation of a macromolecule because any small molecule like ethidium would reorient in a few nanoseconds.

Figure 15a

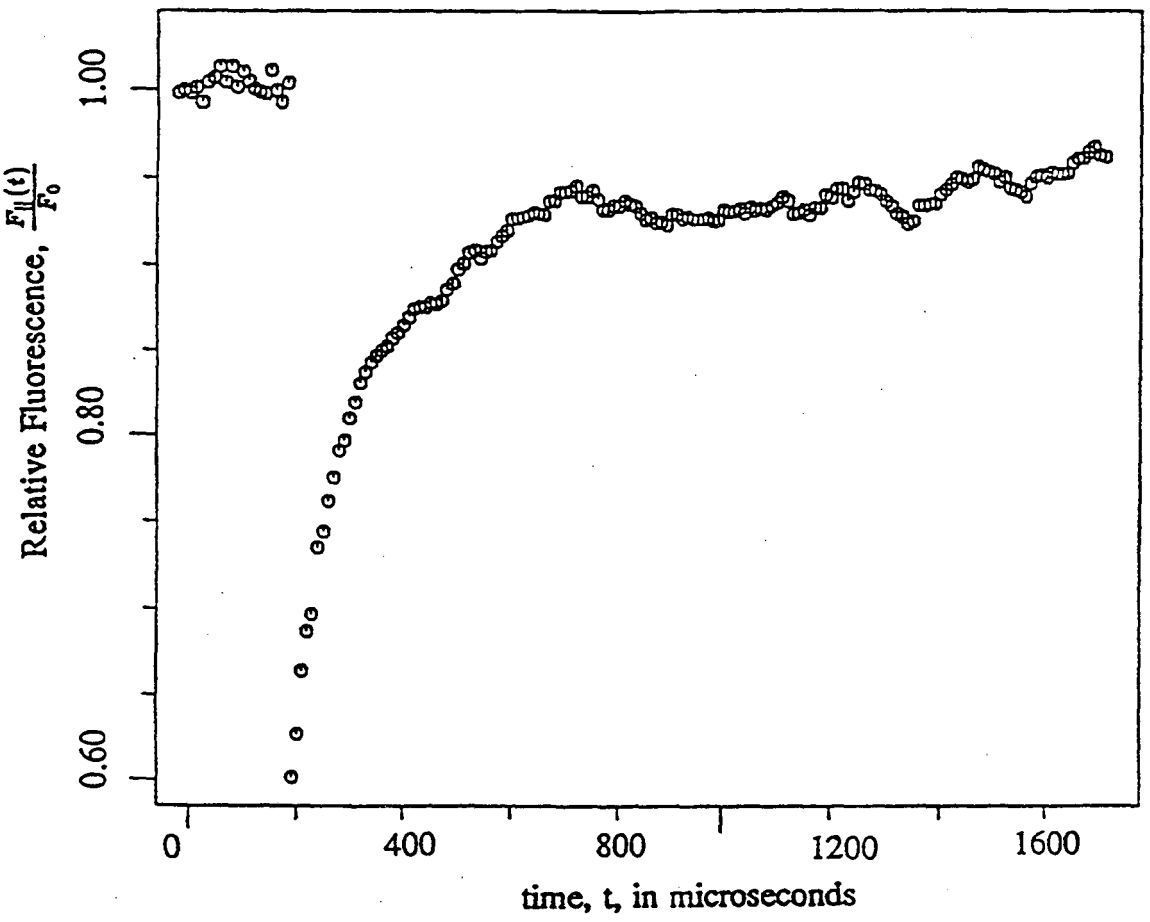
Relative Fluorescence, $\frac{F_{II}(t)}{F_0}$
1.00
0.80
0.60
0
400
800
1200
1600
time, t, in microseconds

Figure 15b

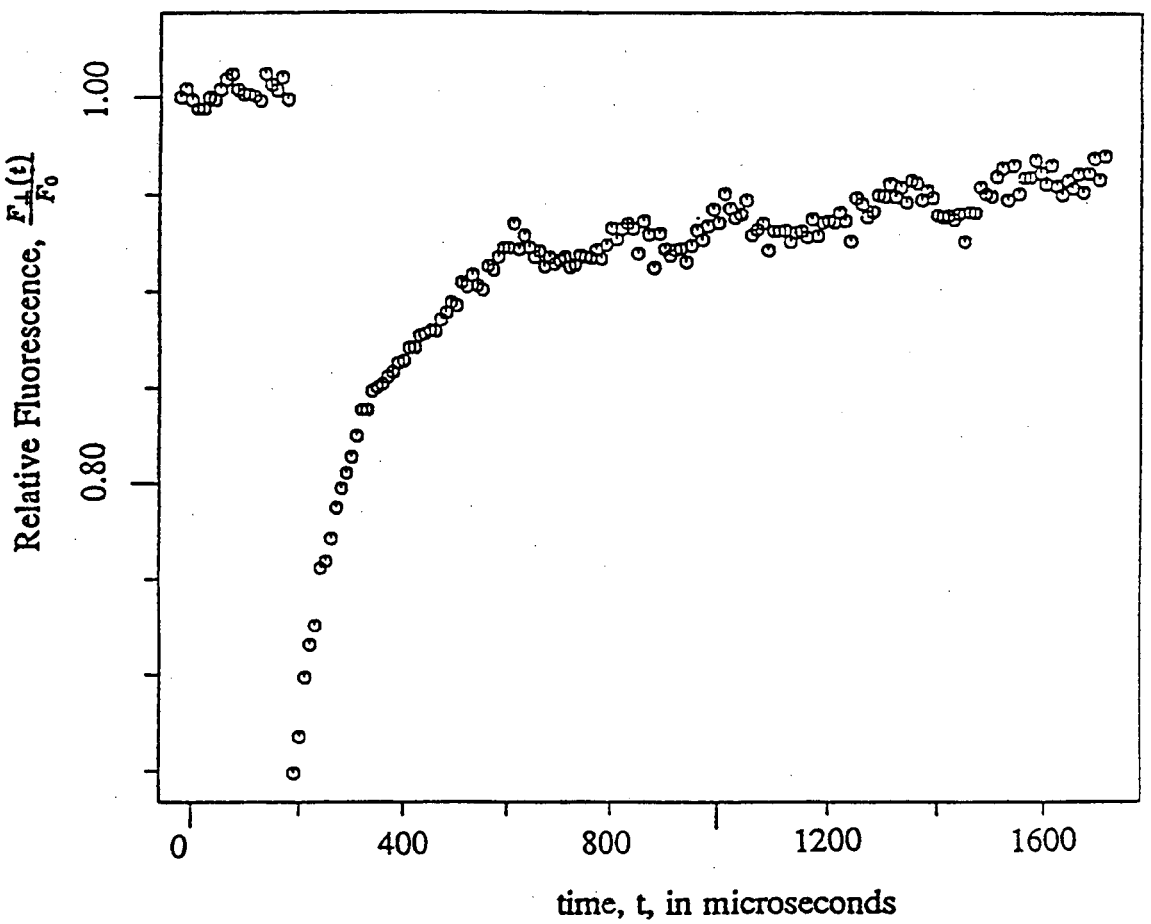
Relative Fluorescence, $\frac{F_A(t)}{F_0}$
1.00
0.80
0
400
800
1200
1600
time, t, in microseconds

Figure 15c

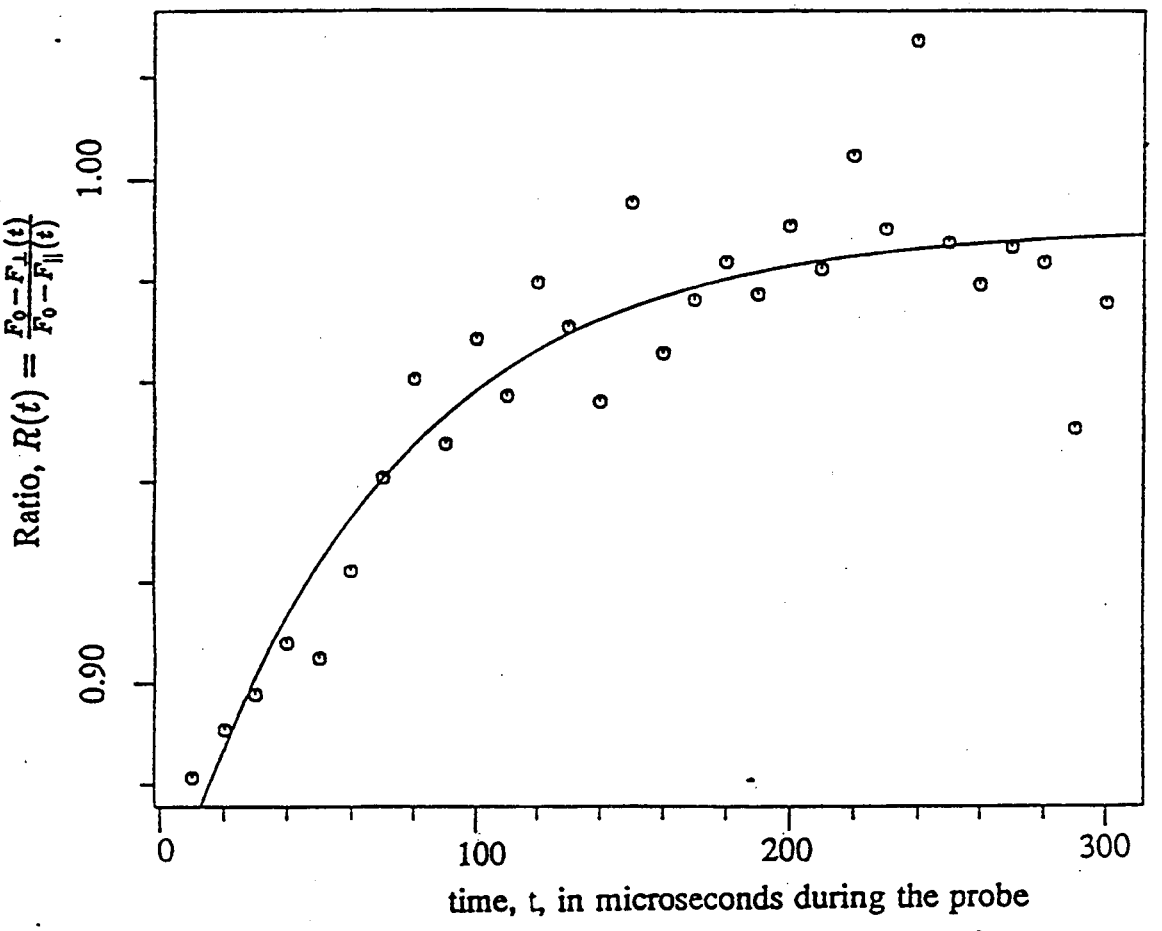
Ratio, $R(t) = \frac{F_0 - F_\perp(t)}{F_0 - F_\parallel(t)}$
1.00
0.90
0
100
200
300
time, t, in microseconds during the probe

References for Chapter 6

1. D. Axelrod (1979) Carbocyanine dye orientation in red cell membrane studied by microscopic fluorescence polarization. Biophys. J. **26**: 557.

2. L.M. Smith, R.M. Weis and H.M. McConnell (1981) Measurement of rotational motion in membranes using fluorescence recovery after photobleaching. Biophys. J. **36**: 73.

3. D. Axelrod (1987) Manuscript in Preparation.

4. A. Savitzky and M.J.E. Golay (1964) Smoothing and differentiation of data by simplified least squares procedures. Anal. Chem. **36**: 1627.

5. D.E. Graves, L.W. Yielding, C.L. Watkins and K.L Yielding (1977) Synthesis, separation and characterization of the monoazide and diazide analogs of ethidium bromide. Biochim. Biophys. Acta **479**: 98.

6. P.E. Rouse (1953) A theory of the linear viscoelastic properties of dilute solutions of coiling polymers. J. Chem. Phys. **21**: 1272.

7. B.H. Zimm (1956) Dynamics of polymer molecules in dilute solution: Viscoelasticity, flow birefringence and dielectric loss. J. Chem. Phys. **24**: 269.

8. R.A. Harris and J.E. Hearst (1966) On polymer dynamics. J. Chem. Phys. **44**: 2595.

9. S. Fujime (1971) Quasi-elastic light scattering from solutions of macromolecules. III. Detectability of internal modes of motion. J. Phys. Soc. Japan **31**: 1805.

10. K.S. Schmitz and J.M. Schurr (1973) Rotational relaxation of macromolecules determined by dynamic light scattering. II. Biopolymers **12**: 1543.

Chapter 7

FCS Experiments

As mentioned in Chapter 3, FCS is a method of monitoring slowly relaxing molecular dynamics. However, FCS has not seen wide application primarily because the technique suffers from signal to noise difficulties. The origin of the problem may be understood as follows. Consider the quantity $n\beta$—the average number of detected photons per dye molecule per sample time. If an FCS experiment is run in the so-called 'low count regime' (*i.e.* $n\beta \lesssim 1$) the signal to noise ratio for $C(\tau)$ can be shown to be directly proportional to $n\beta$.[1] Therefore in an FCS experiment signal to noise will generally improve as the light intensity and, consequently, $n\beta$ increase. Unfortunately, an intense beam tends to induce bleaching of the dye. The main obstacle in FCS work has, therefore, been the limitation that fluorophore bleaching places on signal to noise.

In recent years our understanding of the phenomena that lead to photobleaching has improved and ways to circumvent the problem have been discovered. It has been shown, for example, that dye solutions containing a small quantity of an oxygen scavenging chemical such as sodium dithionite will exhibit markedly enhanced resistance to photobleaching[2] (see figure 16). This discovery should substantially alleviate the signal to noise difficulties in FCS experiments. Improvements in the machines that compute correlation functions have also extended the time domain that can be monitored

with the technique. The first correlators that were built typically took several hundred microseconds to carry out the multiplications and additions required to compute the correlation function.[3] Therefore, at sampling times that were faster than about 100 μsec the machines became inefficient at processing and acquiring data. Correlators can now routinely do real time sampling as fast as 100 nanoseconds.[4] It is our hope that the FCS technique can now be fruitfully exploited in studies of macromolecular dynamics.

Here we will present some preliminary correlation studies of the translational diffusion of DNA. The translational diffusion coefficient is an important molecular parameter because it is sensitive to size, shape and environment. These experiments utilized an older Saicor correlator. In the future this work will be extended with a new, more versatile Brookhaven machine.

FCS has been used to monitor both the translational motion and flow of ethidium bromide labeled DNA.[5,6] In the ethidium bromide-DNA system the polymer must be heavily labeled with dye to mask effects from the millisecond on-off kinetics of the probe. In this study the DNA is covalently labeled and therefore we need not worry about reversible binding of the fluorophore.

7.1 Translational Correlations and Beam Divergence

Before the FCS data is presented and analyzed it is important to note that the fluctuation theory developed in chapter 3 (see equations 3-7a,b) may not accurately model one aspect of these experiments. Recall that expressions 3-7a,b are valid only if the radius of the beam does change appreciably as the light traverses the sample (*i.e.* beam divergence is small). We will now make the concept of beam divergence mathematically

precise and then calculate the extent of divergence through a typical sample.

As a Gaussian beam propagates it will spread. Specifically, if a TEM_{00} wave front is focused down to a spot of size ω_0 in the focal plane of a lens, the width of the beam $\omega(z)$ will increase with distance z from this plane. The functional relationship between ω and z is[7]

$$\omega(z) = \omega_0[1 + (\frac{z}{z_r})^2]^{\frac{1}{2}} \qquad (7-1a)$$

where

$$z_r = \frac{\pi\omega_0^2}{\lambda}. \qquad (7-1b)$$

Here λ is the wavelength of the light. Note that z_r, the Rayleigh length of the beam, can be thought of as the propagation distance over which the area of the spot doubles.

We now estimate z_r for the typical experiment described here. The objective produces a spot of radius $\omega_0 \approx 1\mu$m, and the wavelength of the light is $\lambda = 0.5154\mu$m. We find

$$z_r = \frac{\pi\omega_0^2}{\lambda} = \frac{\pi 1\mu m^2}{.5145\mu m} \approx 6\mu m. \qquad (7-2)$$

It is apparent that if a sample is more than several microns thick, the spread of the beam will be significant and translational motion will not manifest itself precisely as predicted by equations 3-7a,b.

There are several ways to eliminate the beam divergence problem. One possibility is to make the sample very thin. We did not have much success with thin solutions; the DNA may have been sticking to the slides. Therefore, typically samples that were several hundred μm in thickness were studied. We finally decided to put an image plane aperture in front of the phototube; the aperture obstructs most fluorescence except that which

originates from a small z distance around the focal plane of the microscope objective.[8] Note however, that even with an aperture in the system, light collection extends over $\approx$ 10 μm in the z direction; therefore, the translational FCS data cannot be expected rigorously to follow equations 3-7a,b.

7.2 FCS Apparatus

The apparatus used in the FCS experiments is shown schematically in figure 17. The machine is actually used for translational photobleaching and correlation spectroscopy. The light source is a 4 watt Lexel argon-ion laser. The beam is spatially filtered to ensure that its profile is truly Gaussian. The light is then incident on two sets of beam splitters that are used to switch between bleach and probe illumination in photobleaching experiments. For the FCS work the beam splitters are simply a source of light that is directed onto a photodiode. The photodiode output follows variations in the laser light intensity and is subtracted from the fluorescence current (as discussed below). A lens, L, of focal length f=30 cm directs the beam into a standard epi-illumination microscope. This lens can be translated along the direction of light propagation; the size of the spot in the focal plane of the microscope objective varies as L is moved. The objective used in the translational FCS experiments had a 50X (or 75X) magnification and a numerical aperture of 0.65 (or 1.00). Glass microslides (obtained from Vitro Dynamics Inc.) of several hundred microns in thickness held all samples. As mentioned earlier an image plane aperture passes primarily the fluorescence emitted by dye molecules that are within 5-10 microns of the focal plane of the objective.

In the FCS work the photomultiplier tube was operated in the analog (or current)

mode. Analog detection was utilized because the Saicor correlator could not process photon pulses. The output of the PMT was sent into a pre-amplifier. An amplifier is used to scale the magnitude of the fluorescence signal to the output of the diode; these two signals are then fed into a differential amplifier. The output of the differential amplifier is the difference of the two inputs (x100); the differential amplifier serves to eliminate laser fluctuations. Finally, the signal is filtered to remove high frequency electronic noise and the correlation function is computed.

In the experiments described here the correlator sampled the fluorescence photocurrent in 500 μsec or 1 millisecond intervals. The correlation function was computed using a standard algorithm.[3] The filter was set for a bandwidth of 300 or 1000 hertz. Data were given a 5 point cubic smooth.[9] Curve fits were performed by IMSL routine ZXSSQ.

7.3 FCS Experimental Results

To demonstrate that a decay of correlation had its origin in translational motion the data were subjected to the following tests: (1) The time constant had to exhibit an approximate quadratic dependence on the size of the illuminated region of sample. (2) The amplitude of $\frac{G(\tau)}{\langle i \rangle^2}$ had to decrease as the number of fluorescing DNA's increased. (3) The time constant, τ_D, had to be independent of laser power.

7.3.1 Translational Diffusion of PBR 322

In figure 18 are shown three representative correlation functions obtained from a solution of PBR 322 in TE buffer ($\approx 100 \frac{\mu g}{ml}$). The dye to DNA ratio for these samples was approximately 100:1. The illuminated region of the sample was varied in these experiments by translating the lens L (see figure 17) from the position that produces the

minimum spot size in the focal plane of the microscope objective. The data were fit to the simple hyperbolic relationship of equation 3-7a. The best-fit time constant is a monotonically increasing function of spot size. Moreover, the amplitude of the correlation function $\frac{G(\tau)}{\langle i \rangle^2}$ decreases as the radius of the illuminated region increases. The quantitative results are summarized in table 1. Note also an important qualitative observation. The noise, *i.e.* the scatter in the data associated with a correlation function, increases as the beam is defocused. Finally, the time constants were tested for dependence on light intensity. The correlation time did not vary detectably under changes in laser power. Each of these points will be considered in more detail in section 7.4.

7.3.2 Translation of an 18 Base Pair Oligomer

We also looked at the translational diffusion of a synthetic 18mer. Experimental work with the 18mer was more difficult than with PBR because the ratio of dye to oligomer had to be kept near unity. The data (not shown) were subjected to the tests enumerated above. Correlation decay was typically an order of magnitude faster than in the PBR experiments.

7.4 Interpretation of FCS Data

7.4.1 Source of Correlation Decay

It is important to demonstrate that the decay of correlation shown in figure 18 had its origin in translational fluctuations. Indeed, during the early stages of the FCS work it was found that the response function of the low-pass filter, line noise, etc. could all be observed in the data. However, a correlation function could always be identified as 'spurious' when its amplitude and temporal variation were invariant under changes in

dye concentration, spot size etc. When the instrumental difficulties were eliminated we began to observe correlation data that varied systematically as the sample conditions were changed.

The following characteristics of the correlation functions in figure 18 indicate that the data do represent DNA translation. (1) As the size of the spot, ω, and the number of molecules in the beam, $N = \pi\omega^2 LC$, increase the amplitude of the correlation function falls and the time constant, τ_D, grows. This qualitative observation can be made quantitative in the following fashion. If the data behave as predicted by equations 3-7 and 3-8 we anticipate that the product $\tau_D \times C(0) = \frac{\omega^2}{4D_0} \times \frac{\langle i \rangle^2}{\pi\omega^2 LC} = \frac{\langle i \rangle^2}{4\pi C D_0 L}$ will be independent of the illuminated area of sample. Therefore if the x and y axes for each of the individual correlation functions in figure 18 are rescaled by $C(0)$ (*i.e.* plot $\frac{C(\tau)}{C(0)}$ vs. $\tau C(0)$) the resulting curves should superimpose.[8] The rescaled data are displayed in figure 19. It is apparent that a universal curve is obtained from this procedure. (2) The signal to noise is clearly governed by light intensity; as the spot size increases and the intensity at the sample decreases the scatter in the correlation data grows (all other experimental variables are equal). Since in these studies $n\beta < 1$ this sort of variation in noise with light intensity is consistent with our previous statement that the magnitude of $n\beta$ governs signal to noise in a fluctuation experiment. (3) The time constants are independent of laser power, therefore, dye bleaching was not the origin of correlation decay.

7.4.2 Diffusion Coefficient of PBR and 18mer

There are several ways to extract a translational diffusion coefficient from the FCS data. If the beam waist is known D_0 is easily determined from relationship 3-7b. The

Gaussian waist can be measured quite accurately by translating a knife edge in front of the laser light.[10] The value of ω_0 for our fluorescence set-up was found in this manner to be 0.75μm. The PBR time constant when the lens was positioned so as to produce the minimal illuminated area was approximately 83 milliseconds (see table 1). We find $D_0 = \frac{.75^2}{4(.083)} = 1.7 \pm 0.4 \times 10^{-8} \frac{cm^2}{sec}$. The error in this number was determined from an analysis of multiple experiments. In the case of the oligomer there was more scatter in the data; the diffusion coefficient was found to be $D_0 = 20 \pm 9 \times 10^{-8} \frac{cm^2}{sec}$. Both of these values for D_0 are in reasonable agreement with diffusion coefficients that have been measured for similarly sized DNA's using light scattering and sedimentation techniques.[11-13] Note also that the above values for D_0 must reflect DNA motion because the diffusion coefficient of an ethidium molecule is $\approx 10^{-6} \frac{cm^2}{sec}$.

Alternatively it has been shown by Sorcher and Klein that measurement of τ_D as a function of spot size will yield D_0.[14] This approach was used to measure the diffusion coefficient of ethidium bromide-labeled SV40 DNA. The value of D_0 obtained from this method (for SV40) is in good agreement with that reported here for the similarly sized PBR molecule.

Figure 16

Plot of the temporal variation in the fluorescence emitted by the fluorophore acriflavine in the absence (curve B) and presence (curve A) of $Na_2S_2O_4$ (0.02 Molar). 405 nanometer light from a 200 watt Hg-lamp was focused onto the sample through a 100x objective. Note the very substantial reduction in the rate of irreversible photobleaching of the dye. This $Na_2S_2O_4$ associated inhibition of bleaching has been reported for a large number of important dyes including the DNA stains ethidium and acridine (see table). Adapted from Reference 2.

Figure 16

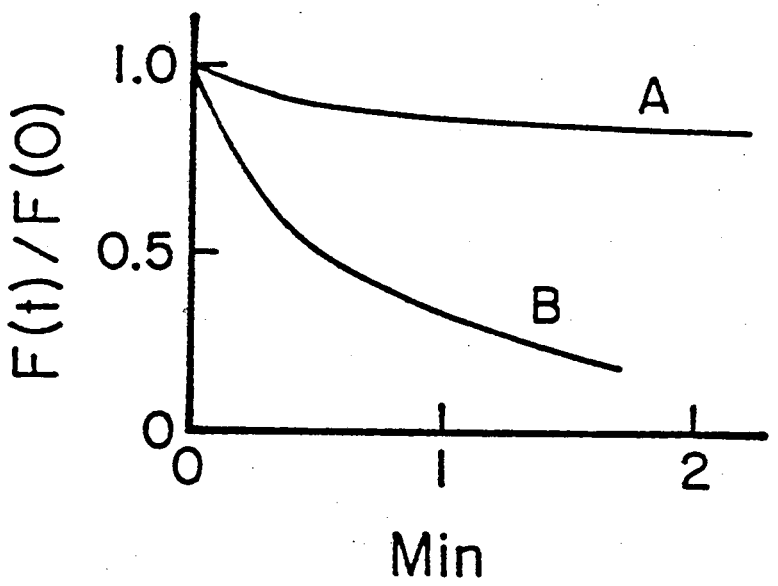

Fluorophore	F(2 min)/F(0) Buffer	$+Na_2S_2O_4$
Fluorescein[a]	0.67	1.00
Acridine orange	0.55	1.00
33258 Hoechst[b]	0.87	1.00
Acriflavine	0.22	0.90
Ethidium-Br[7]	0.27	0.87
Berberine	0.92	1.00
Quinacrine - 2 HCl	0.64	0.65
Rhodamine 3G[e]	0.54	0.62
ANS[11]	<0.1	<0.1
Quercetin-Al^{3+}[d]	(0.30)	(0.88)

Figure 17

Optical apparatus used in the autocorrelation and photobleaching experiments. The light source is a Lexel argon-ion laser. The interlock shutter is a safety feature. The beam is spatially filtered to remove high frequency noise from the TEM_{00} Gaussian intensity profile. The light is then split into bleach and probe beams. The intensity of the two beams can be independently adjusted (reduced) at the attenuator. A mechanical shutter is placed in the path of each beam and will block or pass the light as desired. The bleach and probe light is then recombined at a second 'beam-splitter.'

The photodiode monitors variation in the intensity of the excitation beam. The pin-hole blocks stray light. A lens of focal length f=30 cm can be translated along the optic axis. At one position of the lens the size of the laser spot at the 'infocus' sample is minimized. As the lens is moved from this position the illuminated region of the 'infocus' sample grows.

Finally the beam is steered into a standard epi-illumination microscope set-up. A dichroic mirror reflects the exciting laser light down towards the sample and passes the longer wavelength fluorescence on toward the phototube. The mirror also serves to block scattered laser light. An image plane aperture restricts the effective sample length over which fluorescence is collected. The fluorescence signal is then incident on a photomultiplier tube. Electronic processing then proceeds as described in section 7.2.

Figure 17

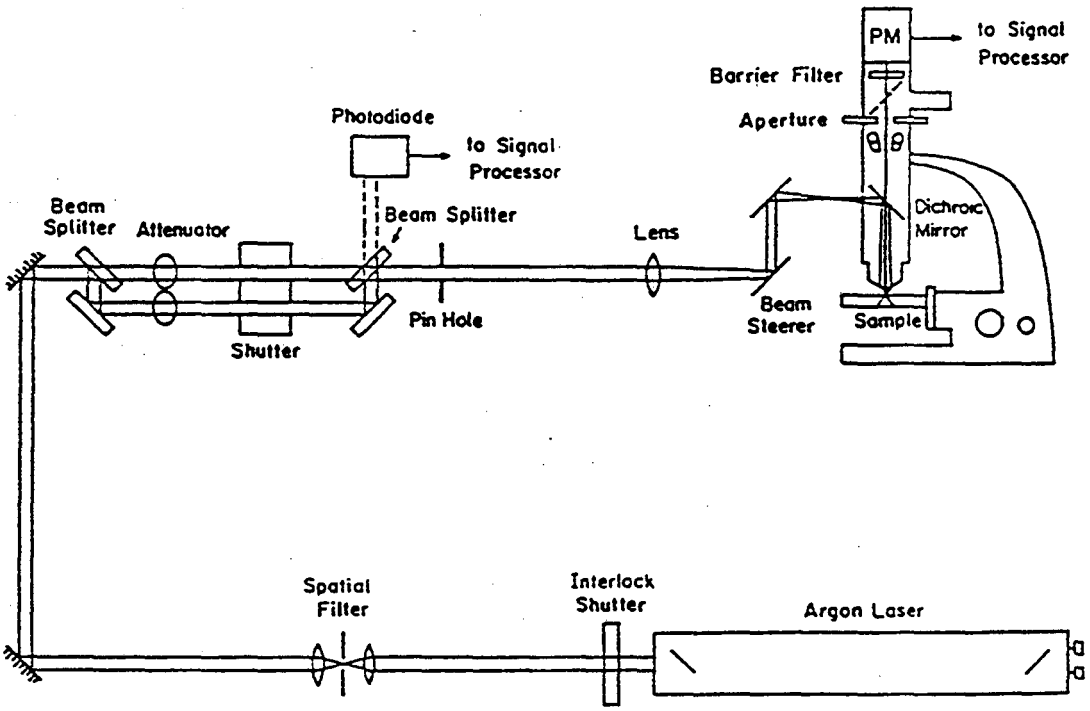
PM
to Signal Processor
Barrier Filter
Aperture
Photodiode
to Signal Processor
Beam Splitter
Attenuator
Beam Splitter
Lens
Dichroic Mirror
Pin Hole
Beam Steerer
Sample
Shutter
Spatial Filter
Interlock Shutter
Argon Laser

Figure 18

Autocorrelation data obtained from a solution of PBR 322 in TE buffer ($100\frac{\mu g}{ml}$). The unit of time along the x axis is 1 millisecond. The three fluctuation measurements were made for different positions of the lens L and hence correspond to diffusion in spots of distinct radii, ω. The correlation function 18a was obtained when the lens was positioned so as to produce the smallest illuminated area in the focal plane of the objective. The data displayed in 18b and 18c correspond to progressively larger beam spots. Note that $\langle i \rangle$ does not change as the lens is moved and, therefore, we do not explicitly distinguish between $C(\tau)$ and the normalized autocorrelation function $\hat{C}(\tau) = \frac{C(\tau)}{\langle i \rangle^2}$.

Figure 18a

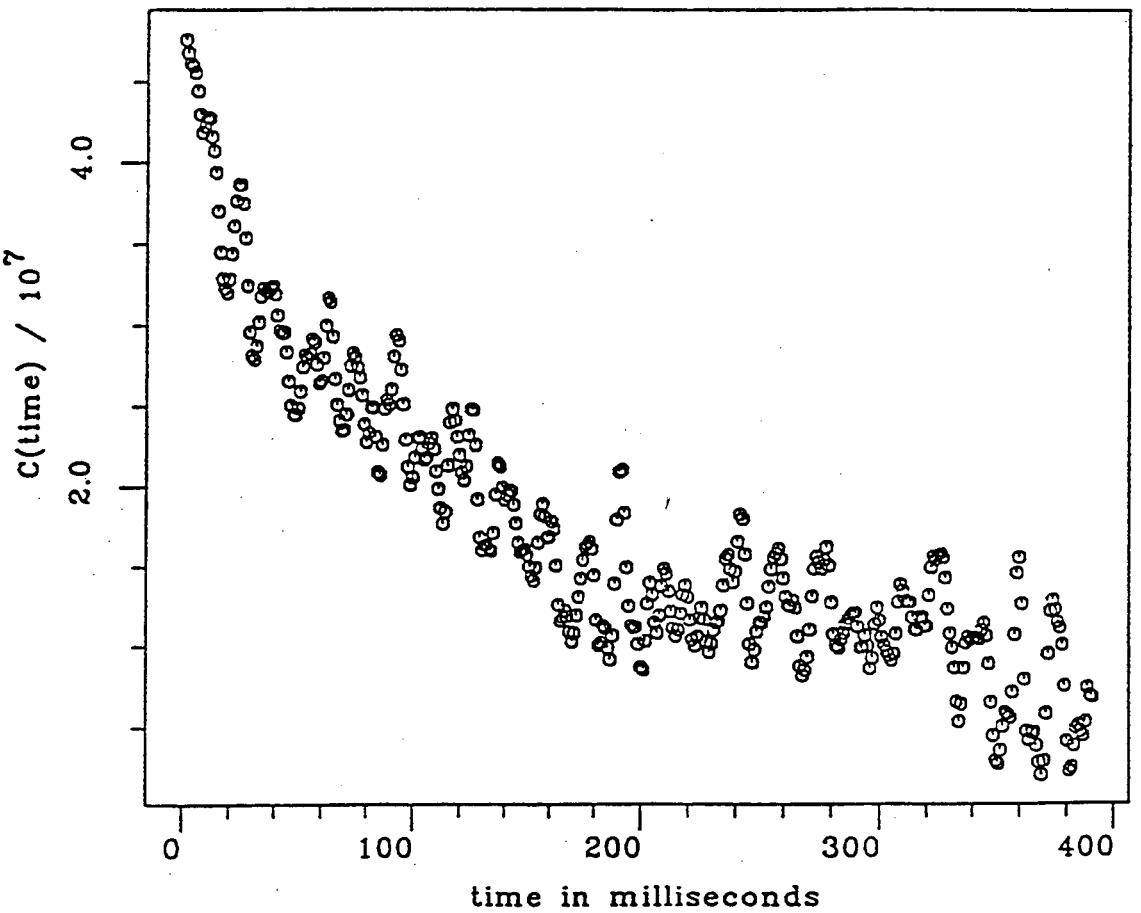

Figure 18b

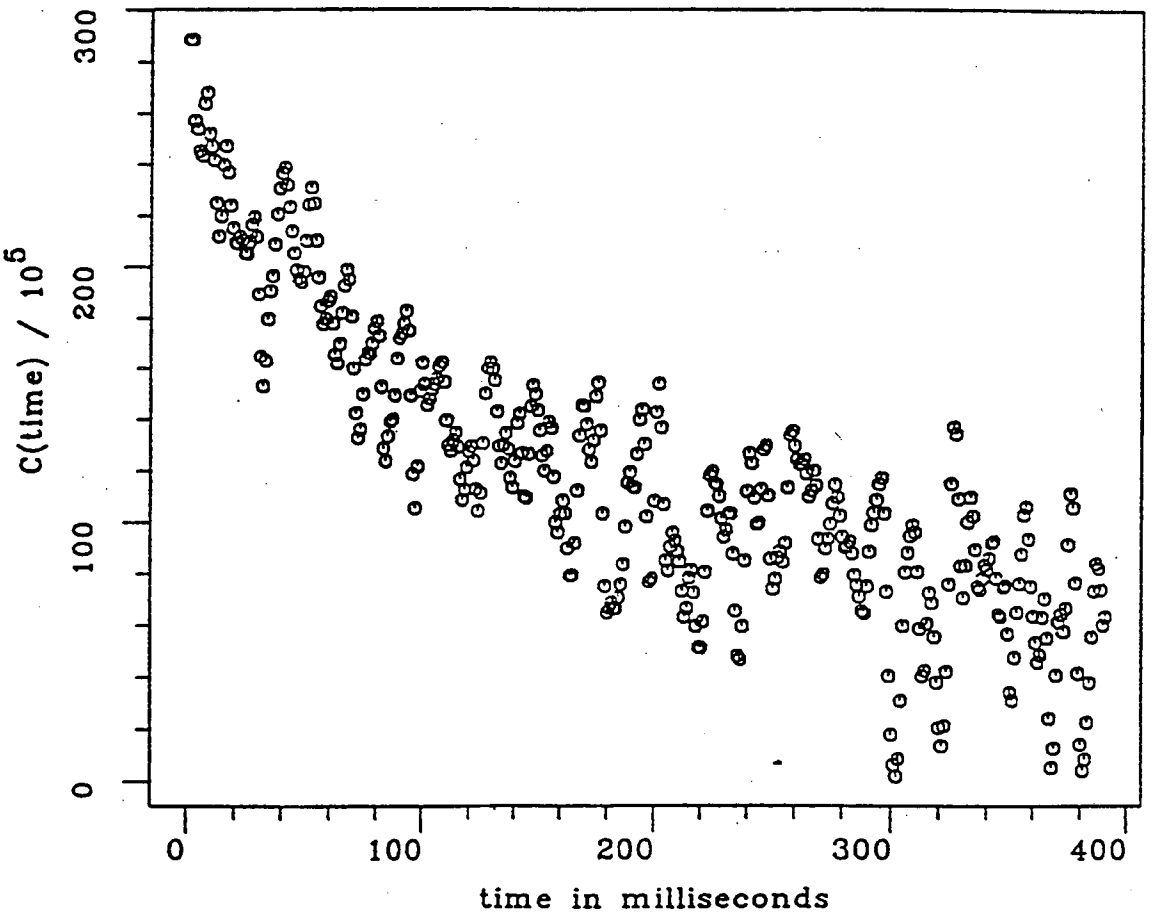

Figure 18c

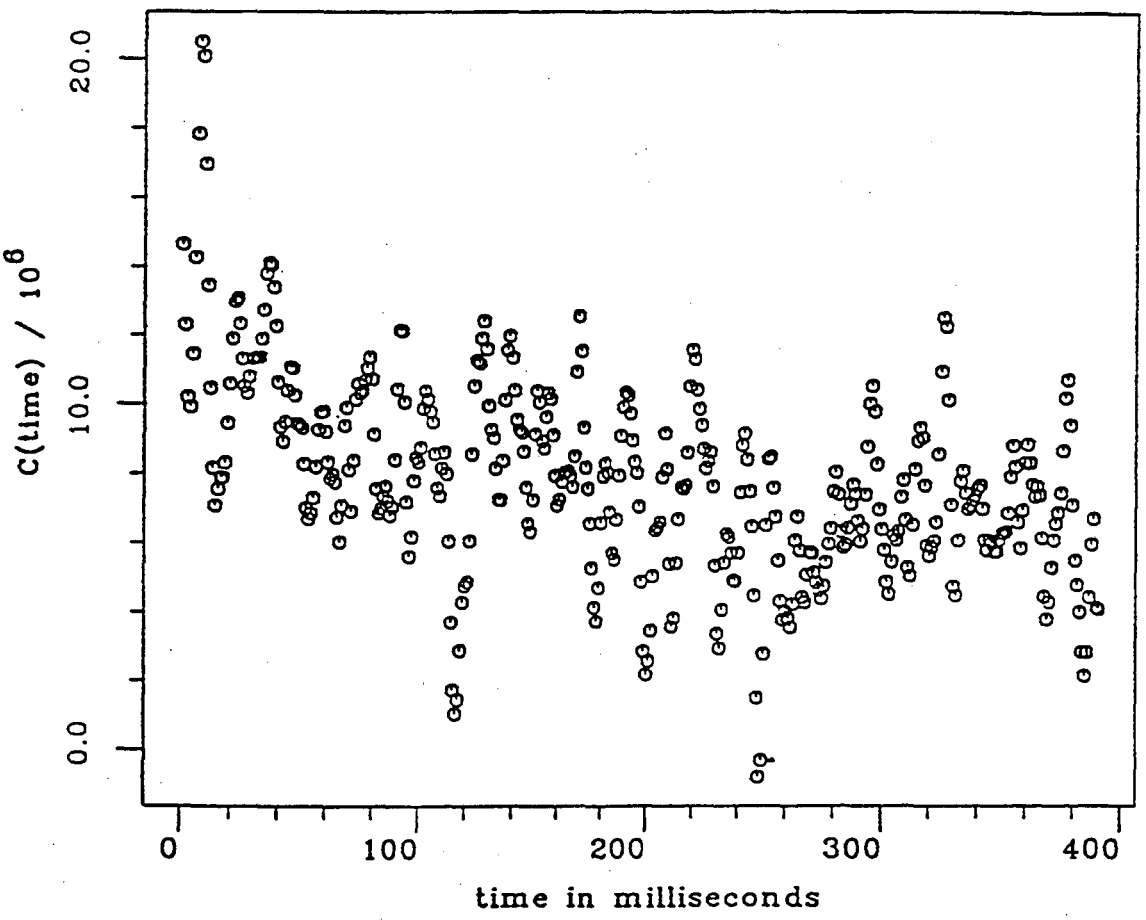

Table 1

Tabulated best-fit amplitudes and time constants for the correlation functions displayed in figure 18.

	minimal spot	intermediate spot	large spot
Amplitude = C(0)	4.9	2.9	1.16
Time Constant = τ_D	83 milliseconds	121 milliseconds	367 milliseconds
$C(0) \times \tau_D$	407	351	426

Figure 19

Rescaled versions of the PBR correlation functions displayed in figure 18. The circles, triangles and crosses correspond to data sets 18a, 18b and 18c respectively. The scaled ordinate is $\frac{C(\tau)}{C(0)}$; the abscissa is $\tau \times C(0)$. The three scaled curves superimpose indicating that the data in figure 18 follow relationships 3-7 and 3-8.

Figure 19

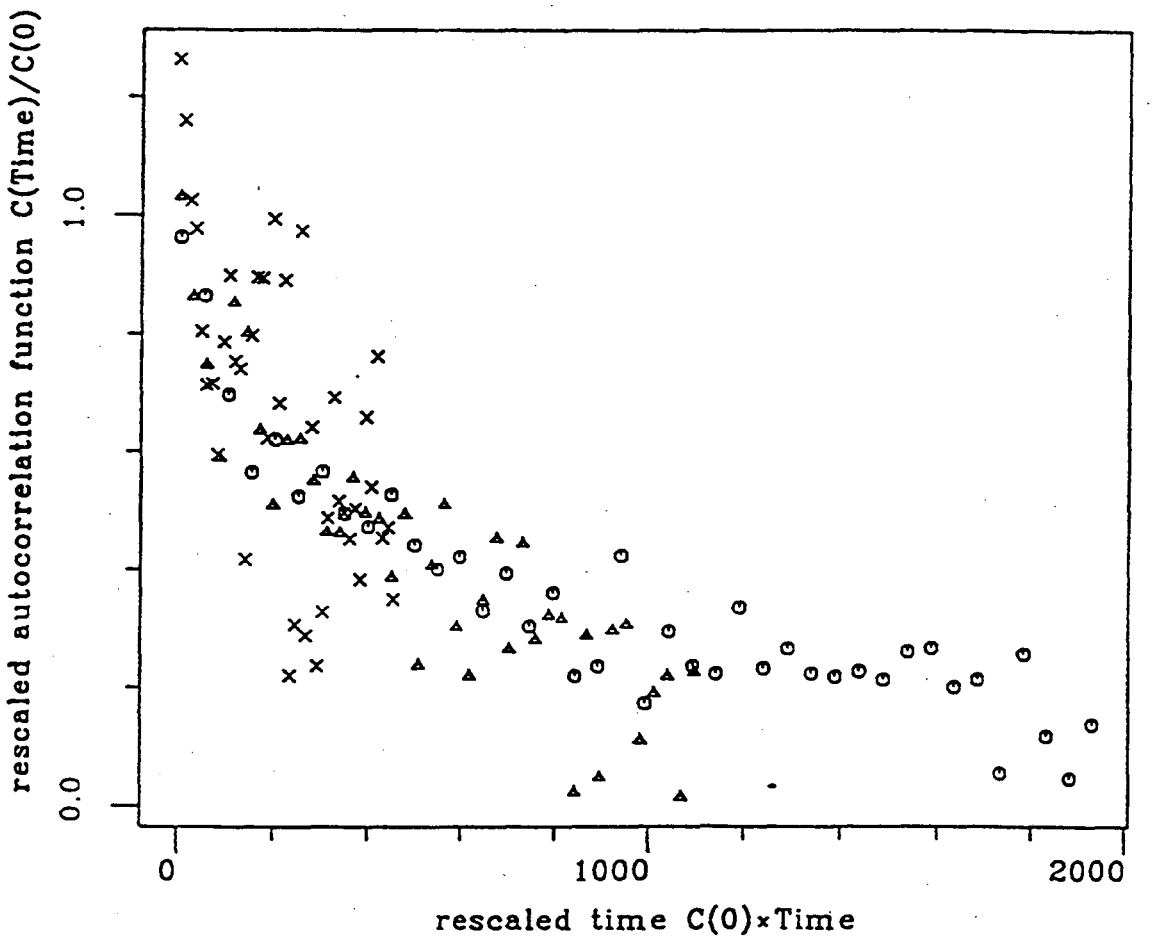
rescaled autocorrelation function C(Time)/C(0)
1.0
0.0
0
1000
2000
rescaled time C(0)×Time

References for Chapter 7

1. D.E. Koppel (1974) Statistical accuracy in fluorescence correlation spectroscopy. Phys. Rev. A **10**: 1938.
2. D. Gill (1979) Inhibition of fading in fluorescence microscopy of fixed cells. Separatum Experientia **35**: 400.
3. Honeywell Test Instruments Division (1973) *Instruction Manual: Model sai-43A Correlation and Probability Analyzer*, section 3.
4. Brookhaven Instruments Corporation (1983) *Instruction Manual: Model BI-2030 Digital Correlator*, section 1.
5. S.M. Sorcher, J.C. Bartholomew and M.P. Klein (1980) The use of fluorescence correlation spectroscopy to probe chromatin in the cell nucleus. Biochim. Biophys. Acta **610**: 28.
6. M. Weissman, H. Schindler and G. Feher (1976) Determination of molecular weights by fluctuation spectroscopy: Application to DNA. Proc. Nat. Acad. Sci. USA **73**: 2776.
7. A. Yariv (1975) *Quantum Electronics*. John Wiley and Sons, Inc., New York, 111.
8. D.E. Koppel, D. Axelrod, J. Schlessinger, E.L. Elson and W.W. Webb (1976) Dynamics of fluorescence marker concentration as a probe of mobility. Biophys. J. **16**: 1315.
9. A. Savitzky and M.J.E. Golay (1964) Smoothing and differentiation of data by simplified least squares procedures. Anal. Chem. **36**: 1627.
10. Y. Suzaki and A. Tachibana (1975) Measurement of the μm sized Gaussian laser

beam using the scanning knife-edge. Appl. Opt. **14**: 2809.

11. R.J. Lewis and R. Pecora (1986) Comparison of predicted Rouse-Zimm dynamics with observations for a 2311 base pair DNA fragment. Macromolecules **19**: 2047.
12. K.S. Schmitz and J.M. Schurr (1973) Rotational relaxation of macromolecules determined by dynamic light scattering. II. Temperature dependence for DNA. Biopolymers **12**: 1543.
13. R.J. Lewis, J.H. Huang and R. Pecora (1985) Rotational and translational motion of supercoiled plasmids in solution. Macromolecules **18**: 944.
14. S.M. Sorcher and M.P. Klein (1980) Profile of a focussed collimated laser beam near the focal minimum characterized by fluorescence correlation spectroscopy. Rev. Sci. Instr. **51**: 98.

Chapter 8

Conclusions

In conclusion we summarize the fluorescence data and its dynamic interpretation. Extensions of this work will also be considered.

8.1 Experimental Results

The data obtained in the steady state fluorescence depolarization and photobleaching experiments demonstrate that photolysed ethidium monoazide/DNA complexes exhibit nanosecond and microsecond internal motions. The temporal and spatial extent of the very fastest components of DNA reorientation can be inferred from the depolarization data. An effective angular amplitude, α, for the motion of the complex during the lifetime of the excited state can be extracted from the steady state anisotropy r (see section 3.1) by invoking the relationship[1]

$$r = r_0[\frac{3\langle cos^2\,\alpha\rangle - 1}{2}]. \qquad (8-1)$$

Here r_0 is the limiting anisotropy of the molecules in a very viscous solution. The anisotropy and polarization (see section 5.2) are equivalent quantities and are related to one another through the expression[1]

$$r = \frac{2P}{3-P}. \qquad (8-2)$$

The steady state polarization of photolysed azide/DNA complexes in dilute buffer

solutions was found to be 0.32. The corresponding values for the anisotropy and angular amplitude were calculated from equations 8-1 and 8-2; the values are 0.24 and 26 degrees respectively. We note in passing that the displacement $\alpha = 26$ degrees is derived from calf thymus data; however, the extent of fast local motion in DNA is not expected to vary extensively for different types of the nucleic acid. It is highly probable that small amplitude torsional oscillations of the DNA backbone, such as those postulated to exist in ethidium bromide/DNA systems, are responsible for the fast, partial depolarization observed in the steady state polarization experiments.

We now move beyond the temporal resolution of the fluorescence depolarization technique and examine microsecond DNA reorientation as revealed in this FPR work. In the FPR experiments described here, the bleach pulse was 10 μsec long. Therefore, we could not resolve rotational motions which relax in less than 10 microseconds. It was possible, however, to calculate an approximate 'wobble' amplitude for motion during the bleach phase of the FPR experiment. For the large molecule phage Lambda we found that the DNA reoriented in a cone of half angle $\alpha = 70$ degrees during the period encompassing the bleach and the reopening of the phototube. Fast torsional oscillations of the helix backbone and some of the smaller amplitude normal mode deformations of the DNA molecule are most likely responsible for the relaxation detected in this time regime.

In the FPR experiments we could resolve still longer lived components of Lambda reorientation. The temporal characteristics of slow DNA rotation were revealed in the rate of decay of the bleach-induced anisotropy in the angular distribution of dye. It was

possible, in these first experiments, to detect Lambda motions that relax characteristically within 120 μsec after bleaching the sample. Bending deformations of the polymer (modes 20 and higher) contribute substantially to this longest resolved component of DNA reorientation. Note that both the empirical Callis-Davidson formula (see equation 2.1) and the Rouse-Zimm/Hearst-Harris expressions 2-9, 6-3 predict the existence of still more slowly relaxing deformations and/or Brownian rotations; these motions were not detected here.

Finally, rates of translational diffusion can also reveal interesting features about the size, shape and environment of biomolecules. In this work we report fluctuation measurements of translational diffusion coefficients of a covalently labeled plasmid PBR 322 ($D_0 = 1.7 \times 10^{-8} \frac{cm^2}{sec}$) and an oligomeric DNA ($D_0 \approx 10^{-7} \frac{cm^2}{sec}$). The data are in agreement with results obtained in earlier fluorescence correlation experiments that utilized intercalating dyes. This FCS approach should prove particularly useful when it is desired selectively to monitor the motion of one species of molecule immersed in a complicated multicomponent biological system.

8.2 Potential for Future Work

We have utilized fluorescence spectroscopy to map out a wide spectrum of DNA rotational and translational motions. A number of interesting extensions of this work can be considered. As the resolution of the polarized FPR method improves it should be possible, with this technique, to follow the *temporal* evolution of an even broader range of DNA reorientational motions. As mentioned previously, angular correlation measurements hold the potential for revealing new and interesting characteristics of

microsecond and millisecond macromolecular rotation. Finally, a number of important biological systems, such as the RNA polymerase-DNA complex, await investigation with the experimental tools and theoretical concepts discussed here.

References for Chapter 8

1. J.R. Lackowicz (1983) *Principles of Fluorescence Spectroscopy.* Plenum Press, New York, 118.

Appendix 1

Derivation of Equation 3-6.

Throughout this mathematical discussion the polarizations of the parallel and perpendicular mode bleaching beams will define the directions of the laboratory z and y axes. The polarization of the probe beam must then be parallel to z. (Note that these choices for the direction of the bleach and probe beam polarization are not the same as the convention established in chapter 3 or Appendix 3. However, we make this change so that all angular variables can be interpreted as spherical polar coordinates). In our experimental configuration only the z component of the fluorescence is passed to the photomultiplier.

Consider an absorption dipole that wobbles in a cone of half angle α during the bleach pulse and the first (10 μsec) interval over which excitation counts are collected. The cone is centered on an axis whose polar and azimuthal angles in the laboratory frame are θ_0 and ϕ_0 (see figure 6). The orientation of the absorption moment (not the cone) is time dependent and will be denoted by (θ,ϕ).

We analyze the effect of wobble on the initial ratio in the 'weak' bleach limit. The probability that the dye molecule is bleached by z polarized light is then proportional to the ensemble average of $cos^2\,\theta$ over the wobble cone. Similarly the probability that the fluorophore is bleached by y polarized light is proportional to $\langle sin^2\,\theta\, sin^2\,\phi\rangle$. Moreover,

if it is assumed that the *average* orientation of the transition moment does not change significantly as the phototube reopens and the first set of observation counts is collected, the excitation of the dye molecule by the probe beam is also proportional to the average of $cos^2\,\theta$ over the bleach cone. Finally only the z component of the fluorescence is actually passed to the photomultiplier; therefore the detection geometry will also introduce a factor of $\langle cos^2\,\theta \rangle$ into the expression for the fluorescence signal. (We assume here that the absorption and emission moments are parallel). The problem is, then, to evaluate $\langle cos^2\,\theta \rangle$ and $\langle sin^2\,\theta\, sin^2\,\phi \rangle$ and to determine what effect these quantities have on the initial ratio.

It is most convenient to compute the required expectation values in a coordinate system whose z axis is along the average position of the transition moment (θ_0, ϕ_0). It is necessary, therefore, to establish the relationship between the coordinates of a point in the laboratory and wobble frames. The laboratory axes are coincident with the wobble axes after a counterclockwise rotation through an angle $\frac{3\pi}{2} + \phi_0$ about the laboratory z axis; this first rotation is then followed by a counterclockwise rotation of $2\pi - \theta_0$ about the new x axis. Thus the coordinates of a vector relative to the molecular (primed) axes are related to the components of the vector in the laboratory (unprimed) frame by the matrix equation [1]

$$\begin{pmatrix} x \\ y \\ z \end{pmatrix} = \begin{pmatrix} sin\,\phi_0 & cos\,\phi_0\, cos\,\theta_0 & sin\,\theta_0\, cos\,\phi_0 \\ -cos\,\phi_0 & cos\,\theta_0\, sin\,\phi_0 & sin\,\theta_0\, sin\,\phi_0 \\ 0 & -sin\,\theta_0 & cos\,\theta_0 \end{pmatrix} \begin{pmatrix} x' \\ y' \\ z' \end{pmatrix}. \qquad (A1-1)$$

We require the quantities $\langle sin^2\,\theta\, sin^2\,\phi \rangle = \langle (\frac{y}{r})^2 \rangle$ and $\langle cos^2\,\theta \rangle = \langle (\frac{z}{r})^2 \rangle$. Here r is just the conventional radial polar coordinate of a point. The transformation equation A1-1 can be used to rewrite these expectation values in terms of primed (wobble) coordinates.

We have

$$z = -\sin\theta_0 y' + \cos\theta_0 z' \qquad (A1-2)$$

and

$$y = -\cos\phi_0 x' + \cos\theta_0 \sin\phi_0 y' + \sin\theta_0 \sin\phi_0 z'. \qquad (A1-3)$$

Moreover, if (θ',ϕ') specifies the orientation of the transition moment in the molecular frame

$$x' = r\sin\theta'\cos\phi';\ y' = r\sin\theta'\sin\phi';\ z = r\cos\theta'. \qquad (A1-4)$$

After substitution of the relationships A1-4 into equations A1-2 and A1-3 the resulting expressions for z and y can be used to demonstrate that

$$\langle \sin^2\theta \sin^2\phi\rangle = \cos^2\phi_0\langle \sin^2\theta' \cos^2\phi'\rangle + \cos^2\theta_0 \sin^2\phi_0\langle \sin^2\theta' \sin^2\phi'\rangle$$

$$+ \sin^2\theta_0 \sin^2\phi_0\langle \cos^2\theta'\rangle - \cos\phi_0 \cos\theta_0 \sin\phi_0\langle \sin^2\theta' \cos\phi' \sin\phi'\rangle$$

$$- \sin\theta_0 \sin\phi_0 \cos\phi_0\langle \sin\theta' \cos\theta' \cos\phi'\rangle + \cos\theta_0 \sin\theta_0 \sin^2\phi_0\langle \cos\theta' \sin\theta' \sin\phi'\rangle$$

$$(A1-5)$$

and

$$\langle \cos^2\theta\rangle = \sin^2\theta_0\langle \sin^2\theta' \sin^2\phi'\rangle + \cos^2\theta_0\langle \cos^2\theta'\rangle$$

$$-2\sin\theta_0 \cos\theta_0\langle \sin\theta' \sin\phi' \cos\theta'\rangle. \qquad (A1-6)$$

The simplification achieved by the transformation into the molecular frame is now evident. Evaluation of expressions A1-5 and A1-6 simply requires computation of the ensemble average of functions of molecule-referenced angular variables. These averages will be the same for all transition dipoles; if the expectation values were evaluated in the

laboratory frame the answers would, of course, depend on the average orientation of the wobble axis.

The expectation values are easily evaluated analytically for the case we consider *i.e.* the uniform motion model. In this case it is clear that the amount of time spent in a small area $d\Omega'$ about (θ', ϕ') is simply proportional to the area $d\Omega'$. Hence the averages in equations A1-5 and A1-6 are calculated as integrals over $d\Omega' = \sin\theta' d\theta' d\phi'$. The probability of finding a dipole with a given orientation is normalized to the total area of the cone. The limits of integration are simply $0 < \theta' < \alpha$ and $0 < \phi' < 2\pi$. The last three terms in expression A1-5 and the final integral in A1-6 all vanish when ϕ' ranges from 0 to 2π. After explicit evaluation of the nonzero integrals it can be shown that

$$\langle \sin^2\theta \sin^2\phi \rangle = \frac{\cos\alpha(\cos\alpha + 1)}{2}(\sin^2\theta_0 \sin^2\phi_0 - \frac{1}{3}) + \frac{1}{3} \qquad (A1-7)$$

and

$$\langle \cos^2\theta \rangle = \frac{\cos\alpha(\cos\alpha + 1)}{6}(3\cos^2\theta_0 - 1) + \frac{1}{3}. \qquad (A1-8)$$

We now use these uniformly averaged angular quantities to compute the initial ratio as a function of wobble angle. Recall that R(0) is defined as

$$R(0) = \frac{F_0 - F_\perp(0)}{F_0 - F_\parallel(0)} = \frac{1 - \frac{F_\perp(0)}{F_0}}{1 - \frac{F_\parallel(0)}{F_0}}. \qquad (A1-9)$$

The quantity $\frac{F_\perp(0)}{F_0}$ is given by (suppressing common factors) the following expression (see below for rationale)

$$\frac{F_\perp(0)}{F_0} = \frac{\int_0^{2\pi}\int_0^{\pi}(1 - f_B\langle \sin^2\theta \sin^2\phi \rangle)\langle \cos^2\theta \rangle^2 \sin\theta_0 d\theta_0 d\phi_0}{\int_0^{2\pi}\int_0^{\pi}(\langle \cos^2\theta \rangle^2 \sin\theta_0 d\theta_0 d\phi_0)}. \qquad (A1-10)$$

Here f_B is a bleach parameter that is proportional to the intensity of the incident laser light. (An analogous expression for $\frac{F_\parallel(0)}{F_0}$ can be obtained from the relationship above

by replacing $sin\,\theta\,sin\,\phi$ by $cos\,\theta$). The first term in equation A1-10 is proportional to the number of fluorescent molecules with average orientation (θ_0, ϕ_0) at the end of the bleach period. The second and third angular averages (written together as $\langle cos^2\,\theta\rangle^2$ in A1-10) reflect the probability of exciting a wobbling dye molecule with polarized probe light and the contribution of the z component of the fluorescence to the measured signal.

The last step in the calculation involves inserting the expressions for the wobble averaged angular quantities into the equations for $\frac{F_\perp}{F_0}$ and $\frac{F_\parallel}{F_0}$ and then computing the integrals over θ_0 and ϕ_0. Equation A1-9 can then be used to find R(0) as a function of α.

References for Appendix 1

1. H. Goldstein (1950) *Classical Mechanics*. Addison-Wesley Press, Inc., Cambridge, 109.

Appendix 2

The Stochastic Operator Method

Suppose, a general stochastic quantity of interest, X(t), is governed by some evolution equation

$$\frac{dX(t)}{dt} = \epsilon O(t)X(t). \qquad (A2-1)$$

Here, epsilon is a small parameter and O(t) is some operator. It is possible to expand X(t) as

$$X(t) = \sum_i \epsilon^i f^i(t)\langle X(t)\rangle. \qquad (A2-2)$$

Here, the $f^i(t)$ are stochastic operators that satisfy $\langle f^i(t)\rangle = 0$. The mean value of X(t) will satisfy some non-stochastic differential equation of the form

$$\frac{d\langle X(t)\rangle}{dt} = \sum_i \epsilon^i \Omega^i(t)\langle X(t)\rangle. \qquad (A2-3)$$

Here the $\Omega^i(t)$ are non-stochastic: they are equal to their average.

One may find expressions for the $\Omega^i(t)$ by substituting the power series for X(t) and $\langle X(t)\rangle$ into the basic evolution equation for X(t) and then equating powers of epsilon. The general expressions for the expansion coefficients in terms of integrals over the operator O(t) are given in reference 1 of chapter 4. It is shown that

$$\Omega^1(t) = \langle O(t)\rangle \qquad (A2-4)$$

$$\Omega^2(t) = \int_0^t (\langle O(t)O(t_1)\rangle - \langle O(t)\rangle\langle O(t_1)\rangle dt_1. \qquad (A2-5)$$

The expressions for the higher expansion coefficients $\Omega^i(t)$ are more complicated functions of the operator O(t), but in general the $\Omega^i(t)$ are expressible in terms of integrals over ensemble averaged products of O(t). The $\Omega^i(t)$ are evaluated for a specified O(t). Once the $\Omega^i(t)$ are determined the equation of motion for $\langle X(t)\rangle$ may be integrated to find the ensemble average of X(t).

Appendix 3

Derivation of Equation 6-1.

An exact calculation of the maximal temperature rise in a three dimensional absorbing sample that is illuminated with light having a diverging Gaussian intensity profile is complicated. Therefore in this analysis of thermal effects we make two approximations both of which will lead to an overestimate of the maximal bleached induced temperature increase. First, the divergence of the beam is neglected. Second, we compute an approximate ΔT given by the product of the initial rate of temperature increase multiplied by the length of the bleach pulse.

The temperature distribution is governed by the inhomogeneous diffusion equation

$$-\frac{\partial T(\vec{r},t)}{\partial t}+\kappa\nabla^2 T(\vec{r},t)=\frac{A(\vec{r},t)}{c_p\rho}. \qquad (A3-1)$$

In equation (A3-1) $A(\vec{r},t)$ is the power per unit volume deposited by the laser beam at point $\vec{r}$ at time t and κ is the thermal diffusivity of the medium. If the heat source has a nondiverging Gaussian intensity profile $A(\vec{r},t)=\frac{4.6\epsilon CP}{\pi w_0^2}\,exp(\frac{-2r^2}{w_0^2})$. Here r is the standard radial *cylindrical* distance of point $\vec{r}$ from the position of maximal light intensity.

We compute the temperature profile by integrating the three dimensional free space Green's function of equation A3-1 over the inhomogeneous term $A(\vec{r},t)$. The Green's

function of (A3-1) is

$$G(\vec{r}-\vec{r'},t-t') = \frac{1}{[4\pi\kappa(t-t')]^{\frac{3}{2}}} exp[\frac{-(\vec{r}-\vec{r'})^2}{4\kappa(t-t')}] \quad t > t'$$

$$G(\vec{r}-\vec{r'},t-t') = 0 \quad t < t'. \qquad (A3-2)$$

Hence the solution of (A3-1) may be written

$$T(\vec{0},t) = \int_0^t dt' \int d\vec{r'} G(\vec{0}-\vec{r'},t-t') \frac{A(\vec{r'},t')}{c_p\rho}. \qquad (A3-3)$$

For our particular choice of A($\vec{r}$,t) equation A3-3 reads

$$T(\vec{0},t) = B\int_0^t dt' \int_{-\infty}^{\infty} dz' \int_0^{\infty} dr' \frac{2\pi r'}{[4\pi\kappa(t-t')]^{\frac{3}{2}}} exp[\frac{-r'^2-z'^2}{4\kappa(t-t')}] exp(\frac{-2r'^2}{w_0^2}) \qquad (A3-4)$$

where B=$\frac{4.6\epsilon CP}{\pi w_0^2 c_p\rho}$. If we make the change of variable $\beta = \frac{1}{\sqrt{t-t'}}$ it follows that

$$T(\vec{0},t) = \frac{4\pi B}{[4\pi\kappa]^{\frac{3}{2}}} \int_{t^{-\frac{1}{2}}}^{\infty} d\beta \int_{-\infty}^{\infty} dz' \int_0^{\infty} dr' r' exp[-r'^2(\frac{\beta^2}{4\kappa}+\frac{2}{w_0^2})] exp(\frac{-z'^2\beta^2}{4\kappa}). \qquad (A3-5)$$

The goal is to determine the bleach induced temperature rise, ΔT, at the position of maximal beam intensity (r=0). The following approximate relationship holds $\Delta T = \frac{dT}{dt}\Delta t$ where $\frac{dT}{dt}$ is the rate of temperature increase at t=0 and r=0; Δt is the length of the bleach. The derivative of the temperature with respect to time may be determined from the chain rule. It follows that

$$\frac{dT}{dt} = \frac{1}{2}t^{-\frac{3}{2}} \frac{4\pi B}{[4\pi\kappa]^{\frac{3}{2}}} \int_{-\infty}^{\infty} dz' \int_0^{\infty} dr' r' exp[-r'^2(\frac{1}{4\kappa t}+\frac{2}{w_0^2})] exp(\frac{-z'^2}{4\kappa t}). \qquad (A3-6)$$

Evaluation of the integral over r' yields the following expression

$$\frac{dT}{dt} = \pi B t^{-\frac{3}{2}} (4\pi\kappa)^{-\frac{3}{2}} \int_{-\infty}^{\infty} dz' \frac{exp(\frac{-z'^2}{4\kappa t})}{\frac{2}{w_0^2}+\frac{1}{4\kappa t}}. \qquad (A3-7)$$

Finally we compute the integral over z' and find

$$\frac{dT}{dt} = \frac{2B}{1 + \frac{8\kappa t}{w_0^2}}. \qquad (A3-8)$$

Note that the rate of temperature increase at r=0 is maximal at t=0. An upper bound for the bleach induced temperature rise is therefore

$$\Delta T = 2B\Delta t = \frac{9.2\epsilon CP}{\pi w_0^2 c_p \rho}\Delta t. \qquad (A3-9)$$

More precisely the following explicit expression for $T(0,t)$ holds

$$T(0,t) = \frac{2.3\epsilon CP}{2\pi\kappa c_p \rho} ln(1 + \frac{8\kappa t}{w_0^2}). \qquad (A3-10)$$

Equation A3-9 is merely the short time limit of (A3-10).

LAWRENCE BERKELEY LABORATORY
TECHNICAL INFORMATION DEPARTMENT
UNIVERSITY OF CALIFORNIA
BERKELEY, CALIFORNIA 94720